Department of Electrical and Computer Engineering

Villanova University

TECHNICAL REPORT

(11/15/97 - 10/1/98)

BLIND TIME-FREQUENCY ANALYSIS FOR SOURCE DISCRIMINATION IN MULTISENSOR ARRAY PROCESSING

Submitted to

Office of Naval Research

Grant No. N00014-98-1-0176

Principle Investigator

Moeness G. Amin

September 1998

VILLANOVA UNIVERSITY

DEPARTMENT OF ELECTRICAL AND
COMPUTER ENGINEERING

September 29th, 1998

Office of Naval Research
Program Officer: William J. Miceli
Ballston Centre Tower One
800 North Quincy Street
Arlington, VA 22217-5660

Dear Mr. Miceli

Enclosed, please find three copies of the interim (annual) report for ONR grant N00014-98-1-0176.

Sincerely

Moeness G. Amin
Professor
Principle Investigator

cc: Administrator Grant Officer
Director, Naval Research Laboratory
Defense Technical Information Center
Office of Research and Sponsored Projects, VU

800 LANCASTER AVENUE VILLANOVA PENNSYLVANIA 19085-1681 (610) 519-4970 FAX (610) 519-4436

Table of Contents

Topic		Page
Executive Summary		1
1.	Spatial Averaging of Time-Frequency Distributions	1
2.	Fast Computational Time-Frequency Distribution Kernels	2
3.	Blind Spatial Processing for Frequency Diversity Spread Spectrum Communications: Partial Jamming Suppression	3
4.	Adaptive Array Processing for Multipath Fading Mitigation Via Exploitation of Filter Banks	3
Research Team and Collaborations		4
Appendix		5

Executive Summary

Moeness Amin (PI)

This report presents the results of the research work performed under the ONR funding, grant number N00014-98-1-0176 over the period of November 15th, 1997 to September 30th, 1998. The research efforts on this grant have taken four different directions, namely; Array Processing Using Time-Frequency Analysis; Fast Computational Time-Frequency Distribution Kernels; Blind Spatial Processing for Frequency Diversity Spread Spectrum Communications: Partial Jamming Suppression; Adaptive Array Processing for Multipath Fading Mitigation Via Exploitation of Filter Banks. In the following, we highlight the approach adopted in each problem and summarize the respective results and contributions. We include in the appendix all research papers which have come out of the current ONR grant since its inception last November. Some of these papers have already been published, while others are either under review or will be published past October 1st, 1998.

1. SPATIAL AVERAGING OF TIME-FREQUENCY DISTRIBUTIONS

Time-frequency distributions have been recently proposed for applications to array signal processing problems. For this purpose, spatial time-frequency distributions (STFDs) have been introduced and represented in a matrix form. The elements of a spatial time-frequency distribution matrix are the time-frequency distributions and the cross-time frequency distributions of the data received at the multi-sensor array. It has been shown that the relationship between the spatial time-frequency distributions of the sensor data and the time-frequency distributions of the sources is identical to that of the sensor data covariance matrix and the sources' correlation matrix. This key property permits direction finding and blind source separations to be performed using the sources' time-frequency localization properties.

Blind source separation consists of recovering a set of signals of which only instantaneous linear mixtures are observed. This problem has been typically solved using statistical information available on source signals, including second or higher order statistics. Our previous contribution to this area has shown that the spatial time-frequency distributions is an effective alternative to separating sources whose signatures are different in the t-f domain. Successful applications of STFDs to source separation require computing STFD at different time-frequency (t-f) points. The results are then incorporated into a joint-diagnalization technique to estimate the mixing, or the array manifold matrix. This matrix transfers the source signals into sensor data – a process that we must *undo* by blind separation, often up to a multiplicative complex scalar and the order of the sources.

We have continued to focus our research work on array processing using the signal arrivals' time-varying frequency characteristics. We have concentrated our efforts into two different specific problems, namely, high resolution angle of arrival estimation and improved blind source separations. Both problems are approached using the signal power distribution over two joint variables, including time and frequency.

Our first contribution is improving source signal estimation by performing the blind source separation using ambiguity functions rather than time-frequency distributions. Unlike the spatial time-frequency distributions, where the separation is performed using various time-frequency bins, the proposed approach is based on information from the

ambiguity domain. The procedure is similar to that adopted in spatial TFD-based blind source separation. The main difference, however, lies in the domain in which the mixing matrix is estimated. In the proposed technique, the mixing matrix is obtained by joint diagonalization of the spatial ambiguity (SAF) matrices rather than the spatial time-frequency distribution matrices. These SAF matrices are formed from the auto- and cross-ambiguity functions of the data received by the different array sensors. It is shown that at each time-lag and frequency-lag point in the ambiguity domain, the sensors' SAF matrix is related to the sources' ambiguity function matrix in the same fashion as the sensors' and sources' TFDs. Performing blind source separation in the ambiguity-domain, rather than the t-f domain, provides a greater ability to formulate the problem using the signal auto-terms. Avoiding cross-terms both simplifies and improves the performance of joint-diagonalization, and subsequently enhances source estimation.

Our second contribution is the development of a novel approach based on time-frequency distributions (TFDs) for separating signals received by a multiple antenna array. The sources, as stated above, have different time-frequency signatures and are instantaneously mixed at the array sensors. The proposed approach provides a significant improvement in performance over the recently introduced spatial time-frequency distributions, specifically for signals with close time-frequency signatures. In this approach, spatial averaging of the time-frequency distributions of the sensor data is performed to eliminate the interactions of the sources signals in the time-frequency domain, and as such restores the realness property and the diagonal structure of the source TFDs, which are both necessary for source separation. It is shown that the proposed approach yields improved performance over both cases of no spatial averaging and averaging using time-frequency smoothing kernels.

Our third contribution to this area is the introduction of the Time-frequency MUSIC as a new array signal processing method based on time-frequency signal representations. As discussed above, spatial time-frequency distributions have successfully been used to solve the problem of blind source separations for nonstationary signals. We have used the same underlying structure of STFDs to solve the direction finding problem, i.e., angles of arrival (AOA) estimation. A new method for the estimation of the signal subspace and the noise subspace based on time-frequency signal representations has been introduced. The proposed approach consists of the joint block-diagonalization (JBD) of a set of spatial time-frequency distribution matrices. Once the signal and the noise subspaces are estimated, any subspace based approach can be applied for AOA estimation. We propose to use the MUSIC algorithm. The effects of spreading the noise power while localizing the source energy in the time-frequency domain amounts to increasing the robustness of the eigenstructure superresolution method with respect to noise, and hence improves spatial resolution. Performance of the proposed Time-Frequency MUSIC (TF-MUSIC) for different time-frequency kernels was evaluated numerically.

2. FAST COMPUTATIONAL TIME-FREQUENCY DISTRIBUTION KERNELS

Time-frequency distributions (TFDs) are a powerful tool for nonstationary signal analysis in a wide variety of applications. However, the computational burden limits the applicability of the TFD in practice. Hence, design of fast implementation methods are important to utilize TFDs for applications that require on-line processing such as radar systems and nonstationary jammer excision in spread spectrum communications. The TFD is often computed using the following procedure. First, the bilinear data products are computed which form the instantaneous autocorrelation function (IAF). Next, the IAF is smoothed along each time-lag using a time-frequency (t-f) kernel to produce the local autocorrelation function (LAF). Finally, the LAF is Fourier transformed along the time-lag variable to yield the

required TFD. Recognizing the fact that the computations required to compute the DFT are much smaller than those needed to compute the LAF, it becomes logical to target the calculation of the LAF, for significant computational savings.

We have introduced a new recursive structure for efficient computations of the local autocorrelation function. This recursion is achieved by decomposing the t-f kernel along each time-lag into a finite number of cosinusoidal terms. Each term generates one recursive equation to update the LAF. This technique is named the *trigonometric decomposition of time-frequency kernels*, and can be viewed as a frequency sampling design technique of t-f kernels. This proposed class of Trigonometric kernels (also referred to as the frequency sampling (FS) kernels), while providing considerable reduction in the computation of the LAF, retain the Hermitian property of the LAF which simplifies the DFT operations. Further, trigonometric decomposition is amenable to data -dependent kernel design and does not compromise the time-frequency desirable properties.

3. BLIND SPATIAL PROCESSING FOR FREQUENCY DIVERSITY SPREAD SPECTRUM COMMUNICATIONS: PARTIAL JAMMING SUPPRESSION

Frequency diversity spread spectrum (FD-SS) has been recently shown to be a powerful tool for digital detection as well as an effective alternative to the traditional spread spectrum techniques, namely direct sequence (DS-SS) and frequency hopping (FH-SS). In a general context, diversity is conceived by the existence of several replicas (either in code, time space, or frequency). When diversity is available to the receiver either by the structure of the transmitted signal or the architecture of the receiver, optimum spatial signal processing, which is blind to the temporal signal characteristics, can be derived.

We have devised a novel technique to obtain optimum blind spatial processing for frequency diversity spread spectrum (FD-SS) communication systems. The sufficient statistics for a linear combiner, which prove ineffective due to the interferer's spectral location, are modified to yield improved detection under partial jamming in the spectral domain. Robustness to partial time jamming is achieved by extending the notion of replicas over the frequency axis to repetition over the time variable. Analysis and simulations are provided showing the advantages of using FD-SS with spatial diversity to combat interference which is confined to a narrow frequency or time support relative to the desired signal extent in either domain.

4. ADAPTIVE ARRAY PROCESSING FOR MULTIPATH FADING MITIGATION VIA EXPLOITATION OF FILTER BANKS

The spatial-temporal equalization can be achieved by space-time adaptive processing (STAP) to effectively mitigate inter-symbol interference (ISI) and co-channel interference (CCI). Such a scheme consists of an integrated adaptive array and a temporal equalizer to perform jointly optimum spatial and temporal signal processing. However, solving both the CCI and ISI problems simultaneously by conventional STAP methods is difficult. The recent STAP methods require either large scale matrix inversion, recursive calculation or cascaded CCI and ISI cancellers.

We have proposed an efficient subband adaptive array processing method that utilizes filter banks to mitigate both the CCI and ISI effects in land mobile communications. A subband adaptive array has, in effect, the same function as an STAP system, while the implementation is much easier. The subband adaptive array provides sub-optimal performance in the context of frequency-spatial signal processing, which enhances the

signal correlation between multipath rays prior to processing. In subband adaptive arrays, the frequency band of the received signal is divided into smaller bands through the use of filter banks. Analysis filters yield a significant increase in the signal correlation between the multipath rays within each subband. Such an increase is blind in the sense that it does not require a priori knowledge of the arriving signals. As a result of increased correlation, the multipath fading associated with both the desired and the interference signals is reduced, thus yielding faster convergence of the adaptive weight vector as well as fewer degrees-of-freedom (DOF's) required for adequate equalization. The importance to properly choose the analysis and synthesis filters to obtain good equalization performance by subband signal processing is emphasized. The signal correlation enhancements of multipath signals using different filter banks are compared and several simulation examples are provided to confirm the effectiveness of the proposed method.

Research Team and Collaborations

The research team working on this grant at Villanova University are: Professor Moeness Amin (Principle Investigator), Dr. Yimin Zhang (Postdoctoral Fellow), Mr. Weifeng Mu (graduate student), and Mr. Govind Mandapati (graduate student). The work by the two graduate students have not matured to the level of reporting and will be included in the next year report. The work on optimum spatial processing and partial band jamming is performed in collaboration with Prof. Miguel Lagunas at TSC Department, MODULO 5, Barcelona, Spain. The work on fast computation time-frequency kernels is joint with Dr. Gopal Venkatesan at the University of Minnesota. The time-frequency MUSIC is the result of joint collaboration with Dr. Adel Belouchrani at Ecole National Polytechnique, Algeria. The work on subband arrays is in conjunction with Dr. Yimin Zhang while he was in Japan before joining Villanova University as a Postdoctoral fellow, in April 1998, and his colleague Dr. K. Yang.

Appendix

Publications

1. Y. Zhang and M. Amin, "Spatial Averaging of Time-Frequency Distributions," Submitted to International Conference on Acoustics, Speech, and Signal Processing, 1999.

2. M. Amin and A. Belouchrani, " Time-Frequency MUSIC -- An Array Signal Processing Method based on Time-Frequency Signal Representation, "Proceedings of the SPIE, Radar Processing, Technology, and Applications III, San Diego, Ca, July 1998.

3. M. Amin and G. Venkatesan, " Trigonometric Decomposition of Time-Frequency Distribution Kernels, "Proceedings of the 1998-IEEE Int. Symposium on Time-Frequency and Time-Scale, Pittsburgh, Pa, October 1998.

4. M. Amin and A. Belouchrani, "Blind Source separation Using Spatial Ambiguity Functions, " Proceedings of the 1998-IEEE Int. Symposium on Time-Frequency and Time-Scale, Pittsburgh, Pa, October 1998.

5. M. Lagunas, A. Perez, M. Amin, and J. Vida, "Spatial Processing for Frequency Diversity Schemes," Submitted to the IEEE Transactions on Signal Processing, August 1998.

6. Y. Zhang, K. Yang, and M. Amin, "Adaptive Array Processing for Multipath Fading Mitigation via Exploitation of Filter Banks," Proceedings of the IEEE International Symposium on Antennas and Propagation, July 1998.

Submitted to the 1999-IEEE Int. Conf. on Acoustics, Speech, and Signal Processing.

SPATIAL AVERAGING OF TIME-FREQUENCY DISTRIBUTIONS

Yimin Zhang and *Moeness G. Amin*

Department of Electrical and Computer Engineering
Villanova University
Villanova, PA 19085, USA

ABSTRACT

This paper presents a novel approach based on time-frequency distributions (TFDs) for separating signals received by a multiple antenna array. This approach provides a significant improvement in performance over the recently introduced spatial time-frequency distributions, specifically for signals with close time-frequency signatures. In this approach, spatial averaging of the time-frequency distributions of the sensor data is performed to eliminate the interactions of the sources signals in the time-frequency domain, and as such restore the realness property and the diagonal structure of the source TFDs, which are necessary for source separation. It is shown that the proposed approach yields improved performance over both cases of no spatial averaging and averaging using time-frequency smoothing kernels.

1. INTRODUCTION

In this paper, we introduce a new technique for source separation based on time-frequency distribution methods. The sources have different time-frequency signatures and instantaneously mixed at the array sensors. The number of sensors is assumed to be equal to or greater than twice the number of sources. The time-frequency distributions (TFDs) of the data across the array are computed and used to construct spatial time-frequency distribution matrices (STFDs). By forcing the hermition Toeplitz structure of the STFDs and perform spatial symmetric averaging over two parts of the array, we achieve significant improvement of source separation over the case where no spatial averaging is performed.

Recently, time-frequency distributions have been applied to direction finding and blind source separation problems in array processing. The spatial time-frequency distributions are introduced in [1] and represented by a spatial matrix whose elements are the time-frequency distributions of the data across the multi-sensor array. The successful application of STFDs to separating sources with identical spectra, but different time-frequency signatures, is shown in [2]. In this application, STFD matrices computed at different t-f points are incorporated into a joint-diagnalization technique based on generalized Jacobi transform to estimate the mixing, or array manifold, matrix. This matrix is then used to estimate the sources' signals up to a multiplicative complex scalar and the order of the sources. The general theory of solving blind source seperation problems using spatial arbitrary joint variable distributions, including those of time and frequency, is given in [3]. In [4], the two arbitrary variables are chosen as the time-lag and frequency-lag, and the source separation was performed using spatial ambiguity functions. The use of STFDs as an eigenstructure-based approach for direction finding is given in [5], where the Time-Frequency MUSIC technique is proposed to estimate the signal and noise subspaces.

The importance of joint-diagonalization (JD) in the STFD context is that the diagonal structure, the distinct eigenvalues, and the full rank properties of the signal TFD matrix, necessary for source separation, can be easily violated when operating with a single t-f point. The cross time-frequency distributions of the source signals yield non-zero complex values at the off-diagonal elements, rendering the estimation of the mixing matrix difficult, or even impossible. Also, the noise contribution to all matrix elements at low SNR cannot be ignored. As the interactions of the source signals vary over the time-frequency plane, the incorporation of several STFD matrices at different t-f points into JD enhances diagonalization and leads to a successful separation of signal arrivals. It is noted that the primary motivation of using smoothing kernels and resorting to other variables than time and frequency, specifically the ambiguity-domain variables, is to allow the selection of joint-variable points where the interactions of the source signals are insignificant.

The fundamental role of the proposed technique of symmetric spatial averaging of STFDs is the effective elimination of the signals' intermodulations. It effectively restores the diagonal structure and realness property of the signal TFD matrix. Symmetric spatial averaging is a simple, well-known technique in conventional array processing [6]. It uses additional array sensors to reduce cross-correlation in coherent and correlated signal environments, and thereby permits proper angle-of-arrival estimations and source separations. It is shown that adopting this technique in the underlying TFD-based source separation JD problem gives robustness to t-f point selections and leads to improved performance over other TFD-based techniques, specifically for sources whose time-frequency signatures are not very distinct.

2. SPATIAL TIME-FREQUENCY DISTRIBUTIONS

The data vector for N-element array is given by

$$\mathbf{x}(t) = \mathbf{y}(t)+\mathbf{n}(t) = \mathbf{A}\mathbf{s}(t)+\mathbf{n}(t). \quad (1)$$

In vector forms, $\mathbf{x}(t)=[x_0(t), \ldots, x_{N-1}(t)]^T$ is a noisy instantaneous linear mixture of the source signals $\mathbf{s}(t)=[s_1(t), \ldots, s_n(t)]^T$ and $\mathbf{n}(t)$ is the additive noise. The mixing matrix $\mathbf{A}$ is the transfer function between the sources and the array sensors.

This work is supported by ONR under Grant #N00014-98-1-0176.

The discrete-time form of Cohen's class of TFD for signal $x(t)$ is given by [7]

$$D_{xx}(t,f)=\sum_{l=-\infty}^{\infty}\sum_{m=-\infty}^{\infty}\phi(m,l)x(t+m+l)x^{*}(t+m-l)e^{-j4\pi fl} \quad (2)$$

where t and f represent the time index and the frequency index, respectively. The kernel $\phi(m, l)$ characterizes the TFD and is a function of both the time and lag variables. The cross-TFD of two signals $x_i(t)$ and $x_j(t)$ is defined by

$$D_{x_ix_j}(t,f)=\sum_{l=-\infty}^{\infty}\sum_{m=-\infty}^{\infty}\phi(m,l)x_i(t+m+l)x_j^{*}(t+m-l)e^{-j4\pi fl} \quad (3)$$

The spatial time-frequency distribution (STFD) incorporates both equations (2) and (3), and is defined in [2] by,

$$\mathbf{D}_{xx}(t,f)=\sum_{l=-\infty}^{\infty}\sum_{m=-\infty}^{\infty}\Phi(m,l)\otimes\mathbf{x}(t+m+l)\mathbf{x}^{H}(t+m-l)e^{-j4\pi fl} \quad (4)$$

where $\left[\mathbf{D}_{xx}(t,f)\right]_{i,j}=D_{x_ix_j}(t,f)$, for $i, j=0, \ldots, N-1$, $\otimes$ denotes the Hadamard product, and $\left[\Phi(m,l)\right]_{i,j}=\phi_{i,j}(m,l)$ is the time-frequency kernel associated with the pair of the sensor data $x_i(t)$ and $x_j(t)$. Under the linear data model of Eq. (1) and assuming noise-free environment, the STFD matrix takes the following simple structure

$$\mathbf{D}_{xx}(t,f)=\mathbf{A}\mathbf{D}_{ss}(t,f)\mathbf{A}^{H} \quad (5)$$

where $\mathbf{D}_{ss}(t,f)$ is the signal TFD matrix whose entries are the auto- and cross-TFDs of the sources. Eq. (5) is similar to that commonly used in conventional blind source separation and direction-of-arrival (DOA) estimation problems [8,9], relating the signal correlation matrix to the data spatial correlation matrix. If $\mathbf{D}_{ss}(t,f)$ is a full-rank matrix, the two subspaces spanned by the principle eigenvectors of $\mathbf{D}_{xx}(t,f)$ and the columns of $\mathbf{A}$ become identical. In this case, directional finding techniques based on eigenstructures can be applied. If $\mathbf{D}_{ss}(t,f)$ is diagonal, i.e., the signal cross-TFDs at the time-frequency point (t,f) are zeros, the mixture matrix and the signal waveform can be recovered using blind source separation methods [1,2]. In these methods, in order to avoid potential problems associated with using a single STFD, STFDs at different (t,f) points are incorporated into a joint-diagonalization scheme. Although JD of the STFDs is effective in most cases, signals with close time-frequency signatures are still difficult to separate. As shown below, spatial averaging can be used to facilitate signal separation.

3. SPATIAL AVERAGING TIME-FREQUENCY DISTRIBUTIONS

Symmetric spatial averaging method was proposed by Pillai [6] to restore the full-rank property of the signal covariance matrix in the presence of coherent signals. In this section, we extend the spatial averaging method to TFD analysis, and propose the signal separation method by joint diagonalization (JD) based on spatial averaging TFDs.

Without loss of generality, we consider $M=2$, i.e., only two sources, $s_1(t)$ and $s_2(t)$. The result can be easily extended to multiple sources. By ignoring the effect of noise, the received signal at i-th array sensor is represented as

$$x_i(t)=x_i^{(1)}(t)+x_i^{(2)}(t)=s_1(t)e^{-jd_i\omega_1}+s_2(t)e^{-jd_i\omega_2} \quad (6)$$

where $\omega_k=2\pi\sin\phi_k/\lambda$ $(k=1,2)$ is the spatial radian frequency, λ is the RF wavelength, and d_i is the distance between 0-th and i-th array sensors. We assume the array is equi-spaced linear array. The cross-TFD of $x_i(t)$ and $x_j(t)$ is

$$\begin{aligned}&D_{x_ix_j}(t,f)\\&=D_{x_i^{(1)}x_j^{(1)}}(t,f)+D_{x_i^{(2)}x_j^{(1)}}(t,f)+D_{x_i^{(2)}x_j^{(2)}}(t,f)+D_{x_i^{(1)}x_j^{(2)}}(t,f)\\&=\left[D_{s_1s_1}(t,f)+D_{s_2s_1}(t,f)e^{-jd_i(\omega_2-\omega_1)}\right]e^{-j(d_i-d_j)\omega_1}\\&\quad+\left[D_{s_2s_2}(t,f)+D_{s_1s_2}(t,f)e^{jd_i(\omega_2-\omega_1)}\right]e^{-j(d_i-d_j)\omega_2}\end{aligned} \quad (7)$$

Since the cross-terms (second term in each bracket in (7)) are generally complex, it is clear that the TFD matrix $\mathbf{D}_{xx}(t,f)$ will not provide proper phase information for recovering the DOA of the arrived signals when cross-terms are present. However, such phase information can be restored by using spatial averaging methods. The spatial averaging of TFD allows the signal separation even when the TFDs of multiple signals have very similar shapes and are highly overlapping.

Let the number of array sensors be $2N-1$ with the array center is the zeroth sensor, as shown in Fig.1. The TFD of $x_0(t)$ and $x_i(t)$, $i=0, 1, 2, \ldots, N-1$, is

$$\begin{aligned}&D_{x_0x_i}(t,f)\\&=\left[D_{s_1s_1}(t,f)+D_{s_2s_1}(t,f)\right]e^{jd_i\omega_1}+\left[D_{s_2s_2}(t,f)+D_{s_1s_2}(t,f)\right]e^{jd_i\omega_2}\end{aligned} \quad (8)$$

where we note $d_0=0$. Similarly, the TFD of $x_0(t)$ and $x_{-i}(t)$ is

$$\begin{aligned}&D_{x_0x_{-i}}(t,f)\\&=\left[D_{s_1s_1}(t,f)+D_{s_2s_1}(t,f)\right]e^{-jd_i\omega_1}+\left[D_{s_2s_2}(t,f)+D_{s_1s_2}(t,f)\right]e^{-jd_i\omega_2}\end{aligned} \quad (9)$$

The spatial averaging of (8) and (9) is given by

$$\tilde{D}_{xx}^{(i)}(t,f)=\left\{D_{x_0x_i}(t,f)+D_{x_0x_{-i}}^{*}(t,f)\right\}/2=b_1e^{jd_i\omega_1}+b_2e^{jd_i\omega_2} \quad (10)$$

where

$$b_1=D_{s_1s_1}(t,f)+\mathrm{Re}\left\{D_{s_2s_1}(t,f)\right\}$$

$$b_2=D_{s_2s_2}(t,f)+\mathrm{Re}\left\{D_{s_1s_2}(t,f)\right\}$$

Since the terms in the brackets are all real, the TFD in (10) correctly represents the phase information caused by the propagation delay between array sensors, even when the cross-terms are complex. The matrix formed from the TFDs (10)

$$\tilde{\mathbf{D}}_{xx}(t,f)=\begin{bmatrix}\tilde{D}_{xx}^{(0)}(t,f) & \tilde{D}_{xx}^{(1)}(t,f) & \cdots & \tilde{D}_{xx}^{(N-1)}(t,f)\\ \tilde{D}_{xx}^{(1)*}(t,f) & \tilde{D}_{xx}^{(0)}(t,f) & \cdots & \tilde{D}_{xx}^{(N-2)}(t,f)\\ \vdots & \vdots & \ddots & \vdots\\ \tilde{D}_{xx}^{(N-1)*}(t,f) & \tilde{D}_{xx}^{(N-2)*}(t,f) & \cdots & \tilde{D}_{xx}^{(0)}(t,f)\end{bmatrix} \quad (11)$$

is hermitian and Toeplitz. It is referred to as the spatial averaging TFD (SATFD) matrix. In the noise-free environment, the SATFD matrix can be expressed as

$$\tilde{\mathbf{D}}_{xx}(t,f) = \mathbf{A}\tilde{\mathbf{D}}_{ss}\mathbf{A}^H \tag{12}$$

where

$$\tilde{\mathbf{D}}_{ss}(t,f) = \mathrm{diag}[b_1 \quad b_2] \tag{13}$$

are the equivalent TFD of the signal vectors. Note that $\tilde{\mathbf{D}}_{ss}(t,f)$ no longer expresses the actual TFD. Clearly, (12) has the same format as (5), and $\tilde{\mathbf{D}}_{ss}(t,f)$ here is diagonal even when the cross-terms of the TFD of the signals are present. Therefore, the spatial averaging method will ensure the validity of the TFD-based signal separation in the presence of cross-TFD.

4. SIMULATION RESULTS

Equi-spaced 5-element linear array is used for simulation with the interelement spacing 0.5λ. When spatial averaging method is used, two sub-arrays are formed, each with 3 elements. Two sources of chirp signals

$$s_1(t) = e^{-j\mu\frac{t^2}{2}}, \quad s_2(t) = e^{-j\mu\frac{t^2}{2}-j\omega t} \tag{14}$$

are used, where μ and ω are chosen to be 0.008π and 0.02π, respectively. The DOAs of the two signals are assumed 30° and 60° from the broadside direction. No noise is considered here.

Fig.2(a) shows the Wigner-Ville distribution of each source signal, and Fig.2(b) shows the respective distributions after signal separation. It is clear that the array fails to separate $s_1(t)$ and $s_2(t)$.

In the TFD-based signal separation method, applied in Fig. 2, three points (t, f) are used for joint diagonalization at t = 32, 64, and 96. The frequency f is chosen so that the TFD at the first array sensor is the largest for a given t.

To show the effect of using a smoothing kernel, similar simulation is performed with the Choi-Williams kernel [10] with σ = 0.1. The result is shown in Fig.3. A rectangular window with 31 samples in both time and frequency scale is used. Since the two signals are closely spaced in the t-f domain, the cross-terms reduction furnished by the Choi-Williams kernel is limited, and again the array fails to separate the two signals.

Fig.4 shows the separated signals under the same conditions when the proposed spatial averaging method is applied. The signals are perfectly separated, except for their order.

5. CONCLUSIONS

Symmetric averaging of spatial time-frequency distributions has been introduced. The averaging improves the performance of source separation using joint-diagonalization techniques. It amounts to forming a spatial hermition Toeplitze matrix using the time-frequency distributions of the data across one half of the array. This matrix is then added to the spatial matrix corresponding to the other half of the array. The effect of this averaging is to remove interaction between the source signals in the time-frequency domain. Joint digonalization (JD) using a generalization of Jacobi transform is then applied to estimate the mixing matrix. By reducing the interaction of the source signals, the JD algorithm yields improved performance over the case when no averaging is performed. The paper presented an example of separating two chirps signals whose time-frequency signatures are slightly different. The proposed approach has successfully separated the two signatures, while other non-averaging methods fail.

6. REFERENCES

[1] A. Belouchrani and M. Amin, "Source separation based on the diagonalization of a combined set of spatial time-frequency distribution matrices," in *Proc. IEEE ICASSP'97*, Germany, April 1997.

[2] A. Belouchrani and M. Amin, "Blind source separation based on time-frequency signal representation," *IEEE Trans. Signal Processing*, Nov. 1998.

[3] A. Belouchrani and M. Amin, "Blind source separation using joint signal representations," in *Proc. SPIE Conf. on Advanced Algorithms and Architectures for Signal Processing*, San Diego, CA, Aug. 1997.

[4] M. Amin and A. Belouchrani, " Blind source separation using the spatial ambiguity functions," in *Proc. IEEE Int. Symp. on Time-Frequency and Time-Scale Analysis*, Pittsburgh, Pennsylvania, Oct. 1998.

[5] M. Amin and A. Belouchrani "Time-frequency MUSIC: an array signal processing method based on time-frequency signal representation," in *Proc. SPIE Conf. on Radar Processing, Technology and Applications*, San Diego, CA, July 1997.

[6] S. U. Pillai, *Array Signal Processing*, Springer-Verlog, 1989.

[7] L. Cohen, *Time-frequency Analysis*, Prentice Hall, 1995.

[8] L. Tong, Y. Inouye, and R-W. Liu, "Waveform-preserving blind estimation of multiple independent sources," *IEEE Trans. Signal Processing*, vol,41, no.7, pp.2461-2470, July 1993.

[9] A. Belouchrani, K. A. Meraim, H.-F. Cardoso, and E. Muylines, "A blind source separation techniques using second order statistics," *IEEE Trans. Signal Processing*, vol.45, no.2, pp.434-444, Feb. 1997.

[10] H. I. Choi and W. J. Williams, "Improved time-frequency representation of multicomponent signals using exponential kernels," *IEEE Trans. Acoust., Speech, Signal Processing*, vol. 37, no.6, pp.862-871, June 1989.

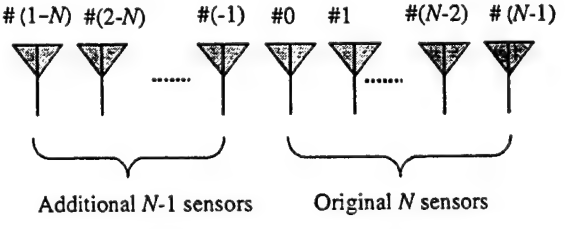

Fig.1 Array configuration for spatial averaging

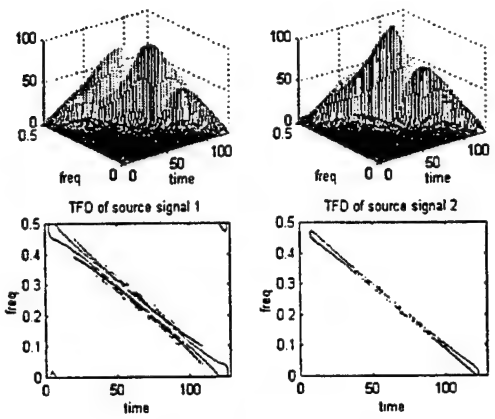

(a) TFD of the sources

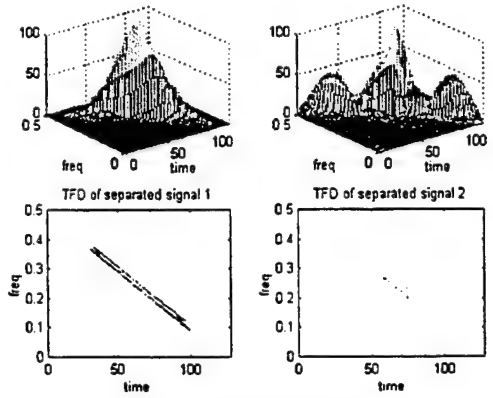

(b) TFD of the separated signals

Fig.2 TFD of the sources and the separated signals using Wigner-Ville distribution

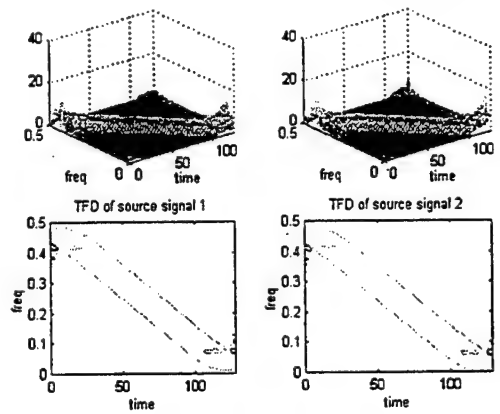

(a) TFD of the sources

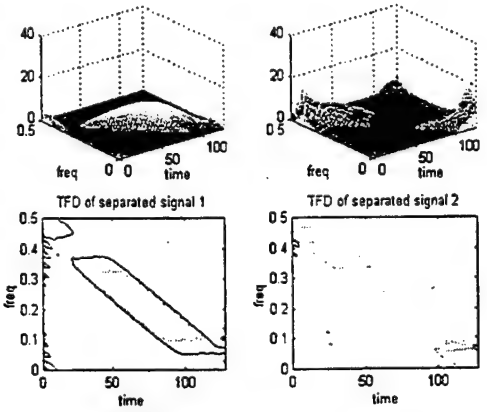

(b) TFD of the separated signals

Fig.3 TFD of the sources and the separated signals using Choi-Williams distribution

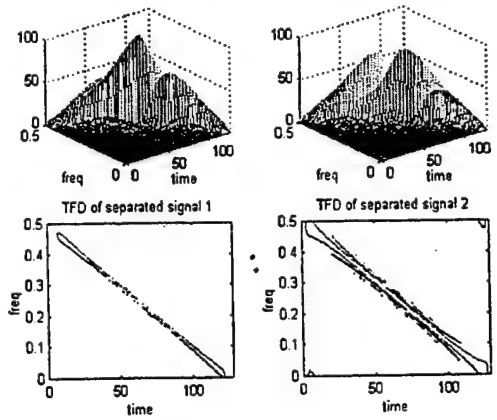

(a) Wigner-Ville distribution

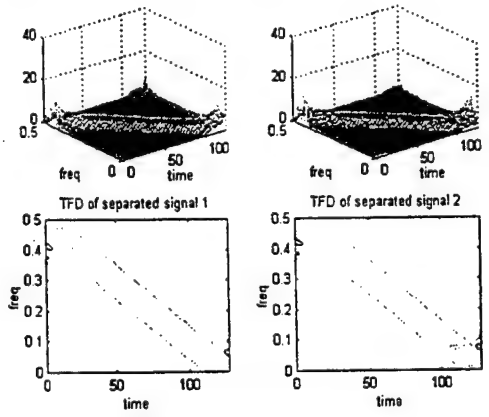

(b) Choi-Williams distribution

Fig.4 Separated signals with spatial averaging

Proceedings of the SPIE, Radar Processing, Technology, and Applications III
Under Review by the IEEE Signal Processing Letters.

Time-Frequency MUSIC: An array signal processing method based on time-frequency signal representation.

Moeness G. Amin* and Adel Belouchrani**
*Dept. of Electrical and Computer Engineering
Villanova University
Villanova, Pa 19085, USA
**Dept. of Electrical Engineering
Ecole national Polytechinque, Algiers, Algeria

ABSTRACT

In previous contributions,[1-3] we have used successfully the concept of spatial time frequency distribution (STFD) to solve the problem of blind source separation for nonstationary signals. In this paper, we propose to apply this same concept to solve the problem of the direction of arrival (DOA) estimation. A new method for the estimation of the signal subspace and noise subspace based on time-frequency signal representation is introduced. The proposed approach consists of the joint block-diagonalization (JBD) of a combined set of spatial time frequency distribution matrices. Once the signal and the noise subspaces are estimated, any subspace based approach can be applied for DOA estimation. Herein, we propose to use the MUSIC algorithm. Performance comparison of the proposed approach with the classical MUSIC method is provided. The influence of the time-frequency kernels on the performance of the newly proposed Time-Frequency MUSIC (TF-MUSIC) is evaluated numerically.

Key Words: DOA estimation, Subspace estimation, Time-frequency representation, Spatial time-frequency distributions, Joint block-diagonalization.

1 Introduction

In many signal processing applications, signals are received on small or large antennas aperture. In some of these applications the multidimensional signal is spatially processed and reduced to one dimension, on which some desired processing are applied. This often occurs when dealing for example with time-frequency signal analysis.[4-6] Typical processing in this case is the signal syntheses from the time-frequency plane. In other applications, the multidimensional signal is directly utilized to estimate some signal parameters. Subspace-based methods exploit this spatial information, which is provided by the multidimensional signal.[7,8] These methods use a geometrical relation involving the exact moments of the data, commonly the data covariance matrix. The desired signal parameters are then extracted by solving the geometrical relation in some approximate sense, and using sample moments instead of the exact ones. This class of methods assumes stationary signals. When the frequency content of the measured data is time-varying, the previous approaches can still be applied. However, they do not use the

*This work is supported by ONR, grant # N00014-98-1-0176

data time-frequency information, which if properly used may significantly improve performance.

We propose to develop new subspace-based methods with a geometrical relation involving no longer the exact moments of the data but their **Spatial Time Frequency Distributions**. The spatial time frequency distribution (STFD) is a generalization of the time frequency distribution to a vector signal. In previous contributions,[1-3] we have used successfully the concept of STFD to solve the problem of blind source separation for nonstationary signals.[9] In this paper , we study the application of this new concept of spatial time frequency signal representations to solve the problem of DOA estimation.

This paper proposes a new approach based on a joint block-diagonalization of several spatial time frequency distribution matrices. It is shown that performing a joint block-diagonalization of a combined set of these matrices provides an improved estimate of the signal and noise subspaces over existing techniques. Once the signal and the noise subspaces are obtained, any subspace based approach[10,11] can be used for the DOA estimation. Experimental performance comparison of the proposed technique with the classical MUSIC[10] is presented. The influence of the time-frequency kernels on the performance of the proposed Time-Frequency MUSIC (TF-MUSIC) is evaluated numerically.

The paper is organized as follows. In section 2, the data model is stated along with the relevant hypothesis. Spatial time-frequency distributions are recalled in section 3. Section 4 presents the proposed method for noise and signal subspace estimation. Section 5 discusses the general conditions that should be satisfied by the spatial time-frequency distributions. Numerical simulations evaluating the performance of the new method are given in section 6.

2 Data Model and Assumptions

Consider an array of m sensors receiving waveforms of n sources ($m > n$). The data snapshot, representing the sensor output vector $\mathbf{x}(t)$, is assumed to obey the following model:

$$\mathbf{x}(t) = \mathbf{A}(\theta)\mathbf{s}(t) + \mathbf{n}(t) \tag{1}$$

where $\mathbf{n}(t)$ is an additive noise, $\theta = [\theta_1, \cdots, \theta_n]^T$, $\mathbf{A}(\theta) = [\mathbf{a}(\theta_1), \cdots, \mathbf{a}(\theta_n)]^T$, and $\mathbf{s}(t) = [s_1(t), \cdots, s_n(t)]^T$ is the signal vector at time t, with the superscript ^{T} denoting the transpose operator. $\mathbf{a}(\theta_k)$ is the transfer vector between $x_k(t)$ and $\mathbf{y}(t)$. The parameter vector θ defines the DOAs.

The signal vector $\mathbf{s}(t)$ is assumed to be a nonstationary multivariate process with

$$(H1): \quad \mathbf{R}_s = \lim_{T\to\infty} \frac{1}{T} \sum_{t=1}^{T} \mathbf{s}(t+\tau)\mathbf{s}(t)^* = \mathrm{diag}[r_{11}(\tau), \cdots, r_{nn}(\tau)] \tag{2}$$

where superscript * denotes the conjugate transpose of a vector, diag[·] is the diagonal matrix formed with the elements of its vector valued argument and $r_{ii}(\tau) = \lim_{T\to\infty} \frac{1}{T} \sum_{t=1,T} \mathbf{s}_i(t+\tau)\mathbf{s}_i^*(t)$ denotes the autocorrelation of $\mathbf{s}_i(t)$. Assumption (H1) means that the component $\mathbf{s}_i(t)$, $1 \leq i \leq n$ are mutually uncorrelated as their cross-correlations are equal to zero.

The additive noise $\mathbf{n}(t)$ is modeled as a stationary, temporally white, zero-mean complex random process independent of the source signals. For simplicity, we also require $\mathbf{n}(t)$ to be spatially white, i.e.

$$(H2): \quad E\left(\mathbf{n}(t+\tau)\mathbf{n}^*(t)\right) = \sigma^2\delta(\tau)\mathbf{I} \tag{3}$$

where $\delta(\tau)$ is the Kronecker delta and $\mathbf{I}$ denotes the identity matrix.

3 Spatial time-frequency distributions

The discrete-time form of the Cohen's class of time-frequency distributions (TFD), for signal $x(t)$, is given by[12]

$$D_{xx}(t,f) = \sum_{l=-\infty}^{\infty} \sum_{m=-\infty}^{\infty} \phi(m,l)x(t+m+l)x^*(t+m-l)e^{-j4\pi fl} \tag{4}$$

where t and f represent the time index and the frequency index, respectively. The kernel $\phi(m,l)$ characterizes the distribution and is a function of both the time and lag variables. The cross-TFD of two signals $x_1(t)$ and $x_2(t)$ is defined by

$$D_{x_1x_2}(t,f) = \sum_{l=-\infty}^{\infty} \sum_{m=-\infty}^{\infty} \phi(m,l)x_1(t+m+l)x_2^*(t+m-l)e^{-j4\pi fl} \tag{5}$$

Expressions (4) and (5) are now used to define the following data *spatial time-frequency distribution* (STFD) *matrix*,

$$\mathbf{D_{xx}}(t,f) = \sum_{l=-\infty}^{\infty} \sum_{m=-\infty}^{\infty} \phi(m,l)\mathbf{x}(t+m+l)\mathbf{x}^*(t+m-l)e^{-j4\pi fl} \tag{6}$$

where $[\mathbf{D_{xx}}(t,f)]_{ij} = D_{x_ix_j}(t,f)$, for $i,j = 1,\cdots,n$.

A more general definition of the spatial time-frequency distribution matrix can be given as,

$$\mathbf{D_{xx}}(t,f) = \sum_{l=-\infty}^{\infty} \sum_{m=-\infty}^{\infty} \mathbf{\Phi}(m,l) \odot \mathbf{x}(t+m+l)\mathbf{x}^*(t+m-l)e^{-j4\pi fl} \tag{7}$$

where $\odot$ designates the Hadamard product, and $[\mathbf{\Phi}(m,l)]_{ij} = \phi_{ij}(m,l)$ is the time-frequency kernel associated with the pair of the sensor data $x_i(t)$ and $x_j(t)$.

Under the linear data model of equation (1) and assuming noise-free environment, the STFD matrix takes the following simple structure:

$$\mathbf{D_{xx}}(t,f) = \mathbf{A}(\theta)\mathbf{D_{ss}}(t,f)\mathbf{A}(\theta)^H \tag{8}$$

where $\mathbf{D_{ss}}(t,f)$ is the signal TFD matrix whose entries are the auto- and cross-TFDs of the sources and the superscript ^{H} denotes transpose conjugation for a matrix. We note that $\mathbf{D_{xx}}(t,f)$ is of dimension $m \times m$, whereas $\mathbf{D_{ss}}(t,f)$ is of $n \times n$ dimension. For narrowband array signal processing applications, matrix $\mathbf{A}(\theta)$ holds the spatial information and maps the auto- and cross-TFDs of the sources into auto- and cross-TFDs of the data.

Expression (8) is similar to that which commonly used in blind source separation[13] and direction of arrival (DOA) estimation problems, relating the signal correlation matrix to the data spatial correlation matrix. The two subspaces spanned by the principle eigenvectors of $\mathbf{D_{xx}}(t,f)$ and the columns of $\mathbf{A}(\theta)$ are, therefore, identical. Since the off-diagonal elements are cross-terms of $\mathbf{D_{ss}}(t,f)$, then this matrix is diagonal for each time-frequency (t-f) point which corresponds to a true power concentration, i.e. signal auto-term. In the sequel, we consider the t-f points which satisfy this property. In practice, to simplify the selection of auto-terms, we apply a smoothing kernel $\phi(m,l)$ that significantly decreases the contribution of the cross-terms in the t-f plane. This kernel can be a member of the reduced interference distribution (RID) introduced in[14] or signal-dependent which matches the underlying signal characteristics.[15,5,16]

4 Noise and Signal Subspace Estimation

By performing the SVD of the steering matrix,

$$\mathbf{A}(\theta) = [\mathbf{E}_s \mathbf{E}_n][\mathbf{D} \quad \mathbf{0}]^T \mathbf{V}^H, \tag{9}$$

and incorporating the results in (8), it is easily shown that

$$\mathbf{D}_{\mathbf{xx}}(t,f) = [\mathbf{E}_s \mathbf{E}_n]\mathbf{D}(t,f)[\mathbf{E}_s \mathbf{E}_n]^H, \tag{10}$$

where $\mathbf{D}(t,f)$ is a block-diagonal matrix given by

$$\mathbf{D}(t,f) = \mathrm{diag}[\mathbf{D}\mathbf{V}^H \mathbf{D}_{\mathbf{ss}}(t,f)\mathbf{V}\mathbf{D} \quad \mathbf{0}]. \tag{11}$$

Since $\mathbf{E}_s$ and $\mathbf{E}_n$, which respectively span the signal subspace and the noise subspace, are fixed and independent of the time-frequency point (t-f), relation (10) reveals that any matrix $\mathbf{D}_{\mathbf{xx}}(t,f)$ is block-diagonalized by the unitary transform

$$\mathbf{E} = [\mathbf{E}_s \ \mathbf{E}_n]. \tag{12}$$

A simple way to estimate the signal and noise subspaces is to perform the SVD on a single matrix $\mathbf{D}_{\mathbf{xx}}(t,f)$. But indeterminacies arise in the case where $\mathbf{D}_{\mathbf{ss}}(t,f)$ is singular. To avoid this problem, we propose to perform a *Joint block-diagonalization* (JBD) of the combined set of $\{\mathbf{D}_{\mathbf{xx}}(t_k,f_k)|k=1..K\}$ by exploiting the joint structure (10) of the STFD matrices. This joint block-diagonalization is achieved by the maximization under unitary transform of the following criterion,

$$C(\mathbf{U}) \stackrel{\text{def}}{=} \sum_{k=1}^{K} \sum_{i,j=1}^{n} |\mathbf{u}_i^* \mathbf{D}_{\mathbf{xx}}(t_k,f_k)\mathbf{u}_j|^2 \tag{13}$$

over the set of unitary matrices $\mathbf{U} = [\mathbf{u}_1, \cdots, \mathbf{u}_m]$.

The BJD criterion allows the structural information contained in each STFD matrix to be jointly integrated in a single unitary matrix. In appendix A, we propose an efficient algorithm for solving (13).

DOA estimation

Once the signal and the noise subspaces are estimated, one can use any subspace-based technique (e.g. MUSIC[10]) to estimate the DOAs. In this paper, the MUSIC algorithm[10] is applied to the noise subspace matrix $\hat{\mathbf{E}}_n$ estimated by the JBD. We obtain the Time-Frequency MUSIC (TF-MUSIC) algorithm which estimates the DOAs by finding the n largest peaks of the localization function,

$$f(\theta) = |\hat{\mathbf{E}}_n^H \mathbf{a}(\theta)|^{-2}. \tag{14}$$

5 Conditions on the time-frequency kernels

It is clear from (13) that from a perspective of the joint block-diagonalization technique, an attractive time-frequency distributions are those which allow the formation of non-singular diagonal matrices $D_{\mathbf{ss}}(t,f)$ at the prospective time-frequency points. This property should be viewed in light of the following observations:

1. The off-diagonal elements of $D_{\mathbf{ss}}(t,f)$ should be zeros, and as such, distributions that mount the cross-terms on the top of auto-terms should be carefully studied and re-examined for qualification under the proposed application and within the above frame work.

2. Time-frequency distributions that spread cross-terms over the entire time-frequency plane should, using the same argument, lead to improved performance over those distributions which localize the cross-terms in the auto-term regions.

3. Time-frequency distributions which reduce, but still localize the cross-terms away from the auto-term regions appear to be most applicable to the diagonal matrix requirements.

4. The time-frequency signatures of the sources, although remain distinct, should intersect as often as possible, producing a large number of candidate points.

5. Time-frequency distributions which reduce the noise variance are of significant importance.[17,18]

It is noteworthy that the time-frequency kernels which handle cross-terms differently in terms of their smoothing and localizations have already been devised. The Wigner,[19] Choi-Williams,[20] and Born-Jordan kernels[12] are good examples of how time-frequency kernels differ in cross-term mitigations. These kernels should be investigated to show their possible distinct offerings in the proposed method. In Section 6, we evaluate the performance of the new technique for these different kernels.

6 Numerical simulations

Herein, the performance of the proposed TF-MUSIC is compared to the MUSIC.[10] For this purpose, we consider a uniform linear array of 4 sensors separated by half a wavelength and receiving signals from 2 sources. The two source signals arriving at $\theta_1 = 10^\circ$ and $\theta_2 = -10^\circ$, respectively, are unit variance. The first source signal is composed of a chirp signal whose frequencies are $\omega_1 = 0.1\pi$ and $\omega_2 = 0.6\pi$. The second source signal is composed of a chirp signal whose frequencies are $\omega_1' = 0.6\pi$ and $\omega_2' = 0.1\pi$. The noise used in this simulation is zero-mean, Gaussian distributed, and temporally white. The noise power σ^2 is adjusted to give the desired $\mathrm{SNR} \stackrel{\mathrm{def}}{=} 10\log_{10}(\sigma^{-2})$. For the TF-MUSIC algorithm, 50 STFD matrices are considered. The variance of the estimated DOAs are computed over 100 independent trials.

Figures 1-4 illustrate the localization of the two sources for different level of the SNR and values of the sample size. In this simulation, the STFD matrices are computed using Choi-Williams kernels. These figures shows that TF-MUSIC performs better than MUSIC for low SNR level.

Next, we compare the performance of TF-MUSIC for the following time-frequency kernels:

1. Wigner kernel
2. Choi-Williams kernel
3. Born-Jordan kernel

and with respect to MUSIC.

Figure 2 displays the variance of the estimated DOA $\hat{\theta}_1$ versus SNR for 500 samples. The solid line presents the classical MUSIC algorithm. The dashed line, dashdot line and the dotted line correspond to the TF-MUSIC using Choi-Williams kernel, the TF-MUSIC using Born-Jordan kernel and the TF-MUSIC using Wigner kernel, respectively. According to this plot, TF-MUSIC using Wigner kernel outperforms the other methods. These results confirm the conditions stated in Section 5 on the time-frequency kernels.

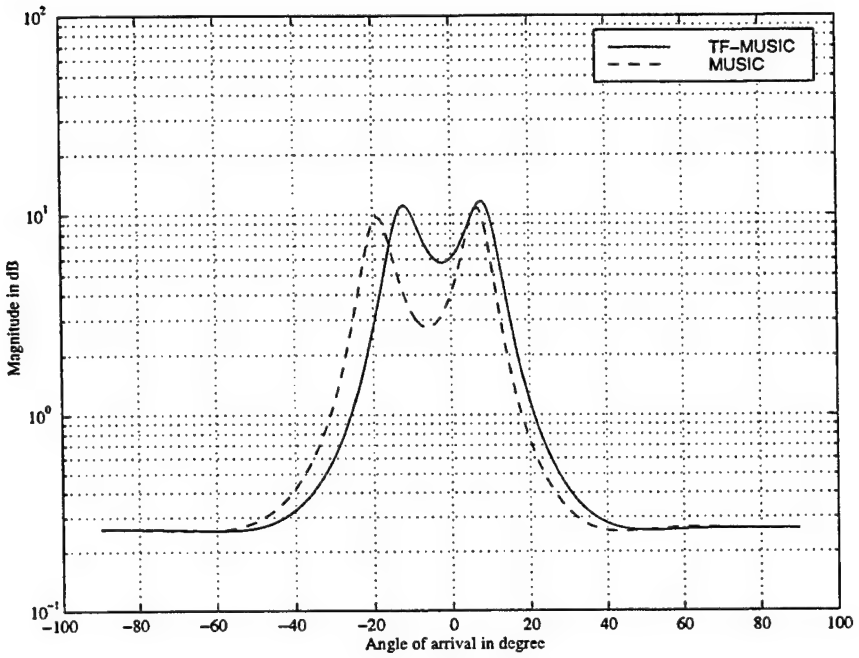

Figure 1: Source localization for SNR=0 dB and 100 samples.

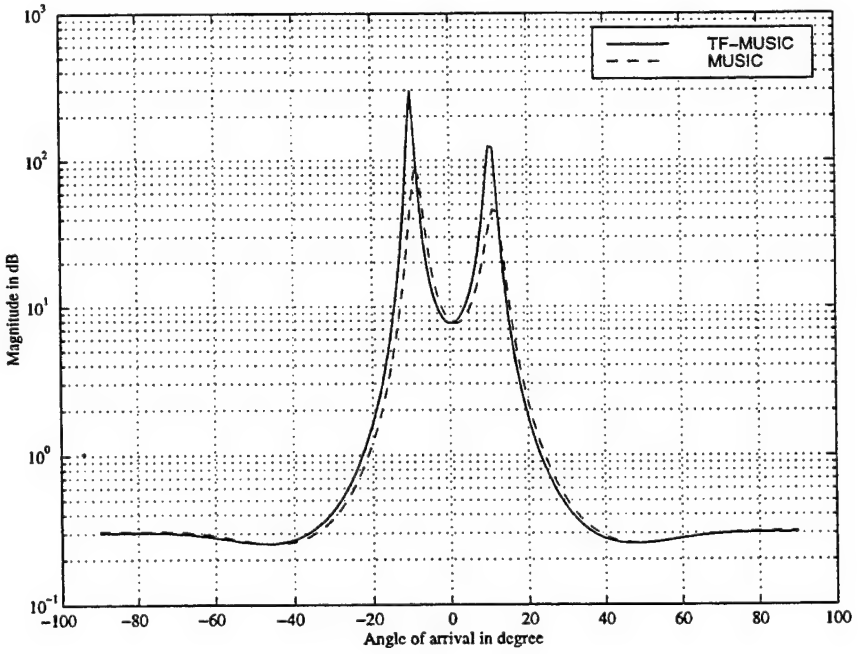

Figure 2: Source localization for SNR=10 dB and 100 samples.

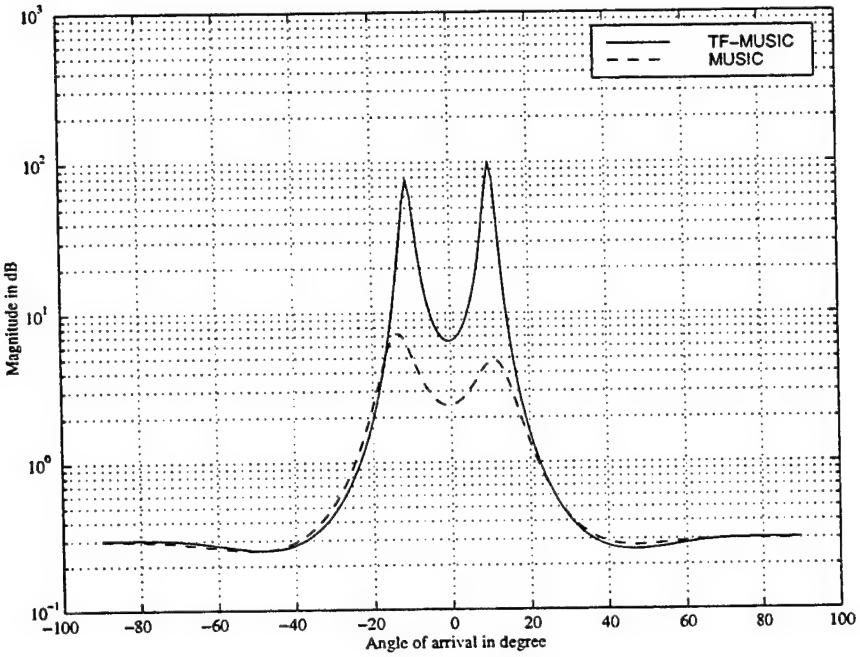

Figure 3: Source localization for SNR=5 dB and 100 samples.

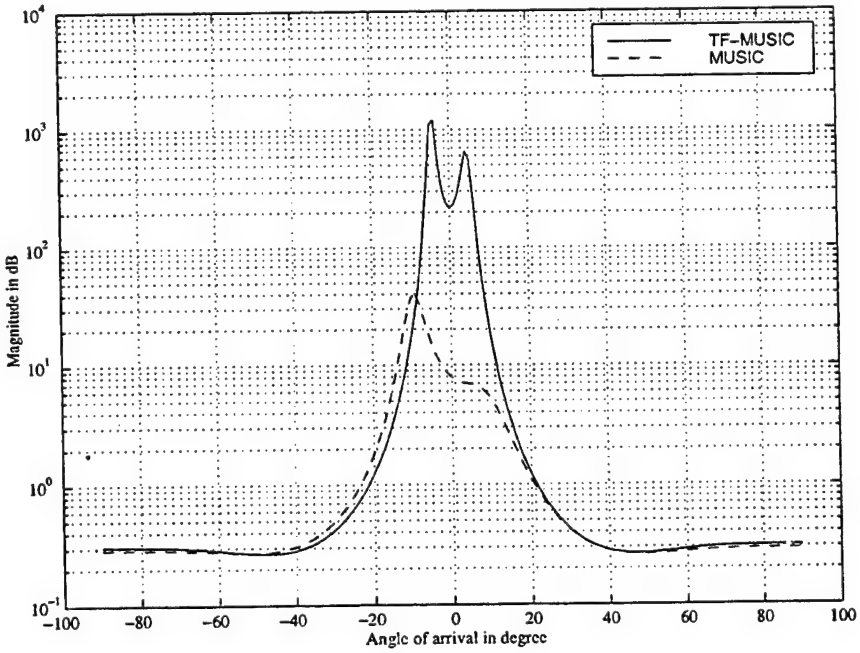

Figure 4: Source localization for SNR=5 dB and 50 samples.

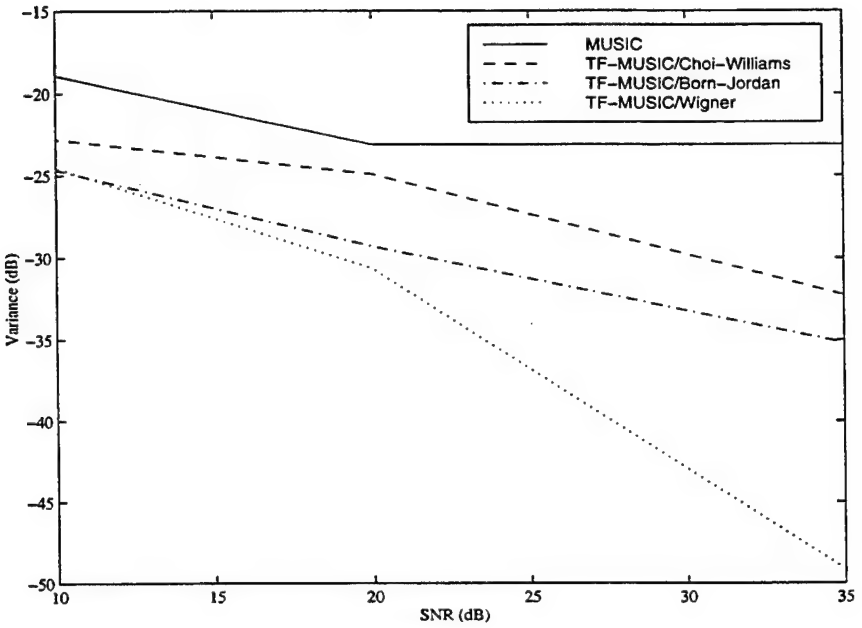

Figure 5: Variance of $\hat{\theta}$ vs SNR.

7 Conclusion

In this paper, a new DOA estimation approach using time-frequency distributions (STFD) is introduced. The new approach is based on the joint block-diagonalization of a combined set of spatial time-frequency distribution matrices. The later are made up of the auto- and cross- TFDs of the data snapshots across the multisensor array and they are expressed in terms of the TFD matrices of the sources. The TFD matrices of the data and sources appear, respectively, in place of the spatial and signal correlation matrices commonly used under stationary environment. The diagonal structure of the TFD matrix of the sources is essential for the proposed approach and is enforced by incorporating only the T-F points corresponding to the signal auto-terms. The off-diagonal elements are cross-terms which become negligible by using a reduced interference distribution kernel. We have focused on the time-frequency distributions of Cohen's class, however, one can use any other bilinear time-frequency signal representations such as the affine and hyperbolic classes.

The effect of spreading the noise power while localizing the source energy in the time-frequency domain amounts to increasing the robustness of the proposed approach with respect to noise. The paper has included numerical experiments of simple nonstationary signals. Performance evaluation of the proposed method for different time-frequency kernels has been provided.

Appendix A: Joint Block-Diagonalization (JBD) algorithm

The proposed algorithm for the joint block diagonalization of a set $\{\mathbf{M}_k = [m_{ij}^{(k)}], k = 1, \cdots, K\}$ of square matrices, inspired from,[13] maximizes the JBD criterion (13) by successive Givens rotations. A unitary matrix

$\mathbf{U} = [u_{ij}]$ is sought such that

$$\mathbf{M}'_k = \mathbf{U}\mathbf{M}_k\mathbf{U}^H, \ k = 1, \ldots, K \tag{15}$$

maximizes criterion (13).

At each Givens step, we choose a pivot pair p,q and make $u_{ij} = \delta_{ij}$ except for the elements $u_{pp} = u_{qq} = \cos(\theta)$, $u_{pq} = e^{j\phi}\sin(\theta)$ and $u_{qp} = -e^{-j\phi}\sin(\theta)$. One can show that optimization of (13) is equivalent to the maximization of

$$\mathbf{Q} \stackrel{\text{def}}{=} \sum_{k=1}^{K}\sum_{j=1}^{n} |\cos(\theta)m_{pj}^{(k)} + e^{j\phi}\sin(\theta)m_{qj}^{(k)}|^2 + |\cos(\theta)m_{jp}^{(k)} + e^{-j\phi}\sin(\theta)m_{jq}^{(k)}|^2 \tag{16}$$

for $p = 1, \cdots, n$ and $q = n+1, \cdots, m$. By defining the vectors

$$\mathbf{v}^T \stackrel{\text{def}}{=} [\cos(\theta), \sin(\theta)\cos(\phi), \sin(\theta)\sin(\phi)] \tag{17}$$

$$\mathrm{g1}_{kj}^T \stackrel{\text{def}}{=} [m_{pj}^{(k)}, m_{qj}^{(k)}, jm_{qj}^{(k)}] \tag{18}$$

$$\mathrm{g2}_{kj}^T \stackrel{\text{def}}{=} [m_{jp}^{(k)}, m_{jq}^{(k)}, -jm_{jq}^{(k)}] \tag{19}$$

$\mathbf{Q}$ also reads

$$\mathbf{Q} = \mathbf{v}^T\mathbf{G}\mathbf{v} = \mathbf{v}^T\,\Re e(\mathbf{G})\,\mathbf{v} \tag{20}$$

where

$$\mathbf{G} = \sum_{j=1}^{n}\sum_{k=1}^{K}(\mathrm{g1}_{kj}\mathrm{g1}_{kj}^T + \mathrm{g2}_{kj}\mathrm{g2}_{kj}^T), \tag{21}$$

and we have used the fact that, $\mathbf{G}$ being hermitian by construction, its imaginary part is anti-symmetric and hence contributes nothing to the above quadratic form. The last step is to recognize that the particular parameterization of $\mathbf{v}$ is equivalent to the condition $\mathbf{v}^T\mathbf{v} = 1$. Maximizing a quadratic form under the unit norm constraint of its argument is obtained by taking $\mathbf{v}$ to be the eigenvector of $\Re e(\mathbf{G}^H\mathbf{G})$ associated to the largest eigenvalue.

A REFERENCES

[1] A. Belouchrani and M. G. Amin, "A new approach for blind source separation using time frequency distributions," *SPIE, Signal and Image processing, Denver, Colorada*, Aug. 1996.

[2] A. Belouchrani and M. G. Amin, "Blind Source Separation using Time-Frequency Distributions: Algorithm and Asymptotic Performance," in *Proc. ICASSP, Germany*, Apr. 1997.

[3] A. Belouchrani and M. G. Amin, "On the Use of Spatial Time Frequency Distributions For Signal Extraction," *Multidimensional Systems and Signal Processing. Special issue on New Developments in Time-Frequency Analysis*, 1997. July.

[4] A. Papandreou, F. Hlawatsch and G. F. Boudreaux-Bartels, "The Hyperbolic Class of Quadratic Time-Frequency Representations Part I: Constant-Q Warping, the Hyperbolic Paradigm, Properties, and Members," *IEEE Trans. on SP*, vol. 41, pp. 3425–3444, Dec. 1993.

[5] B. Ristic and B. Boashash, "Kernel design for time-frequency signal analysis using the Radon transform," *IEEE Trans. on SP*, vol. 41, pp. 1996–2008, May 1993.

[6] F. Hlawatsch and W. Krattenthaler, "Blinear Signal Synthesis," *IEEE Trans. on SP*, vol. 40, pp. 352–363, Feb. 1992.

δ_{ij} denotes the Kronecker operator.

[7] M. Viberg and B. Ottersten, "Sensor Array Processing Based on Subspace Fitting," *IEEE Trans. on SP*, vol. 39, pp. 1187–1199, May 1991.

[8] R. Roy and A. Paulraj and T. Kailath, "ESPRIT a subspace rotation approach to estimation of parameters of cisoids in noise," *IEEE Trans. on ASSP*, vol. 34, pp. 1340–1342, Oct. 1986.

[9] A. Belouchrani and M. G. Amin, " Blind Source Separation Based on Time-Frequency Signal Representation.," *IEEE Trans. on SP*, 1996. Submitted.

[10] R. Schmidt, "Multiple emitter location and signal parameter estimation," *IEEE Trans. on AP*, vol. 34, no. 1, pp. 276–280, 1986.

[11] W.M. Radich and K.M. Buckley , "Robust high-resolution eigenspace DOA estimation," in *Proc. 26th Asilomar Conference on Signals, Systems and Computers*, pp. 204–208, 1992.

[12] L. Cohen, *Time-frequency analysis.* Prentice Hall, 1995.

[13] A. Belouchrani and K. Abed Meraim and J.-F Cardoso and E. Moulines, "A blind source separation technique using second order statistics," *IEEE Trans. on SP*, vol. 45, pp. 434–444, Feb. 1997.

[14] J. Jeong and W. Williams, "Kernel design for reduced interference distributions," *IEEE Trans. on SP*, vol. 40, pp. 402–412, Feb. 1992.

[15] R. Baraniuk and D. Jones, "A signal dependent time-frequency representation: Optimum kernel design," *IEEE Trans. on SP*, vol. 41, pp. 1589–1603, Apr. 1993.

[16] Amin, G. Venkatesan, and J. Carroll, "A Constrained Weighted Least Square Approach for Time-Frequency Kernel Design," *IEEE Trans. on SP*, vol. 44, pp. 1111–1123, May 1996.

[17] S. Hearon and M. Amin, "Minimum variance time-frequency distribution kernels," *IEEE Trans. on SP*, vol. 43, pp. 1258–1262, 1995.

[18] M. Amin, "Minimum variance time-frequency distribution kernels for signals in noise," *IEEE Trans. on SP*, vol. 44, pp. 2352–2356, 1996.

[19] J. Bertrand and P. Bertrand, " A class of affine Wigner functions with extended covariance properties," *J. Math. Phys.*, vol. 33, pp. 2515–2527, July 1992.

[20] H. Choi and W. Williams, "Improved time-frequency representation of multicomponnet signals using exponential kernels," *IEEE Trans. on ASSP*, vol. 37, pp. 862–871, 1989.

TRIGONOMETRIC DECOMPOSITION OF TIME-FREQUENCY DISTRIBUTION KERNELS

Moeness G. Amin*

Department of Electrical and Computer Engn
Villanova University
Villanova, PA 19085
moeness@ece.vill.edu

Gopal T. Venkatesan

Department of Electrical and Computer Engn
University of Minnesota
Minneapolis, MN 55455
gopal@ece.umn.edu

ABSTRACT

Trigonometric decomposition of the time-frequency distribution (TFD) kernels refers to representing each row of the kernel in the time time-lag domain by a finite number of cosinusoidal terms. This allows the local autocorrelation function to be recursively updated, yielding a computationally efficient TFD. Unlike the spectrogram decomposition, where the t-f desirable properties are compromised, the proposed trigonometric decomposition preserves both the support and marginal properties and permits data-dependent kernel design.

1. INTRODUCTION

Time-frequency distributions (TFDs) are a powerful tool for nonstationary signal analysis in a wide variety of applications [1]. However, the computational burden limits the applicability of the TFD in practice. Hence, design of fast implementation methods are important to utilize TFDs for applications that require on-line processing such as nonstationary jammer excision in spread spectrum communications [2].

The discrete-time Cohen's class of TFDs is expressed as

$$\rho(n,k)=\sum_{\ell=-L}^{L}\sum_{m}\phi(n-m,\ell)x(m+\ell)x^{*}(m-\ell)e^{-j4\pi\ell k/K} \qquad (1)$$

where K = 2L + 1. That is, the TFD can be computed using the following procedure. First, the bilinear products $x(m+\ell)x^{*}(m-\ell)$ are found. This two-dimensional function (function of time and time-lag) is called the instantaneous autocorrelation function (IAF). Next, the IAF is smoothed along each time-lag ℓ using the kernel $\phi(m,\ell)$ to produce the local autocorrelation function (LAF). Finally, the LAF is Fourier transformed along the time-lag variable to yield the required TFD. The Hermitian property of the LAF leading to the realness of the corresponding TFD, is obvious on inspection of (1).

Early attempts at devising fast implementation of TFDs used the Hermitian property of the LAF to provide efficient frequency transformations. The method adopted by Martin and Flandrin[3] simply computes the t-f distribution as the real part of the complex one-sided FT of the LAF.

*This work is supported by ONR grant # N00014-98-1-0176.

Boashash and Black [4], on the other hand, have increased the throughput by combining two LAFs in one DFT, and doubling the number of output frequency samples. All the above methods are exact, as they introduce no error in the final result. But they serve to reduce computations only after the LAF has been provided with cumbersome computations. Hence, they are potent only in forming the Pseudo Wigner distribution, i.e., when the IAF is identical to the LAF.

Spectrogram decomposition techniques [5,6], which directly operate on the data, bypass the computation of the LAF. They compute the TFD as a linear combination of the spectrograms (STFT) of the data with different window functions. These window functions are the dominant components arising out of a spectral decomposition of the kernel. These techniques provide approximations of the required TFD and may significantly compromise the kernel's desirable time-frequency (t-f) characteristics (e.g. supports and marginals) unless a large number of decomposition terms are used.

Recognizing the fact that the computations required to compute the DFT is only O(L logL) multiplications whereas the computation of the LAF is O (L^2] multiplications, it becomes logical to target the calculation of the LAF, for significant computational savings. A new class of recursive time-frequency(t-f) kernels that can be used to recursively calculate the LAF in O(L) multiplications has been proposed in [7]. This approach employs modified comb filters to average the bilinear products at different time-lags.

In this paper, we generalize the recursive implementation structure presented in [7] by decomposing the kernel along each time-lag into a finite number of cosinusoidal functions, each generates one recursive equation to update the LAF. This technique is named the *trigonometric decomposition of time-frequency kernels*, and can be viewed as a frequency sampling design technique to generate computationally efficient kernels. It is noteworthy that this proposed class of kernels (also referred to as the frequency sampling (FS) kernels), while providing considerable reduction in the computation of the LAF, retain the Hermitian property of the LAF. Hence, the techniques outlined in [3-5], can be used in conjunction with the recursive computation of the LAF to provide additional computational savings.

2.THE FREQUENCY SAMPLING APPROACH

We first briefly review the frequency sampling approach for filter design and then extend it to the TFD case. The FIR frequency sampling design method uses the DFT to produce a finite impulse response filter. This design method matches the desired frequency response at the equally spaced sampling instants and approximates the desired response between the sampling instants. Let

$$H(k) = M_k e^{j\upsilon_k} \qquad k = 1, 2, .., N-1 \tag{2}$$

be the samples of the desired frequency response at the sampling instances $k\Omega_0$, where M_k and υ_k are the k-th sample amplitude and phase responses, respectively [8]. The IDFT of $H(k)$ gives the corresponding impulse response, $h(n) = \frac{1}{N}\sum_{k=0}^{N-1} H(k) e^{jnk\Omega_0}$ (3)

Setting $\alpha_k = e^{jk\Omega_0}$, the z-domain transfer function of the filter can be expressed as,

$$H(z) = \sum_{n=0}^{N-1}[\frac{1}{N}\sum_{k=0}^{N-1} H(k)\alpha_k^n]z^{-n} = \frac{1-z^{-N}}{N}\sum_{k=0}^{N-1}\frac{H(k)}{1-\alpha_k z^{-1}} \tag{4}$$

It is clear that $H(z)$ has a recursive form even though the impulse response is finite. The number of terms is equation (4) is equal to the number of non-zero frequency samples. This number is equal to the number of frequency samples in the passband, providing that the stopband is comprised of zero values. Therefore, filters with extended stopband characteristics lead to simplified recursions. It is this specific property that makes the frequency sampling method computationally attractive for TFDs.

In the t-f context, the frequency sampling filter is used to process the data bilinear products $x(n+l)x^*(n-l)$ and is considered for each time-lag. Accordingly, the frequency samples are ambiguity-domain variables and can be set equal to the desired values. The kernel that employs these filters at different lags is referred to as the frequency sampling kernel. In the case that all desired filters have zero-phase, the kernel becomes real and symmetric, and is given in the $t-\tau$ domain by

$$\phi_{trig}(n,l) = \frac{1}{N_l}[M_{0l} + \sum_{k=1}^{P_l} M_{kl}\cos(\frac{2\pi kn}{N_l})],$$
$$p_l = (N_l - 1)/2 \tag{5}$$

By taking the z-transform over the time variable, then

$$\Psi_{trig}(z,l) = \frac{z^{\frac{N_l-1}{2}} - z^{-\frac{N_l-1}{2}}}{N_l}[\frac{M_{0l}}{1-z^{-1}} +$$
$$\sum_{k=1}^{P_l}\frac{(-1)^k 2M_{kl}\cos(\frac{k\pi}{N_l})(1-z^{-1})}{1-2\cos(2k\pi/N_l)z^{-1}+z^{-2}}], \tag{6}$$

where the subscript l is added to all variables to indicate possible dependence of the parameters on the lag number.

The recursion equation to update the LAF $r(n,l)$ using the t-f kernel in (6) is given by

$$r(n,l) = \tilde{r}(n+(N-1)/2, l) - \tilde{r}(n-(N-1)/2, l), \tag{7-a}$$

where $\tilde{r}(n,l) = \sum_{k=0}^{N-1} r_k(n,l),$

$$r_k(n,l) = c_{kl} r_k(n-1,l) - r_k(n-2,l) + d_{kl}[x(n+l)$$
$$.x^*(n-l) - x(n-1+l)x^*(n-1-l)], \tag{7-b}$$

$$r_0(n,l) = r_0(n-1,l) + d_{0l}x(n+l)x^*(n-l), \tag{7-c}$$

and

$$c_{kl} = 2\cos(2k\pi/N_l),\ d_{kl} = 2(-1)^k M_{kl}\cos(k\pi/N_l)/N_l,$$
$$d_{0l} = M_{0l}/N_l$$

Time-frequency kernels using expression (5) are referred to as <u>trigonometric kernels</u>. A large stopband, i.e., $M_{kl} = 0$ for high values of k, make them computationally attractive.

To satisfy the frequency marginal, we should have the zeroth frequency sample $\psi(0,l)$=1. Since $M_{0l} = 1$, the first term in the summation (5-b) requires one recursion multiplication. For the time-support property to be satisfied, the number of equally spaced frequency samples N_l at the time-lag ℓ should be $N_l \le 2l+1$. For a cone-shaped kernel, $N_l = 2l+1$. This condition implies that the ambiguity-domain frequency samples must be more widely spaced for smaller lags. As such, for the passband region to include the same number of frequency samples, it must be narrower for higher time-lags. This allows recursion (7) to be completed at the same time for all lags of interest. We maintain that this specific ambiguity domain passband characteristics of the time-frequency kernels are inherent in all low-pass fixed devised kernels including the Choi-Williams, the binomial, and the Cone-shape kernels [1], and is satisfied by all product kernels designed for reduced interference distributions. Fig (1-a) shows the two-term trigonometric kernel corresponding to using two frequency samples in the passband. Notice the pronounced ripples in the passband and stopband. This situation can be improved if, instead of having the response samples go directly from unity in the passband to zero in the stopband, we allow a transition band. Figure (1-b) shows the two-term trigonometric kernel obtained when the second passband sample is halved. Clearly, this kernel is smoother than that shown in Fig. (1-a).

The recursion property of the t-f kernels designed by the frequency sampling method lays the ground for a computationally attractive kernel decomposition technique. By applying the Fourier series expansion to any given t-f kernel and retaining the first K dominant terms, we are, in essence, performing a frequency sampling kernel design in which the ideal kernel is defined by the K frequency samples

corresponding to those terms. In turn, existing symmetric t-f kernels can be made amenable to recursive implementations through trigonometric decomposition in the form (3). Therefore, the frequency sampling kernel design method and the trigonometric kernel decomposition are, respectively, the design and the analysis sides of the same problem, and each can be used to formulate recursive kernels. It is noteworthy that the one-term trigonometric decomposition of all kernels satisfying the marginals and the time-support properties is the well known Born-Jordan kernel [1].

3. SIMULATIONS

To illustrate the significance of the trigonometric decomposition of t-f kernels, we show in Fig. (2-a) the commonly used Choi-Williams distribution kernel truncated to satisfy the time-support property. The two term trigonometric approximation of this kernel is shown in Fig. (2-b). It is evident that the original and the approximated kernels are very much alike, but the trigonometric kernel is superior in computations.

It is well known that for a chirp signal the autoterm is not located near the axes in the ambiguity domain. Hence, traditional fixed kernels will attenuate the chirp autoterm due to their inherent lowpass characteristics. Here we consider the specific case when a signal consists of a chirp and a sinusoid. This compounds the problem further as it introduces crossterms that lie in between the two autoterm components of the signal in the ambiguity domain. A data-dependent kernel designed to "match" the signal characteristics will have values close to unity at the autoterm locations and values close to zero in the crossterm regions. Such a data-dependent kernel can be simply constructed by placing corresponding unit/zero values at the autoterm/crossterm locations. This kernel is, in general, of infinite extent in the time-time lag domain. From the infinite time extent kernel, a finite time-extent recursively implementable kernel can be constructed using the FS method. A plot of this designed kernel is shown in Figure (3-a). Note that this is the minimum-variance solution for the required desired signal characteristics, and is hence, statistically optimal for white noise[9].The TFD obtained by the designed FS kernel is shown in Figure (3-b). The good performance of the FS kernel in depicting the t-f signatures of the two signals is evident.

REFERENCES

[1] L. Cohen, Time-Frequency Analysis, Prentice-Hall, Englewood Cliffs, New Jersey, 1995.

[2] M. Amin," Interference Mitigation in spread spectrum communications using TFDs," IEEE Trans. on SP, vol. 45, January 1997.

[3] W. Martin and P. Flandrin, "Wigner-Ville spectral analysis of non-stationary processes , IEEE Trans. on ASSP, vol. 33, December 1985.

[4] B. Boashash and P. Black, "An efficient real-time implementation of the Wigner distribution," IEEE Trans. on ASSP, vol. 35, Nov. 1987.

[5] M. Amin, "Spectral decomposition of time-frequency distribution kernels," IEEE Trans. on SP, vol. 42, May 1994.

[6] G. Cunningham and W. J. Williams, "Fast implementation of discrete time frequency distributions," IEEE Trans. on SP, June 1994.

[7] M. Amin, "Recursive kernels for time-frequency signal representations," IEEE SP Letters, Jan 1996.

[8] E. Cunningham, Digital Filtering: An Introduction, Houghton-Mifflin Comp., 1992.

[9] S. Hearon and M. Amin ,"Minimum-variance time-frequency distribution kernels," IEEE Trans. on SP, vol. 43, May 1995.

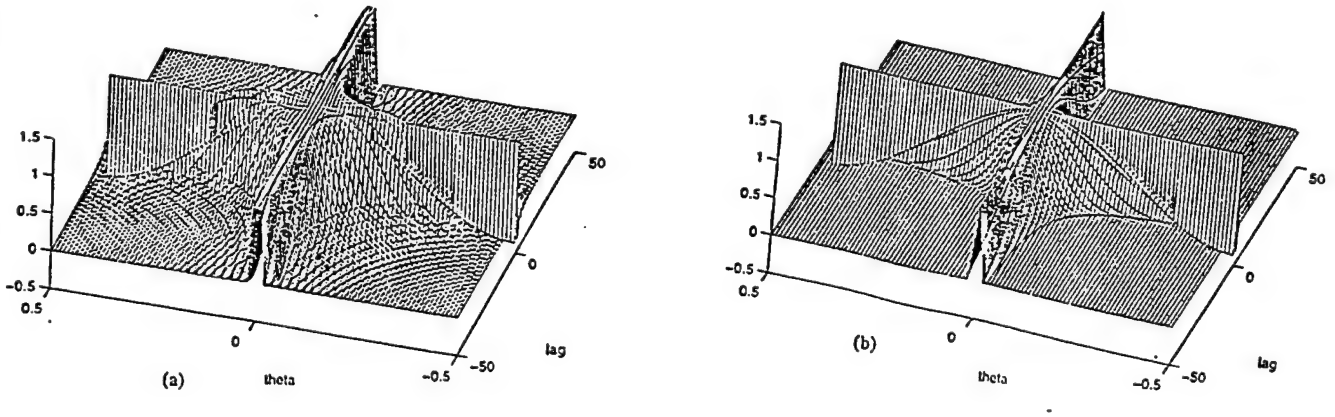

Fig. 1 Frequency sampling kernel (a) without transition band (b) with transition band

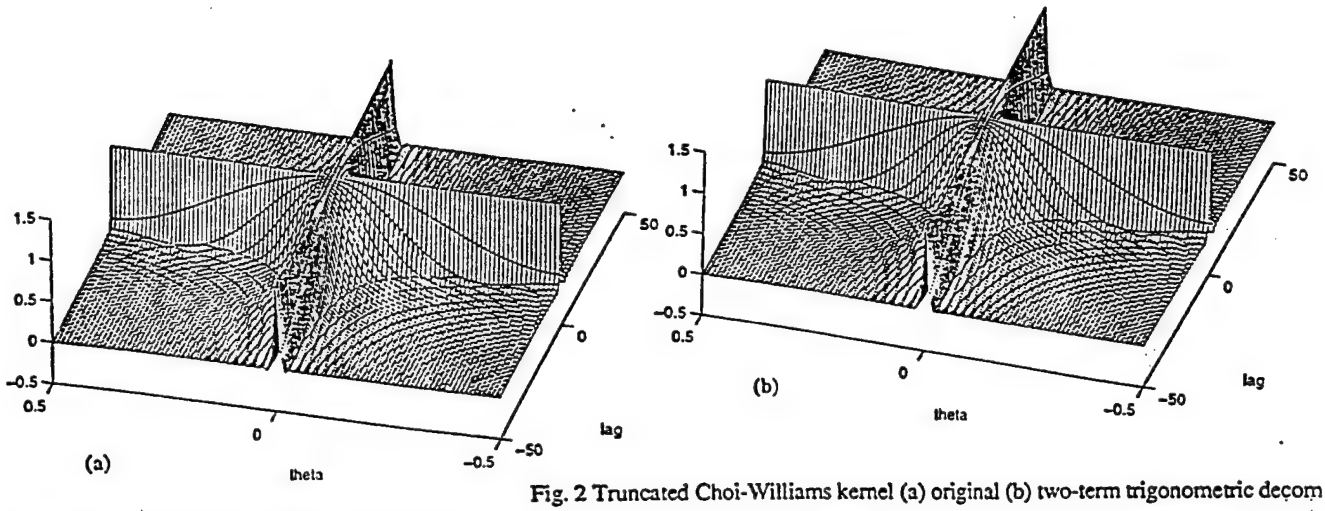

Fig. 2 Truncated Choi-Williams kernel (a) original (b) two-term trigonometric decom

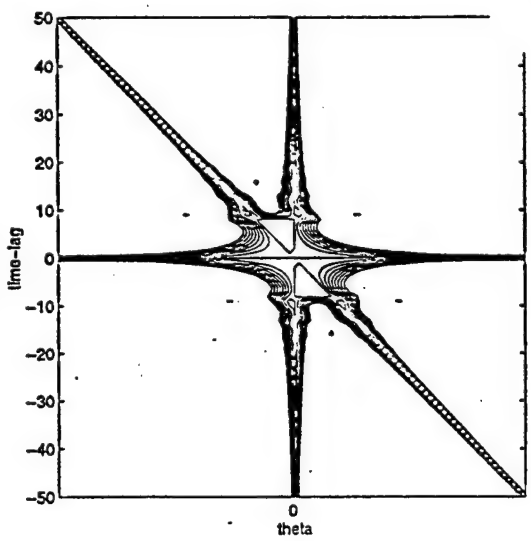

Fig. 3 (a) The FS kernel for chirp+sinusoidal case

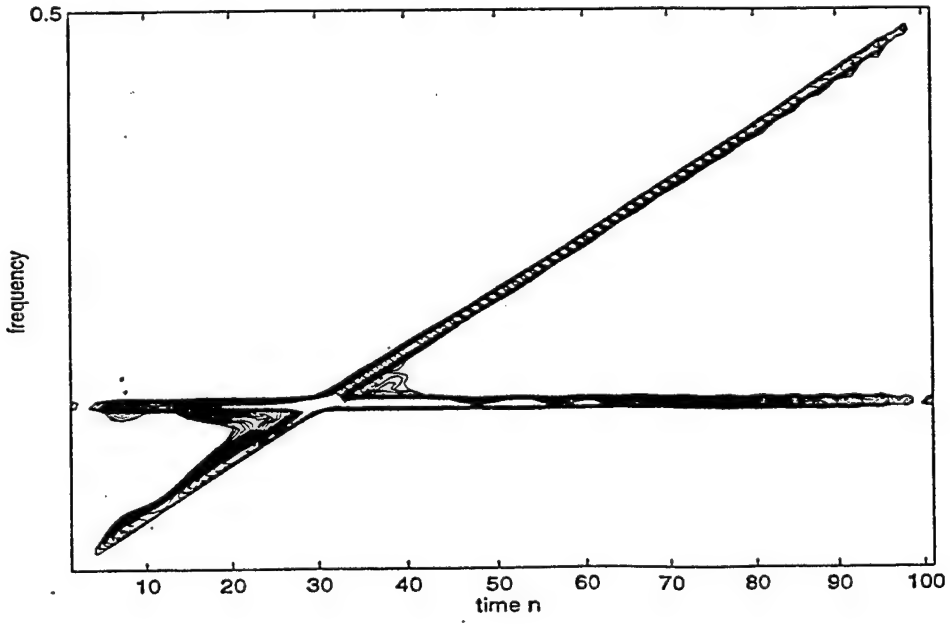

Fig. 3 (b) TFD obtained using FS kernel

BLIND SOURCE SEPARATION USING THE SPATIAL AMBIGUITY FUNCTIONS

Moeness G. Amin*
Department of Electrical and Computer Engn
Villanova University
Villanova, PA 19085
moeness@ece.vill.edu

Adel Belouchrani
Department of Electrical Engineering
Ecole National Polytechinque
Algiers, Algeria
belouchrani@ist.cerist.dz

ABSTRACT

Blind source separation consists of recovering a set of signals of which only instantaneous linear mixtures are observed. This problem has been typically solved using statistical information available on source signals. Recently, we have introduced spatial time-frequency (t-f) distributions as a new and effective alternative to separate sources whose signatures are different in the t-f domain. This paper presents a new blind source separation method, exploiting the difference in the ambiguity-domain signatures of the sources. The approach is based on the digonalization of a combined set of spatial ambiguity functions. In contrast to existing techniques, the proposed approach allows the separation of Gaussian sources with identical spectral shape but with different ambiguity domain localization properties.

1. INTRODUCTION

The evaluation of quadratic time frequency distributions of the data snap shots across the array yields, which was defined in [1] as spatial time-frequency distributions, permits the application of eigenstructure subspace techniques to solving a large class of channel estimation and equalization, blind source separation, and high resolution direction of arrival estimation problems. The spatial time-frequency distribution techniques are most appropriate to handle sources of nonstationary waveforms that are highly localized in the time-frequency domain, or any other domain of a different joint variable signal representations.

In the area of blind source separation, the spatial time-frequency distributions allow the separation of Gaussian sources with identical spectral shape, but with different time frequency localization properties, i.e., different signatures in the time-frequency domain. On the other hand, for direction of arrival estimation problems, the effects of spreading the noise power while localizing the source energy in the time-frequency domain amounts to increasing the robustness of the eigenstructure superresolution methods, which are based on both signal and noise subspace estimations, with respect to noise, and hence improve resolution performance.

*This work is supported by ONR grant # N00014-98-1-0176.

In this paper, we present a new approach for blind separation of sources with different t-f signatures. Unlike the spatial time-frequency distributions, where the separation is performed using various time-frequency bins, the proposed approach is based on information from the ambiguity domain. The procedure is similar to that adopted in spatial TFD-based blind source separation. The main difference, however, lies in the domain in which the mixing matrix is estimated. In the proposed technique, the mixing matrix is abstained by join diagonalization of the spatial ambiguity (SAF)matrices rather than the spatial time-frequency distributions matrices. These SAF matrices are formed from the auto- and cross- ambiguity functions of the data received by the different array sensors. It is shown that the sensor spatial ambiguity function matrix is related to the source ambiguity function matrix in the same fashion as in the well known relationship between the sensor and source covariance matrices[2,3].

Performing blind source separation in the ambiguity-domain rather the time-frequency domain provides a greater ability to formulate the problem using the source autoterms rather than crosssterms. Avoiding cross-term points in any joint variable representation leads to improved source separation, as it will have a positive effect on the performance of the joint-diagonalization algorithm, as discussed in [1,4].

2. TECHNICAL APPROACH

TFDs are a powerful tool in nonstationary signal analysis[5,6]. So far, most of the work on this subject has focused on temporal signal processing without much attention given to the spatial variable. In the following, we introduce a new approach for blind signal separation in a multisensor array using the ambiguity function. In order to present the spatial ambiguity function, we first recall that the generalized auto- and cross-ambiguity functions of two signals $x_1(t)$ and $x_2(t)$ are given by

$$D_{x_i x_i}(\theta,\tau) = \phi_i(\theta,\tau)\int_{-\infty}^{\infty} x_i(u+\tau/2)x_i^*(u-\tau/2)e^{j\theta u}du$$

$$D_{x_i x_j}(\theta,\tau) = \phi_{ij}(\theta,\tau)\int_{-\infty}^{\infty} x_i(u+\tau/2)x_j^*(u-\tau/2)e^{j\theta u}du \qquad (1)$$

for i,j=1,2. τ and θ represent the time-lag index and the frequency-lag index, respectively. The ambiguity-domain kernel $\phi(\theta,\tau)$ is a function of the above two variables. Expressions (1) are now used to define the following data spatial ambiguity function (SAF) for n sources and m sensors

$$D_{xx}(\theta,\tau)=\phi(\theta,\tau)\int_{-\infty}^{\infty} x(u+\tau/2)x^{*}(u-\tau/2)e^{j\theta\tau}du \quad (2)$$

where

$$[D_{xx}(\theta,\tau)]_{ij}=D_{x_i x_j}(\theta,\tau),\ \ for\ \ i,j=1,2,\ldots,m.$$

In several applications such as semiconductor manufacturing process, factor analysis, narrowband array processing, and image reconstruction, the following linear data model is assumed,

$$x(t)=As(t)+n(t) \quad (3)$$

where the m x n matrix A is referred to as the spatial matrix, which may be a mixing matrix or a steering matrix, depending on the application under consideration. The elements of the m x 1 vector x(t), which represent the measured data, are weighted sums of the source signals, and as such, are multicomponent signals. On the other hand, the elements of the n x 1 vector s(t) are source signals and, therefore, are likely to be the monocomponent signals. n(t) is an additive noise, often assumed zero mean, white and Gaussian distributed process. Due to the linear data model, the SAF takes the following structure

$$\mathbf{D}_{xx}(\theta,\tau)=\mathbf{A}\mathbf{D}_{ss}(\theta,\tau)\mathbf{A}^{H} \quad (4)$$

where the noise is neglected as a first step. The superscript "H" denotes the complex conjugate transpose of a matrix and $D_{ss}(\theta,\tau)$ is the SAF matrix of s(t). We note that $D_{xx}(\theta,\tau)$ is a matrix of dimension m-x-m, whereas $D_{ss}(\theta,\tau)$ is of n-x-n dimension. For narrowband array signal processing applications, A holds the spatial information, and through a similarity transformation, it maps the auto- and cross-AFs of the monocomponent signals into auto- and cross-AFs of the data.

Expression (4) is similar to that which has been commonly used in blind source separation and direction of arrival (DOA) estimation problems, relating the signal correlation matrix to the data spatial correlation matrix. Here, these correlation matrices are replaced by spatial ambiguity function matrices. This means that we can solve these problems in various applications using the new formulation which is more tuned to nonstationary signal environment.

The two subspaces spanned by the principle eigenvectors of $D_{xx}(\theta,\tau)$ and the columns of A are, therefore, identical. Since the off- diagonal elements are cross-terms of $D_{ss}(\theta,\tau)$, then this matrix is diagonal for all (θ,τ)points which correspond only to the signal autoterms. In practice, to simplify the selection of such points of high power localization, the kernel $\phi(\theta,\tau)$ that significantly decreases the contribution of the cross-terms should be applied and the ambiguity-domain points near the vicinity of the origin should be selected.

3. JOINT DIAGONALIZATION USING SAFs

The joint diagonalization for blind source separation using spatial ambiguity functions consists mainly of the following two steps:

A. Whitening

Let W denotes mxn matrix such that $(\mathrm{WA})(\mathrm{WA})^{H}=\mathrm{UU}^{H}=\mathrm{I}$, i.e., WA is a mxm unitary matrix (This matrix is referred to as a whitening matrix, since it whitens the signal part of the observations). Pre- and post-multiplying the spatial ambiguity function matrix $D_{xx}(\theta,\tau)$ by W yields the whitened SAF matrix

$$\overline{D}_{xx}(\theta,\tau)=WD_{xx}(\theta,\tau)W^{H} \quad (5)$$

From the definition of and equation (5), we may express $\overline{D}_{xx}(\theta,\tau)$ as

$$\overline{D}_{xx}(\theta,\tau)=UD_{ss}(\theta,\tau)U^{H} \quad (6)$$

Since matrix U is unitary and $D_{ss}(\theta,\tau)$ is diagonal, expression (6) shows that any whitened data SAF matrix is diagonal in the basis of the columns of the matrix U (the eigenvalues of $\overline{D}_{xx}(\theta,\tau)$ being the diagonal entries of $D_{ss}(\theta,\tau)$). If, for the (θ_i,τ_i) point, the diagonal elements of $D_{ss}(\theta_i,\tau_i)$ are all distinct, the missing unitary matrix U may be 'uniquely' (i.e. up to permutation and phase shifts) retrieved by computing the eigendecomposition of $\overline{D}_{xx}(\theta,\tau)$. However, when the $\theta-\tau$ signatures of the different signals are not highly overlapping or frequently intersecting, which is likely to be the case, the selected (θ_i,τ_i) point often corresponds to a single signal auto-term, rendering matrix $D_{ss}(\theta_i,\tau_i)$ deficient. That is, only one diagonal element of $D_{ss}(\theta_i,\tau_i)$ is different from zero. It follows that the determination of the matrix U from the eigendecomposition of a single whitened data SAF matrix is no longer 'unique' in the sense defined above. The situation is more favorable when considering simultaneous diagonalization of a combined set $\{\overline{D}_{xx}(\theta_i,\tau_i)\mid i=1,\ldots,p\}$ of p SAF matrices. This amounts to incorporating several $\theta-\tau$ points in the source separation problem. It is noteworthy that two source signals with identical $\theta-\tau$ signatures can not be separated even with the inclusion of all information in the $\theta-\tau$ plane.

B. Joint diagonalization :

The joint diagonalization(JD) [7] can be explained by first noting that the problem of the diagonalization of a single n x n normal matrix M is equivalent to the minimization of the criterion [8]

$$C(M,V)\overset{def}{=}-\sum_{i}\ \mid v_i^{*}Mv_i\mid^{2} \quad (7)$$

over the set of unitary matrices $V=[v_1,...,v_n]$. Hence, the joint diagonalization of a set $\{M_k \mid k=1..k\}$ of K arbitrary n x n matrices is defined as the minimization of the following JD criterion:

$$C(V) \stackrel{def}{=} -\sum_k C(M_k,V) = -\sum_{ki} | v_i^* M_k v_i |^2 \qquad (8)$$

under the same unitary constraint. An efficient joint approximate diagonalization algorithm exists in [7] and it is a generalization of the Jacobi technique [8] for the exact diagonalization of a single normal matrix.

Equations (5-8) constitute the blind source separation approach based on SAF which is summarized by the following steps:

- Determine the whitening matrix $\hat{W}$ from the eigendecomposition of an estimate of the covariance matrix of the data (see [7] for more details)
- Determine the unitary matrix $\hat{U}$ by minimizing the joint approximate diagonalization criterion for a specific set of whitened SAF matrices $\{\underline{D}_{xx}(\theta_i,\tau_i) \mid i=1,...,p\}$,
- Obtain an estimate of the mixture matrix $\hat{A}$ as $\hat{A} = \hat{W}^{\#} \hat{U}$, where the superscript # denotes the Pseudo-inverse, and an estimate of the source signals $\hat{s}(t)$ as $\hat{s}(t) = \hat{U}^H Wx(t)$.

4. SIMULATIONS

In Figure 1, we show an example of the application of spatial ambiguity functions to the blind source separation problem. In this example, we have two sources and three sensors. One source has four sinusoids, whereas the other has four impulses. The TFDs of the two waveforms are shown in Fig. 1-a. The TFDs and AFs at the first two sensors are shown in Fig. 1-b. Using the spatial ambiguity functions, we are able to recover the original signals from only their observed mixture, as shown in Fig.1-c. It is clear that the recovered signals are very much alike the transmitted ones, which shows that the proposed technique undoes the mixing caused by the propagation channel.

CONCLUSIONS

A new blind source separation technique has been introduced. This technique is based on the ambiguity functions of the data received by the different sensors of the antenna array. The proposed technique is geared towards the applications in which the sources have nonstationary waveforms that are localizable in the ambiguity domain. The key advantage of performing source separation using spatial ambiguity functions rather than spatial time-frequency distributions, as previously suggested, is that in the former, the knowledge of the signal autoterms being positioned near the origin simplifies the selection of the appropriate signature points to be used in the joint diagonalization procedure leading to signal estimation.

REFERENCES

[1] A. Belouchrani and M. Amin, "Blind Source Separation using t-f distributions: algorithm and asymptotic performance," Proc. ICASSP, Germany, April 1997.

[2] R. Schmidt, "Multiple emitter location and signal parameter estimation," IEEE Trans. on AP, vol. 34, no. 1, pp. 276-280, 1986.

[3] R. Roy and T. Kailath, "ESPRIT-Estimation of signal parameters via rotational invariance techniques," IEEE Trans. on Acoustics, Speech, and Signal Processing, vol.37, no.7, pp. 984-995, July 1989.

[4] A. Belouchrani and M. Amin, " Blind source separation using joint signal representations," Proceedings of the SPIE Conference on Advanced algorithms and Architectures for Signal Processing, San Diego, CA , August 1997.

[5] L. Cohen, Time-frequency analysis. Prentice Hall, 1995.

[6] S. Qian and D. Chen , Joint Time-Frequency Analysis -methods and applications, Prentice Hall, 1996.

[7] A. Belouchrani and K. Abed Meraim and J.-F Cardoso and E. Moulines, "A blind source separation technique using second order statistics," IEEE Trans. on SP, Feb. 1997.

[8] G. H. Golub and C.F. Van Loan, Matrix Computations, The Johns Hopkins University Press, 1989.

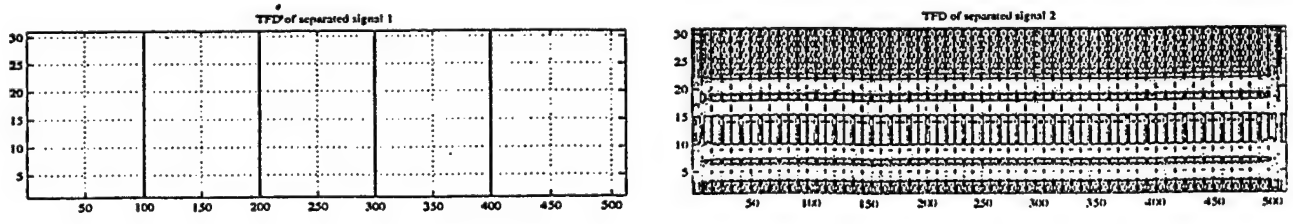

TFDs of the separated signals

Fig. 1-a

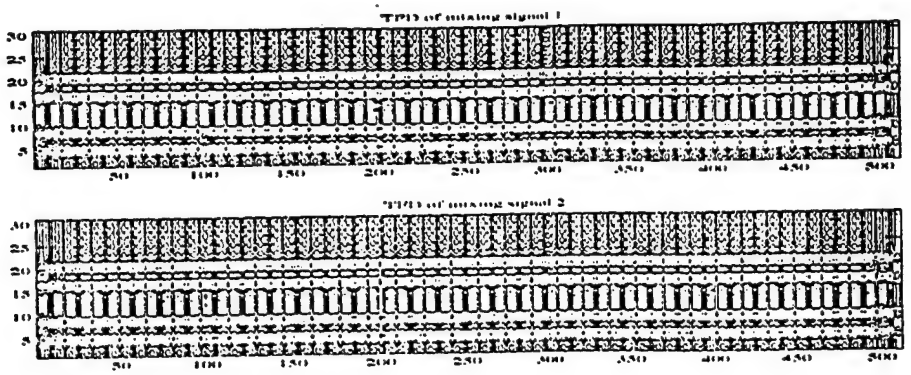

TFDs of the mixed signals

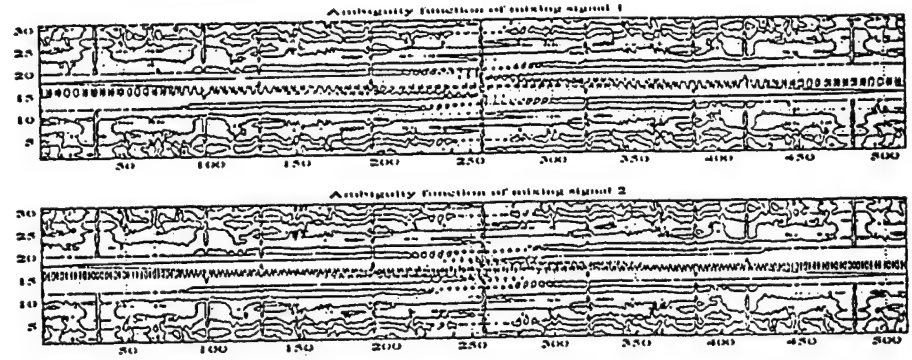

Ambiguity functions of the mixed signals

Fig. 1-b

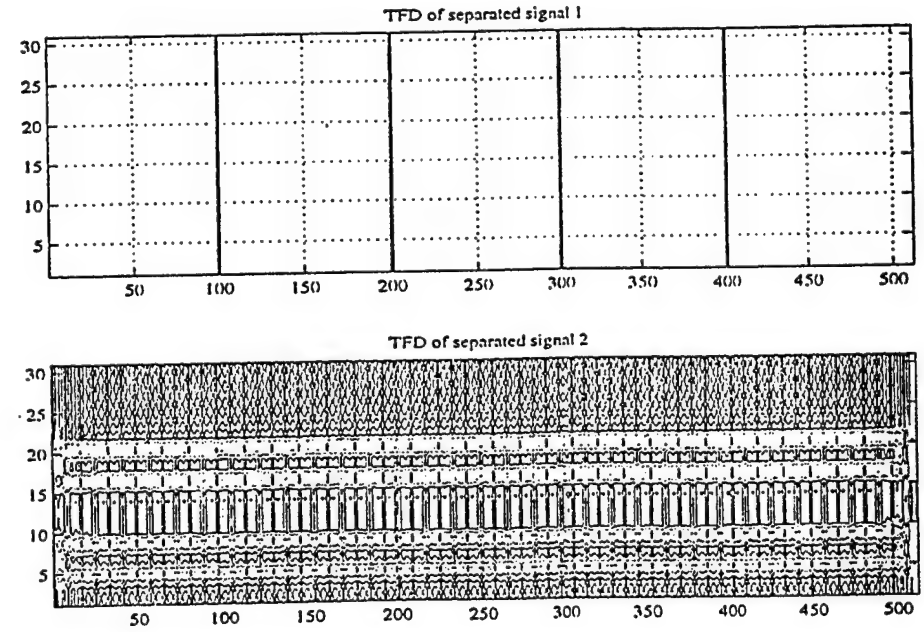

TFDs of the separated signals

Fig. 1-c

SPATIAL PROCESSING FOR FREQUENCY DIVERSITY SCHEMES[1]

Miguel A. Lagunas[2], Ana I. Perez, Moeness G. Amin* and J. Vidal

TSC Department, Modulo D5
Campus Nord UPC, c/Gran Capita s/n
08034 BARCELONA, SPAIN
Phone 34-3-4016446 Fax 34-3-4016447 e-mail miguel@gps.tsc.upc.es

***Department of Electrical and Computer Engineering**
Villanova University
Villanova, PA 19085, USA

EDICS: SP 3.6.2

ABSTRACT

A novel technique to obtain optimum blind spatial processing for frequency diversity spread spectrum (FDSS) communication systems is introduced. The sufficient statistics for a linear combiner, which prove ineffective due to the interferer's frequency characteristics, are modified to yield improved detection under partial jamming in the spectral domain. Robustness to partial time jamming is achieved by extending the notion of replicas over the frequency axis to a repetition over the time variable. Analysis and simulations are provided showing the advantages of using FDSS with spatial diversity to combat the interference when it is confined to a narrow frequency band or short time interval relative to the desired signal extent in either domain.

Under review by the IEEE Transactions on Signal Processing

[1] This work has been supported by CICYT of Spain and CIRIT of Catalunya.
[2] Corresponding author.
* Dr. Amin is supported in part by ONR under grant # N00014-98-1-0176

1. INTRODUCTION

Frequency diversity spread spectrum (FDSS) has been recently shown [1][2] to be a powerful tool for digital detection as well as an effective alternative to the traditional spread spectrum techniques, namely direct sequence (DSSS) and frequency hopping (FHSS)[3]. In a general context, diversity is conceived by the existence of several replicas (either in code, time, space, or frequency). When diversity is available to the receiver either by the structure of the transmitted signal or the architecture of the receiver, optimum spatial signal processing, which is blind to the temporal signal characteristics, can be derived.

In this paper we consider the spatial-frequency diversity problem in wireless communication systems. We derive optimum spatial processing for FDSS systems under partial band jamming. The principle condition for the optimality in these systems is to have at least one frequency band contaminated by the interference and another band that is jammer free. These two bands will here in be refered to as the 'hit' and 'free' bands, respectively.

In partial band jamming, the above condition is often satisfyed, as the desired signal is present in all the frequency bands in which the transmission bandwidth is slotted, whereas the jammer is only active in few bands due to its narrowband frequency characteristics. In this case, the optimum spatial combiners can be obtained in a two-step design procedure as follows. First, the spatial combiner of the free band is computed by minimizing the mean square error (MSE) between the spatial combiners' outputs of the free and the hit bands. In order to avoid trivial solutions, leading to null beamformer or simultaneous removal of the desired signal in all bands, the cross-correlation of the two band outputs is set equal to a nonzero value. Once the spatial combiner for the free band is provided, the corresponding output signal is used as a time reference to design the spatial combiners for the rest of the bands. It is shown that this spatial design procedure is blind to the desired signal waveform and does not require the proper labeling of the hit and the free bands to reach the optimum solution.

The sum of the likelihood of the different bands forms the sufficient statistics for optimal symbol by symbol detection. This requires the knowledge of the jammer level in every hit band [1]. On the other hand, the sufficient statistics in a suboptimum receiver is formed only the bands free of jammer energy. The performances of both receivers, however, become approximately the same under high jammer-to-noise ratio in the hit bands. The offering of spatial processing to improved detection is in its ability to remove the jammer contamination in the hit bands prior to incorporating them into the detection scheme. The quality of jammer suppression in the hit bands, however depends on the angular separation of the waveforms received by the different antennas. As the jammer and desired signal become closely spaced, removal of the jammer power through linear combining of signal arrivals render ineffective. In this case, suboptimal and optimum receivers converge to the same solution. It is noted that shadowing occurs when the angles of arrival of the jammer and the desired signal coincide. We present the proper mechanism to form a sufficient statistic robust to the shadowing effect.

Section 2 provides the general structure of the FDSS systems [5] as well as the mathematical description of the desired signal. Section 3 establishes the optimum receiver for the frequency diversity spread spectrum signal and presents the decision variable and probability of error under partial band jamming. In section 4, we introduce spatial processing for improved detection in FDSS systems and derive the optimum solution for the spatial weights in the hit and free bands. Section 5 describes the optimum receiver robust to the shadowing effect. Section 6 includes an adaptive algorithm as an alternative to the block processing described in section 4. Section 7 reports key features of the proposed design procedure for optimum spatial processing. It is shown that any information transmission system using coded waveforms, such as FDSS, permits blind optimum spatial processing, implying that the allocation of dedicated time or frequency slots for reference framing is unnecessary. Section 7 also includes the mechanism for exploiting the temporal structure of the desired signal to blind beamforming for partial time jamming. Finally, a set of simulations illustrating the advantages of using FDSS combined with spatial diversity are provided in section 8.

2. SPREAD SPECTRUM AND FREQUENCY DIVERSITY

Direct Sequence and Frequency Hopping are the most familiar techniques, among those that use spread spectrum, to combat bandlimited Gaussian interferers. In both cases, the transmitted signal is controlled by properly coding the carrier waveform. The role of coding is to enlarge the transmission bandwidth either by fast keying in the time domain or/and in the frequency domain. However, the performance of FHSS is sensitive to partial band jamming [2]. In DSSS systems, high levels of partial band jamming may force the receiver to employ a whitening filter, together with a sequence detector to remove Inter-Symbol Interference (ISI) caused by the whitening stage. In addition to the highly undesired ISI, the interference excision filters increase the receiver complexity and give rise to self-noise, which is the induced correlation across the PN sequence. To mitigate the aforementioned problems, the FDSS system was proposed in [1] which encompasses the principles of the two systems DS and FH. The FDSS can be viewed as a DS scheme where successive chip frames, within a symbol, are transmitted in parallel over different non overlapping frequency bands. On the other hand, the major difference between traditional FH communication systems and the system implementing FDSS is that in the later, the information symbol is repeated, coded or uncoded, in several frequency bands, instead of using a single band at time. A simple mixture of both systems is to transmit the block of chip symbols, of the first scheme, simultaneously in different frequency bands, with or without hopping. The flexibiliy of mixing the DS and FH schemes grows dramatically when a single information symbol produces the coded symbols through a channel encoder. Since all possible combinations are amenable to spatial diversity processing, the transmitted signal architecture depicted in Figure 1 will be used to introduce the proposed spatial FDSS scheme. This architecture, which was used by several authors (see [5] as an example) to encompass all SS techniques currently reported, allows the presentation of the different alternatives offered by channel encoding, waveform coding, and frequency diversity, to spread the spectrum of the transmitted signal.

The first stage of the scheme in Figure 1 contains the channel encoder. Within this block, the information symbol is converted into coded symbols. The coded symbols are packed in blocks of N_1

symbols and these blocks are arranged in N branches. Without loss of generality, it is assumed that all the bands have the same bandwidth. In this case the bandwidth is controlled by the number of branches N as well as by the number N_1 of coded symbols per branch. This presents the basic contribution of the channel encoder to the bandwidth structure of the transmitted signal. When the number of symbols per branch is equal to one, and the coded symbols are presented in the N channels at the information symbol rate, there will still be a coding gain at the receiver even when using a pure repetition code. This type of coding amounts to the lowest complexity case, i.e. N_1 is equal one and the information symbol is presented simultaneously to all branches (pure repetition code (N,1)).

The second stage is the waveform coding. Every branch is multiplied by different, or equal, chip signals γ_i (t) (i=1,N). The chip rate τ_c, as a fraction of the coded symbols rate T_s, determines the bandwidth for every branch. A special case is when the chip rate and the symbol rate coincide. In this case, there is a single chip symbol $\gamma_{m,i}$ per branch, and no spreading is produced. Furthermore, when the alphabet for the chip symbols is (0,1), the transmitted signal can be viewed as associated with a Frequency Hopping system. In fact, traditional (single band) FH, within this framework, requires a single chip is to be on per a symbol interval , i.e. a single branch is activated at a time.

The third stage, the last in this sequence, contains the pulse shaping. The shaping functions $\psi_i(t)$ have different frequency support. Multicarrier CDMA or OFDM can be encompassed in the proposed scheme, depending on the design of this last stage in the overall structure of signal generation. Assuming non-overlapping frequency support for the shaping functions produces a transmitted signal which is usually referred to as Frequency Diversity spread spectrum signal. The non-overlapping frequency bands often have the same bandwidth B_0. This bandwidth, which includes the roll-off factor, has to be the minimum bandwidth expected from the jammer. This choice guarantees that no narrowband intereferer is present for every frequency diversity band; otherwise, a whitening filtering, together with a Viterbi equalizer to remove the ISI, will be needed. The filter bank is implemented as a polyphase filter [6].

Finally, note that within a FDSS band, the system may have independent frequency hopping [4], allowing phase continuity and coherent optimal combining of the received replicas.

The formulation of the transmitted signal is shown in (1) for the general case when code, time, and frequency diversity are used simultaneously to spread the spectrum. In (1) $\Pi(.)$ denotes the rectangular pulse, N_c the number of chips per coded symbol interval, T_s the symbol duration, N_1 the number of coded symbols in every branch per information symbol, and τ_c the chip duration.

$$X_T(t)=\sum_{i}\sum_{m=1}^{N}\sum_{n=1}^{N_1}\sum_{l=1}^{N_c} a_{i,n,m}\ \Pi\left(\frac{t-iT_s-n(T_s/N_1)-l\tau_c}{T_s/(N_1*N_c)}\right)\gamma_{i,n,m,l}\ \psi_m(t-iT_s) \tag{1}$$

In the case of no spreading, $N_1=1$, and equation (1) simplifies to (2).

$$X_T(t)=\sum_{i}\sum_{m=1}^{N}\sum_{l=1}^{N_c} a_{i,m}\ \Pi\left(\frac{t-iT_s-l\tau_c}{T_s/N_c}\right)\gamma_{i,m,l}\ \psi_m(t-iT_s) \tag{2}$$

Finally, for a single chip per symbol interval and the repetition code, the transmitted signal is (3).

$$X_T(t)=\sum_{m}\sum_{i=1}^{N} a_i\ \gamma_{i,m}\ \psi_m(t-iT_s) \tag{3}$$

This signal, referred to as FDSS signal, will be used from now on without loss of generality.

3. OPTIMUM RECEIVER FOR FDSS

This section highlights the differences between optimum and suboptimum detection in terms of performance versus complexity. It includes results from [1] which are most pertinent to the underlying problem and which serve the derivation of the optimum receiver, including spatial diversity, in the following sections.

The decision variable Λ_i is a sufficient statistic to perform optimum symbol by symbol detection. This decision variable contains the following terms: the received samples, after matched filtering and

sampling at the symbol rate, $z_{i,m}$; the chip symbol, assumed to be known by the receiver $\gamma_{i,m}$; and, factors F_m which depends on the spectral density of the noise plus the jammer in every frequency band m.

$$\Lambda_i = \sum_{m=1}^{N} z_{i,m}\gamma_{i,m}^{*}F_m \tag{4}$$

Since the bandwidth of every band is equal or less than the jammer's bandwidth, the jammer and the noise are assumed to have flat spectral densities, given by J_o and N_o respectively. In this case, the factor F_m in the above equation is given by (5).

$$F_m = 1/\left(1+\left[\frac{J_o}{N_o}\right]\right) \quad \text{for bands hit by the jammer} \tag{5}$$

$$F_m = 1 \quad \text{for free bands}$$

The decision for the received symbol $\hat{a}_i$ is the alphabet symbol a_i which maximizes Re (a_i . Λ_i), where Re(.) indicates the real part of a complex argument. The resulting probability of a symbol error is,

$$P_e = Q\left(\sqrt{\left(\frac{2E_s}{N_o}\right)\beta}\right) \tag{6}$$

where E_s is the received energy per symbol, Q(.) is the error function, and β is the loss factor which reflects the degradation due to the presence of jammer. This factor depends only on the spectral density of the jammer, normalized by the noise density, as well as the number of hit and free bands, denoted by N_h and N_f respectively, relative to the total number of frequency bands N.

$$\beta = \frac{1}{N}\left\{\sum_{N_h}\frac{1}{1+J_o/N_o}+\sum_{N_f}1\right\} \tag{7}$$

The above factor can be modified accordingly in the case of unequal jammer strength for every band. When the jammer has the same strength in all the hit bands, the above formula can be expressed as

a function of the fraction of bands hit η. This factor is the key parameter in the performance of FDSS systems [2].

$$\beta = \left\{ \left(\eta \Big/ \left(1 + \left(J_o \Big/ N_o \right)\right) \right) + (1-\eta) \right\} \tag{8}$$

A suboptimum receiver does not use the side information corresponding to the jammer strength, and the decision variable Λ_i is only formed by the free bands. The probability of symbol error in such a case is given by (9), which shows that the loss factor β is equal to 1-η, being independent of the jammer strength.

$$P_e = Q\left(\sqrt{\left(2E_b \Big/ N_o \right)(1-\eta)} \right) \tag{9}$$

Note that both receivers degrade in performance when η gets close to one; in other words, when the jammer spreads its bandwidth covering the entire transmission band. A detailed study of both receivers and their comparison with DS and FH systems can be found in [1,2,4], showing the advantages in many respects of FDSS over traditional DSSS and coherent, or incoherent, FHSS for partial band jamming. It should be noted that for a DSSS, the processing gain is, in essence $1/\eta$, and the equivalent β is given by:

$$\beta_{DS} = \left(\frac{1}{1+\eta\left(\frac{J_o}{N_o} \right)} \right) \tag{10}$$

which is always lower than that of in the FDSS optimum receiver.

Spatial diversity in FDSS is next introduced in order to alleviate, whenever it is possible, the impact of the hit bands on the receiver performance. This is to say that spatial processing strives to reduce the effective η, by removing jammer contamination in the hit bands.

4. SPATIAL PROCESSING IN FDSS SYSTEMS

As mentioned in the previous Section, when the number of bands hit by the interference is close to N, the total number of frequency bands, both the optimum and suboptimum receivers degrade in performance. Furthermore, high levels of jamming tend to impair the performance of both receivers, rendering all efforts of labeling every band useless. As it is typical in digital transmission, when temporal processing is insufficient to counteract interferences, spatial diversity may be introduced to remove, or or at least reduce, the jammer contamination of the desired signal, independent of its temporal characteristics. Taking advantage of the frequency diversity available in FDSS systems, we propose a procedure to design optimum spatial diversity processing that is blind to the desired signal waveform. In fact, the procedure is valid for all the SS schemes which implement the architecture of Figure 1 for the transmitted signal generation, providing N is greater than one.

It is assumed that the desired signal is present in all the frequency bands. It is also assumed that the labeling of hit bands is properly done (This assumption is latter relaxed). All the air interfaces, down conversion, and filtering channels are calibrated. Full coherence is assumed for the desired signal across spatial diversity channels.

Let us assume that $\underline{X}_{f,n}$ and $\underline{X}_{h,n}$ are the snapshots, at time n, of the free and hit bands, respectively. Both bands are selected to start up the design of the respective optimum spatial combiners $\underline{w}_f$ and $\underline{w}_h$. Once the chip symbol is removed for the two bands selected, i.e. $\underline{X}_{f,n} \Rightarrow \gamma^*_{f,n} \cdot \underline{X}_{f,n}$ and $\underline{X}_{h,n} \Rightarrow \gamma^*_{h,n} \cdot \underline{X}_{h,n}$, the desired signal, which is present in both bands can act as the reference signal. The design of both combiners can then be performed through the quadratic cost function minimization:

$$\xi = \mathrm{E}\left\{\left|\underline{w}_f^H \underline{X}_{f,n} - \underline{w}_h^H \underline{X}_{h,n}\right|^2\right\} \tag{11}$$

The undesired solutions to the above objective are either the null vector for both combiners, or the case when the desired, together with the jammer, is nulled out simultaneously. A suitable technique to avoid both solutions is to set the cross-correlation of both combiner's outputs to some chosen value,

$$\mathrm{Re}\left\{E\left[\underline{w}_f^H \underline{X}_{f,n} \underline{X}_{h,n}^H \underline{w}_h\right]\right\} = \phi \tag{12}$$

where ϕ is some constant different from zero

Naming the array autocovariances and cross-covariance of the two frequency channels as,

$$\begin{aligned} \underline{\underline{R}}_f &= E\left[\underline{X}_{f,n} \underline{X}_{f,n}^H\right] \\ \underline{\underline{R}}_h &= E\left[\underline{X}_{h,n} \underline{X}_{h,n}^H\right] \\ \underline{\underline{P}}_{f,h} &= E\left[\underline{X}_{f,n} \underline{X}_{h,n}^H\right] \end{aligned} \tag{13}$$

the minimization problem becomes:

$$\text{Minimize } \xi = \underline{w}_f^H \underline{\underline{R}}_f \underline{w}_f + \underline{w}_h^H \underline{\underline{R}}_h \underline{w}_h - \underline{w}_f^H \underline{\underline{P}}_{f,h} \underline{w}_h - \underline{w}_h^H \underline{\underline{P}}_{f,h}^H \underline{w}_f \tag{14.a}$$

$$\text{Constrained to } \underline{w}_f^H \underline{\underline{P}}_{f,h} \underline{w}_h + \underline{w}_h^H \underline{\underline{P}}_{f,h}^H \underline{w}_f = \phi \tag{14.b}$$

Forming the Lagrangian and setting partial derivatives equal to zero, the optimum spatial combiners are obtained as:

$$\underline{\underline{R}}_f \underline{w}_f = (1+\lambda)^2 \underline{\underline{P}}_{f,h} \underline{\underline{R}}_h^{-1} \underline{\underline{P}}_{f,h}^H \underline{w}_f \tag{15.a}$$

$$\underline{w}_h = (1+\lambda) \underline{\underline{R}}_h^{-1} \underline{\underline{P}}_{f,h}^H \underline{w}_f \tag{15.b}$$

where λ is the Lagrange multiplier. Since ξ is minimum for minimum λ, the optimum combiner for the jammer free band is the eigenvector of (15.a) associated with the minimum eigenvalue. After $\underline{w}_f$ is found, the combiner for the hit band is just the Wiener solution for the cross-correlation vector $\underline{\underline{P}}_{f,h}^H \underline{w}_f$. Once

the combiner of the free band is derived, the rest of the combiners can be derived by using the band free output as a time reference for all other bands. The unconstrained minimization procedure is shown in (16.a), together with the solution for the combiners in (16.b). Since every frequency band has to be calibrated in the front-end, the reference combiner is normalized for response equal to one in a preselected diversity channel (i.e. $w_f(1)=1$) before it is used in (16.b); at the same time this normalization also helps the weights implementation with finite register length.

$$E\left[\left|\underline{w}_f^H \underline{X}_{n,f} - \underline{w}_h^H \underline{X}_{n,h}\right|^2\right]_{min} \text{ min.} \qquad \text{for } h \neq f \tag{16.a}$$

$$\underline{w}_h = \underline{\underline{R}}_h^{-1} \underline{\underline{P}}_{h,f} \underline{w}_f \tag{16.b}$$

It is noteworthy that, since the jammer is uncorrelated from one band to another due to the chip demodulation, any two bands can be selected to start up the design in (16.a). Once a combiner is derived, its output provides a time reference for the rest of the bands. This implies that labeling is not essential to design the spatial processor. Nevertheless, when required, a suitable procedure to determine the free and the hit bands, to be used in (15.a), is to choose the two bands with minimum and maximum received power respectively.

Note that when the transmission bandwidth is very small compared with the central frequency, and adequate labeling of free and hit bands is available, there is a great saving in computations since the combiners derived in (15), for a pair of free and hit bands, can be applied directly in the rest of the bands.

To gain insight into the design method, we inspect the design equation for the case when the desired signal is a point source; in this case, the cross-covariance matrix is rank one,

$$\underline{\underline{P}}_{f,h} = \kappa_o \underline{P}_f \underline{P}_h^H \tag{17}$$

the corresponding equations for the optimal combiners reduce to

$$\underline{w}_f \propto \underline{\underline{R}}_f^{-1} \underline{P}_f \tag{18.a}$$

$$\underline{w}_h \propto \underline{\underline{R}}_h^{-1} \underline{P}_h \tag{18.b}$$

as expected from the optimum combiner equations, when the vectors of the second term of (17) are known. Nevertheless, the rank one approximation of the cross-covariance provides poor performance when the number of snapshots used in its estimation is small. In general, the formulation (15) offers much better results than the outlined rank one approximation procedure. Further, the rank one procedure requires the point source model for the desired signal, which, in general, is no longer the case in radio communication systems.

5. OPTIMUM DETECTION AND CROSS-OVER

It is often the case that the effect of the spatial processing on subsequent stages in the receiver is ignored. In the underlying problem, it is important to include such an effect, specifically, when the spatial combiner varies from a frequency channel to another for both the suboptimum and optimum receivers. The changes in the power of both the desired signal and the jammer, as they marsh through the spatial structures alter the sufficient statistic for optimum detection. The sufficient statistic for optimum detection depends on the combiner response to all sources impinging the aperture, and is given by

$$\Lambda_i = \sum_{m=1}^{N} z_{m,i} \left(\frac{w_{md}^*}{J_o \left| w_{mj} \right|^2 + N_o \left| \underline{w}_m \right|^2} \right) \tag{19}$$

where $z_{m,i}$ is the combiner output of the frequency channel m at symbol i after chip de-spreading and matched filtering. The scalars w_{md} (i.e. $w_{md}=\underline{w}_m^H.\underline{S}_d$. $\underline{S}_d$ is the steering of the desired in the optic channel) and w_{mj} are the responses of the combiner $\underline{w}_m$ to the desired signal and to the jammer, respectively.

From (19) it is clear that the response of the combiners is required in order to determine the sufficient statistics for optimum detection. Furthermore, it may occur that the spatial signature of the

jammer completely mask the desired signal. This is the case when the jammer cross-over the DOA of the desired source in an optic channel. In consequence, it is necessary to keep control of the adequate labeling at the combiners' outputs. From the three values involved in each term in (19), only the norm of the combiner is directly available to the designer; the other two must be estimated from data. It can readily be shown that, by taking the free band in (15 a) as a reference band, the factor Fn for the rest of the bands is

$$F_n = \left(\frac{\left(\frac{w_{nd}}{w_{fd}} \right)^*}{\left(\frac{J_o \left| w_{nj} \right|^2 + N_o \left| \underline{w}_n \right|^2}{N_o \left| \underline{w}_f \right|^2} \right)} \right) \quad ; \forall\, n \neq f \tag{20}$$

The term corresponding to the spectral density of the noise N_o can be determined from the noise eigenvalues of $\underline{\underline{R}}_f$. The numerator, in the above equation can be provided using the following indentity

$$\left(\frac{w_{nd}}{w_{fd}} \right)^* \approx \frac{\underline{w}_f^H \underline{\underline{P}}_{fn} \underline{w}_n}{\underline{w}_f^H \underline{\underline{R}}_f \underline{w}_f} \tag{21}$$

As for the estimation of the denominator in (20), we use two key formulations of the design criterion for the combiners. The first expression is the MSE incorporating (16.b);

$$MSE(n) = \underline{w}_f^H \left(\underline{\underline{R}}_f - \underline{\underline{P}}_{nf}^H \underline{\underline{R}}_n^{-1} \underline{\underline{P}}_{nf} \right) \underline{w}_f \tag{22}$$

the second relationship, comes from the definition of the minimization criterion. The MSE is lower bounded by the residuals levels of jammer and noise.

$$MSE(n) \geq J_o \left| w_{nj} \right|^2 + N_o \left(\left| \underline{w}_n \right|^2 + \left| \underline{w}_f \right|^2 \right) \tag{23}$$

The equality holds for the case where the jammer does not shadow the desired signal and it is properly cancelled in the MSE. Thus, using (21), (22) and (23) in (20), we obtain an estimate of the factor to be used in the decision variable for the bands different from the reference band.

$$F_n = \frac{\dfrac{\underline{w}_n^H \underline{\underline{P}}_{nf} \underline{w}_f}{\underline{w}_f^H \underline{\underline{R}}_f \underline{w}_f}}{\left(\left[\dfrac{MSE(n)}{N_o \left| \underline{w}_f \right|^2} \right] - 1 \right)} \tag{24}$$

Note that this factor is smaller than the optimum weigthing since the inequality (23) is used to estimate the denominator. This factor accounts for the residual loss from the spatial diversity processing due to the presence of the jammer. In the case where the desired source is completely shadowed by the jammer, the factor F_n depicts negligible contribution of the hit bands to the decision variable, when compared with the terms of the bands free of jammer.

6. ADAPTIVE DESIGN

This section describes an adaptive algorithm to the constrained minimization described in Section 4. It should be emphasized that the fundamental step is to find the response of the free-band combiner $\underline{w}_f$; once this combiner is found at each iteration, the update of the rest of the combiners, including $\underline{w}_h$, is done in a time reference combining framework, where the output of $\underline{w}_f$ acts as the reference waveform. As stated in Section 4, the presence of chip symbol modulation decorrelates the jammer from one band to another. Under this premise, the band selection is no longer crucial in the resulting performance of the method.

The basic update of the selected beamformers is done with the instantaneous gradient of the Lagrange objective ξ,

$$\xi = \left|y_{f,n} - y_{h,n}\right|^2 - (\lambda_n - 1)2.\mathrm{Re}\left[y_{f,n}.y_{h,n}^*\right] = \left|y_{f,n} - y_{h,n}\right|^2 - (\lambda_n - 1)\phi_n \tag{25}$$

where (λ_n-1) is the Lagrange multiplier and

$$\begin{aligned} y_{f,n} &= \underline{w}_{f,n}^H \underline{X}_{f,n} \\ y_{h,n} &= \underline{w}_{h,n}^H \underline{X}_{h,n} \end{aligned} \tag{26}$$

are the combiners' output. The update equations are then given by:

$$\begin{aligned} \underline{w}_{f,n+1} &= \underline{w}_{f,n} - \mu_{f,n} \underline{X}_{f,n} \left(y_{f,n}^* - \lambda_n y_{h,n}^*\right) \\ \underline{w}_{h,n+1} &= \underline{w}_{h,n} - \mu_{h,n} \underline{X}_{h,n} \left(y_{h,n}^* - \lambda_n y_{f,n}^*\right) \end{aligned} \tag{27}$$

The Lagrange multiplier has to be set such that the new weights, prepared for snapshot n+1, hold the constraint at snapshot n. In other words, the updated combiners have to satisfy (28).

$$\phi_n = 2.\mathrm{Re}\left[\underline{w}_{f,n+1}^H \underline{X}_{f,n} \underline{X}_{h,n}^H \underline{w}_{h,n+1}\right] \tag{28}$$

The step-size parameters are set to (29),

$$\mu_{f,n} = \frac{\alpha}{W_{f,n}} \; ; \; \mu_{h,n} = \frac{\alpha}{W_{h,n}} \tag{29}$$

The denominators in the above equation are the snapshot powers defined by

$$\begin{aligned} W_{f,n} &= \left|\underline{X}_{f,n}^H \underline{X}_{f,n}\right| \\ W_{h,n} &= \left|\underline{X}_{h,n}^H \underline{X}_{h,n}\right| \end{aligned} \tag{30}$$

Including the weight updates in (28) and assuming that the past weights satisfy the constraint, the following equation provides the selection for λ_n

$$\lambda_n^2 \phi_n \alpha + \lambda_n (P_{f,n} + P_{h,n})(1-\alpha) + \phi_n (\alpha - 2) = 0 \tag{31}$$

where

$$P_{f,n} = \left| \underline{w}_{f,n}^{H} \underline{X}_{f,n} \right|^2$$
$$P_{h,n} = \left| \underline{w}_{h,n}^{H} \underline{X}_{h,n} \right|^2 \quad (32)$$

Since the parameter α has to be set equal to small values, usually below 0.02, to obtain reasonable levels of missadjusment, the terms including α in (31) can be neglected in favor of the two terms which do not contain it. This results in

$$\lambda_n = \frac{\phi_n}{(P_{h,n} + P_{f,n})} \quad (33)$$

since the constraint acts like an automatic control gain for the system, the numerator of the above formula can be set to a constant value. Note that this constant will be, on the average, the power at the output of the free band. This value was set to one in the simulations included in this section. It is interesting to note that, at the steady state, as the output powers tend to be equal, the Lagrange multiplier will tend to one. On the other hand, at the start up, when P_f and P_h are expected to be different, the multiplier will be smaller than one. In other words, the Lagrange multiplier acts like a flag indicating to the updating algorithm how both output signals have to be compared to provide a proper error correction.

A realistic set-up of the algorithm demands some smoothing of the instantaneous powers defined previously. The resulting performance, in terms of convergence rate, does not show high sensitivity to this parameter, providing it is above a threshold. For different scenarios, the values of the smoothing factor which are above 0.8 shown small impact in the learning curve.

In Figure 2 depicts the learning curve (i.e. the smoothed MSE versus number of snapshots) for two different scenarios, which differ in the angular separation between the desired source and the jammer. The rest of parameters are: FDSS of 6 bands, η equal to 50%, 5 sensors half wavelength ULA array, the desired and jammer signals are 1 dB and 10 dB respectively, α=0.01 and β=0.9. From this Figure, it is

clear that the adaptive algorithm exhibits good behavior which makes it a candidate alternative to frame processing method suitable for TDMA which has been reported in Section 4.

7. COMMENTS AND EXTENSSIONS OF THE PROCEDURE

It is important to note that the proposed method is based merely on the coded structure of the desired signal in the frequency domain. We should stress, however, that the applicability of this method is granted irregardless of the nature of the code, i.e., wether it is being pure repetitive or otherwise. With the same perspective, it is easy to realice that, as long as the desired signal has a structure (we refer to "a structure" as any repetition in any diversity axis like encode, frequency, time, etc.), optimum spatial processing is attainable.

From the above perspective, spatial processing methods, referred to as blind, are not enterely blind, since some information concerning the signal structure is used at the receiver to obtain optimum processing . In communications systems, this structure is provided for proper matching between modulation and demodulation schemes at both ends of the communications channels.

A way around to describe the underlaying advantages of FD systems for blind beamforming is to traduce the signal structure to the property of exact prediction. The structure of the FDSS transmitted signal, in essence, has allowed the desired signal to be exactly predicted from one band to another, and thereby serves as a reference. Since this scheme is using predictability in the frequency domain it is evident that some correspondence has to exist in the time domain. This possibility was outlined in Section 2, when it was proposed to divide the chip signal in several segments within a symbol and to transmit every slot in a different frequency band. The time domain dual is the transmissions of these slots sequentially in time; time diversity, to counteract partial time jamming [7]. With time diversity, the segments, within an information symbol, can be predicted which are then used to form the blind combiner. For clarity of the presentation, let us assume that the chip signal within a symbol is divided in

two segments, as indicated in Figure 3. Note that the pure repetition code is also included within this general scheme (i.e. the same chip code is used twice per symbol interval).

Since the described structure in the time domain is exactly the same as that of the FDSS in the frequency domain, the optimum spatial combiner for the corresponding desired signal can be derived from the minimization of ξ defined as (34),

$$\xi = E\left\{\left|\underline{w}_f{}^H \underline{X}_{n,1} - a(n)\underline{w}_h{}^H \underline{X}_{n,2}\right|^2\right\} \tag{34}$$

where $\underline{X}_{n,1}$ and $\underline{X}_{n,2}$ are the snapshots corresponding to segments one and two respectively. This formulation is adequate for partial time jamming, as the desired signal temporal structure allows exact prediction. More interesting is the case where the minimization of (34) is carried over a single combiner, which is possible if the jammer remains uncorrelated from time segment to segment ,

$$\xi = E\left\{\left|\underline{w}^H \underline{X}_{n,1} - a(n)\underline{w}^H \underline{X}_{n,2}\right|^2\right\} \tag{35}$$

Since the jammer and the noise are assumed uncorrelated for the two segments selected, the optimum combiner will select only the signal which is exactly predicted by a(n), i.e. the desired signal. Of course, the additional constraint used for FDSS has to be added in order to avoid the trivial solution to the minimization of (35). The exact prediction required for the procedure, outlined previously, can be also provided by the channel encoder. Note that using the same combiner precludes optimal detection, but reduces the complexity in the suboptimum detector.

For further illustration of the notion of signal prediction and diversity we selected below the case of an unmodulated carrier at baseband frequency f_o. Assuming that the maximum time for coherence in the jammers is smaller than t_o (This is the case when t_o is greater than the inverse of the interferer's symbol rate), the minimization objective is (36).

$$\xi = E\left\{\left|\underline{w}^H \underline{X}_n - \exp(-j2\pi f_o t_o)\underline{w}^H \underline{X}_{n+t_o}\right|^2\right\} \tag{36}$$

This objective, which is constrained by the non-zero value of the cross-correlation between the two outputs produces adequate nulling of the jammer at the combiners' output. Defining

$$\underline{\underline{R}} = E\left(\underline{X}_n \underline{X}_n{}^H\right) \underline{\underline{P}} = E\left(\underline{X}_n \underline{X}^H{}_{n+t_o}\right)\exp(-j2\pi f_o t_o) \tag{37}$$

the optimum combiner is the eigenvector associated with the minimum eigenvalue of

$$\underline{\underline{R}}\underline{w} = \lambda \underline{\underline{P}}\underline{w} \tag{38}$$

Figure 4 shows an example using the exact prediction property of an unmodulated carrier. The top part of this Figure shows the beamformer response (top) whereas the bottom part depicts the beamforming scheme, which reflects the low complexity of the reference loop. The scenario contains two BPSK interferers (10 and 3 dB of SNR) at symbol rate greater than t_o^{-1} with DOAs equal to 0 and 10°, together with the desired unmodulated carrier (0 dB.) impinging from –20°. The baseband frequency is 0.25 for all sources. The adequate response of the combiner designed from 500 snapshots (250 each set), using the afforementioned procedure is clearly evident.

It is noteworthy that this system requires only the nominal frequency of the desired signal and does not need phase synchronism which is very convenient in practice. This allows a great saving in complexity and threshold margin for very low SNRIs.

Finally, note that since frequency structure effectively remove partial band jamming, time structure does the same with partial time jamming. In consequence, if the structure of the transmitted signal has simultaneously time and frequency diversity, the receiver will be robust against these two undesired jamming effects.

8. SIMULATIONS

The most important issue concerning the usefulness of spatial combining for frequency diversity is the adequate weighting of every term of the sum forming the decision variable Λ_m in (19). This factor reflects the limitations of the combiner when the jammer shadows globally or partially some bands of the FD system. The estimate of this factor is proposed in (23), as is shown in Figure 5 presents this estimate for different DOA separation between the jammer and the desired signal. For every separation, a set of 400 snapshots has been used. The variation of the DOA separation was set from 0° (complete shadowing) up to 20°.The SNR of the jammer was in all cases 10 dB (SJR=-10dB). No chip modulation has been used in the simulations; in consequence, the jammer is fully correlated from band to band, and the performance reported can be considered, in practice, as a lower bound. The desired signal is BPSK modulated and its power is changed from 10 dB down to 0 dB (step 1 dB). The desired signal permanent location was set equal to 10° from the broadside. The FDSS system has six frequency bands out of which bands 1, 2 and 4 are hit by the jammer (η= 50%) at 10 dB of Jammer to Noise Ratio (JNR) each. The labeling of the free and hit bands was done from a power detector. The aperture was an ULA array of 5 sensors. The estimate of the shadowing factor F_n improves when the SNR of the desired is high, that is Fn is close to zero for zero degrees of sources separation and close to one when the jammer is impinging on the aperture from secondary lobes (for this case the spatial bandwidth of the aperture at the central frequency was 20 °). Performance deterioration for low signal to noise ratio is expected, since the difference between the free and the hit bands decreases, with high levels of noise. When factor F_n was used in the detector statistics, the Bit Error Rate (BER) was always below or equal (complete shadowing) to the resulting one for the suboptimum detector (BER corresponding to SNRd plus the number of free bands (10.log3 dB), plus the number of spatial diversity channels, (10log5 dB)).

It is also interesting to measure for the same scenario the change in the SNR over the different bands at the combiners' outputs for different SJRs. Figure 6 shows (top) for the hit bands and (bottom) for the free bands the average of the actual SNR for each group, together with the impact of the corresponding shadowing. The input SNRd is set to 1 dB. It is important to note that the contribution of

the SNR in the free bands increases with increased jammer power and with the shadowing effect. The worst case is represented by a 30 dB jammer above the desired in every hit band and DOA equal to the same as desired signal. The result is 1 dB less than the case when there is two degrees of separation between the jammer and the desired signal. This plot provides evidence that the new front-end is able to resort at any time to the suboptimum detector. This is because the free bands remain almost unaffected by the spatial combiner processing. The role of spatial processing for improving SNR in the hit bands should be well appreciated. This traduces in an effective reduction in factor η which, for this aperture, reduces to zero when the separation of the desired and the source is greater than 6 degrees.

9. CONCLUSIONS

It has been shown that the use of diversity, basically frequency diversity, in the sense of several replicas of the desired signal, allows the optimum design of the spatial combiners blind to the source waveform. In a wide sense, it can be stated that whenever the desired signal along any diversity axis has an exact representation over diversity components, the spatial combiner can be optimally designed without additional diversity slots for a reference signal. The propossed design procedure minimizes the MSE between two selected diversity components, as in an exact prediction problem, with the constraint of a cross-correlation factor different from zero. It is remarked that the diversity could be time, frequency, encode or any mixture of them. The procedure is blind to the desired signal waveform. Since the spatial diversity may collapse, depending if the jammer may sign in all diversity components, the optimum detector demands for an estimate of this effect in order to properly adjust the likelihood in every diversity branch. To cope with this problem, an estimate has been derived from the design parameters. This estimate almost loads the detector to operate only on the jamming free diversity branches when the jammer shows strong presence. This is, in essence, an automatic convergence to the so-called sub-optimum receiver. It has been outlined that, whenever any kind diversity allows exact prediction of only the desired signal over two diversity components, blind spatial processing is always available.

10. REFERENCES

[1] G.K. Kaleh, "Frequency Diversity Spread Spectrum Communications System to counter Bandlimited Gaussian Intereference," IEEE Trans. on Communications, Vol. 44, No.7, pp. 886-893, July 1996.

[2] G.K. Kaleh, "Performance comparison of Frequency Diversity and Frequency Hopping Spread Spectrum Systems," IEEE Trans. on Communications, Vol. 45, No. 8, pp. 910-912, August 1997.

[3] J.G. Proakis, Digital Communications, Third Edition, Mac-Graw Hill, Chapters 12-15, 1995.

[4] E. Lance, G.K. Kaleh, "A diversity Scheme for a Phase- Coherent Frequency-Hopping Spread Spectrum System," IEEE Trans. on Communications, Vol. 45, No. 9, pp. 1123-1129, September 1997.

[5] R. Prasad, S. Hara, "An Overview of Multicarrier CDMA," Proc. of IEEE Fourth International Symposium on Spread Spectrum Techniques and Applications. pp. 107-113, Mainz Germany, December 1996.

[6] R. E. Crochiere, L.R. Rabiner, "Multirate Digital Signal Processing," Englewood-Cliffs, Prentice Hall, NJ, 1983.

[7] R.E. Blahut, Digital transmission of information, Reading, MA: Addison Wesley 1990.

FIGURE CAPTIONS

Figure 1. General transmitter scheme for spread spectrum digital communications.

Figure 2. Learning curve for the adaptive algorithm, i.e. the smoothed MSE versus snapshots used, for DOA separations of 1° (top) and 15° (bottom) between the desired signal and the jammer. The scenario and algorithm parameters are: 6 bands, 50% bands jammed, 1dB and 10dB of SNR for desired signal and jammer respectively, α= 0.01, β=0.9 and 5 sensors half wavelength ULA array.

Figure 3. The code structure within time diversity: A segment of the desired signal can be exactly predicted from the previous segment.

Figure 4. Beamforming response based on the exact prediction of the desired signal. Desired (unmodulated carrier) and jammers are labeled with lines in both plots on top. Bottom the beamforming architecture with the reference loop.

Figure 5. The shadowing factor F_n as a function of the DOA separation of the desired versus the jammer for several SNR (SNRd) of the desired signal.

Figure 7. Average actual SNR for the hit bands (top) and for the free bands (bottom) versus Signal to Jammer Ratio (SJR), for different DOA separation between the desired source and the jammer.

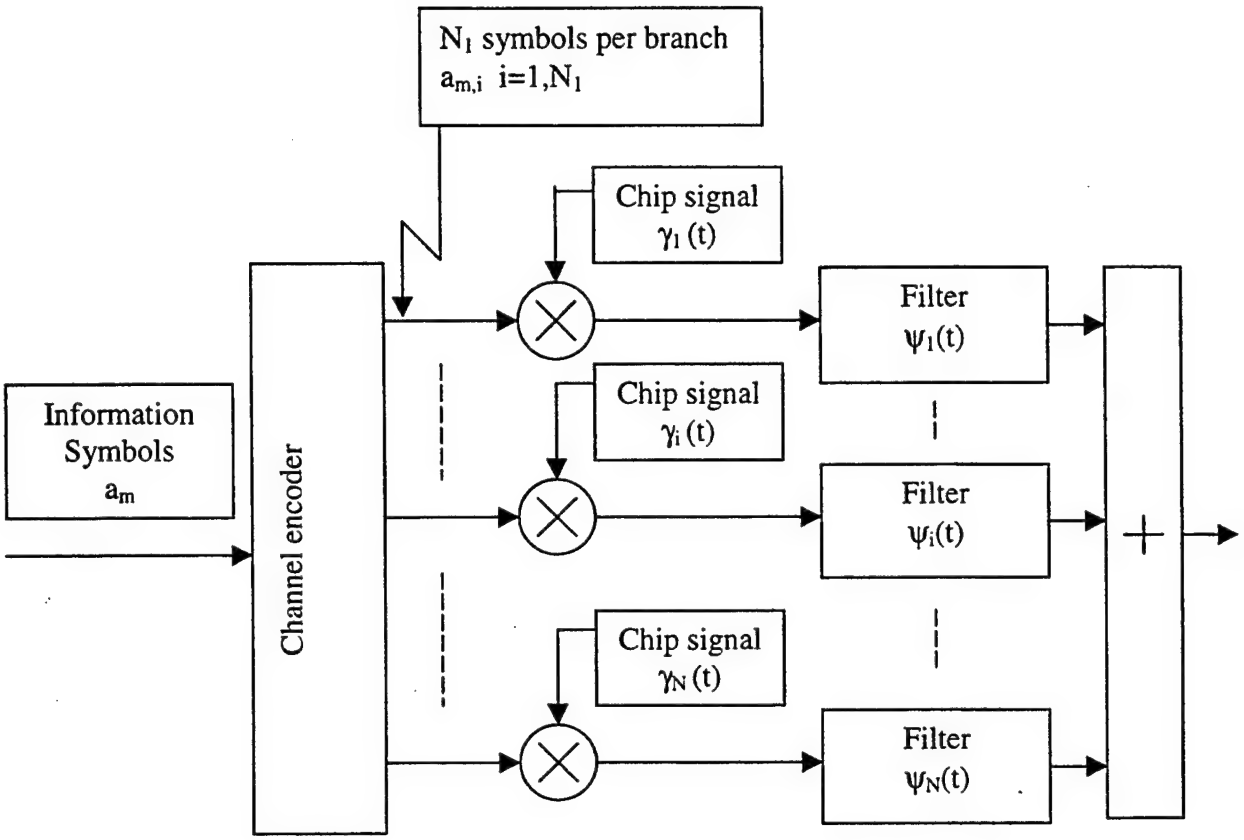
N_1 symbols per branch
$a_{m,i}$ i=1,N_1
Chip signal
γ_1 (t)
Chip signal
γ_i (t)
Chip signal
γ_N (t)
Information
Symbols
a_m
Channel encoder
Filter
ψ_1(t)
Filter
ψ_i(t)
Filter
ψ_N(t)

FIG. 1

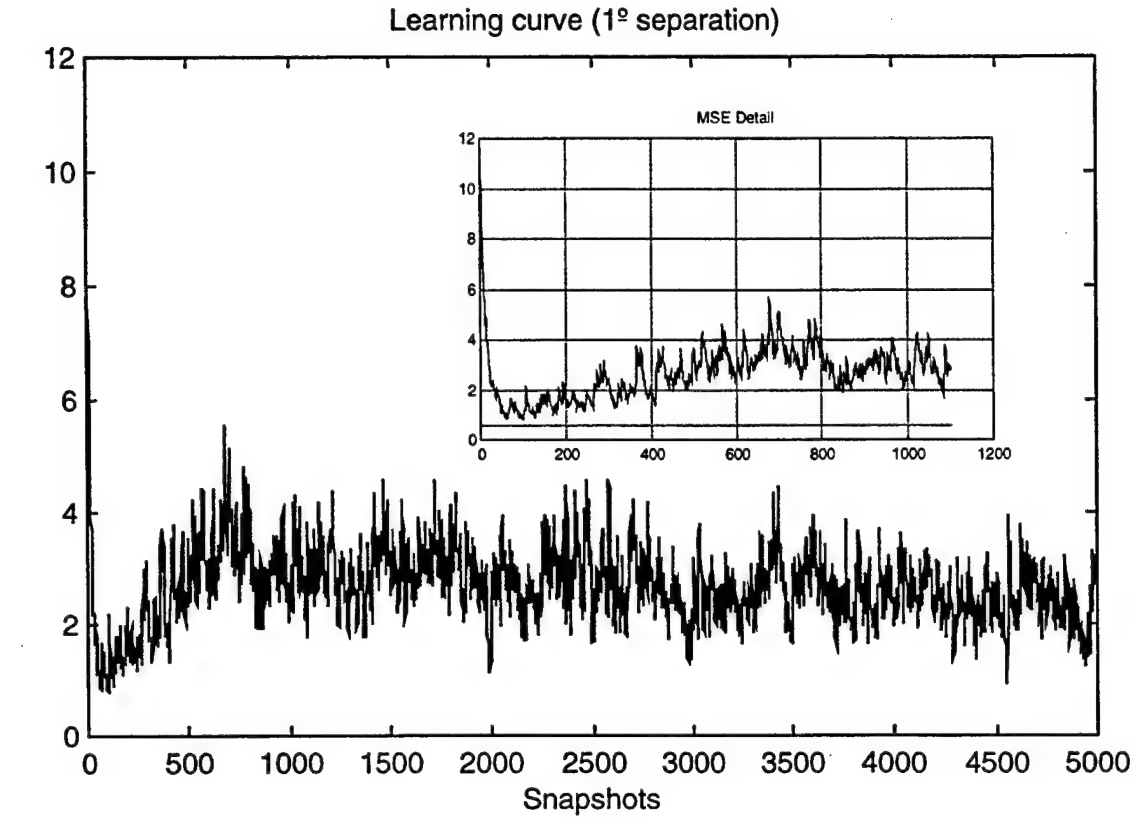
Learning curve (1º separation)
MSE Detail
Snapshots

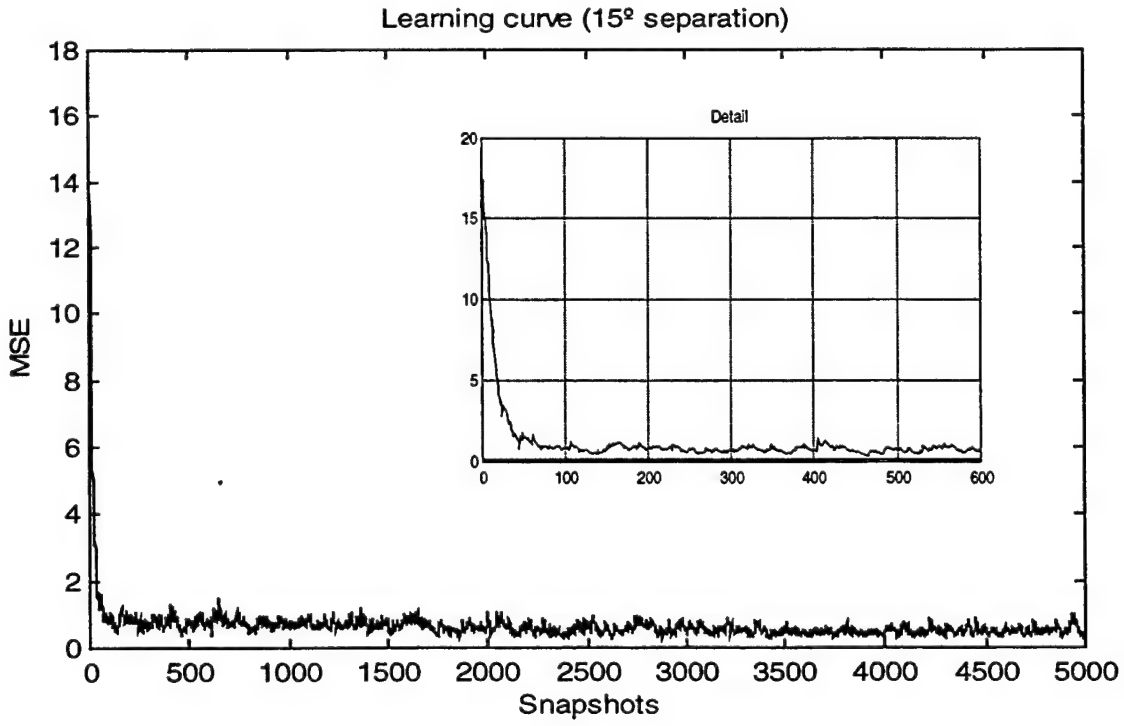
Learning curve (15º separation)
Detail
MSE
Snapshots

FIG. 2

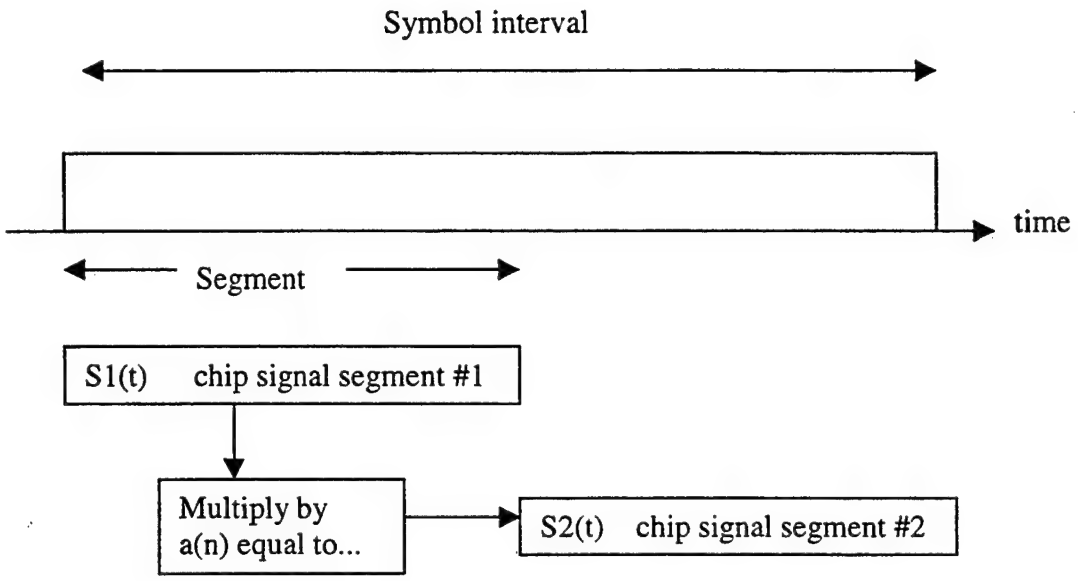
Symbol interval
time
Segment
S1(t) chip signal segment #1
Multiply by
a(n) equal to...
S2(t) chip signal segment #2

FIG. 3

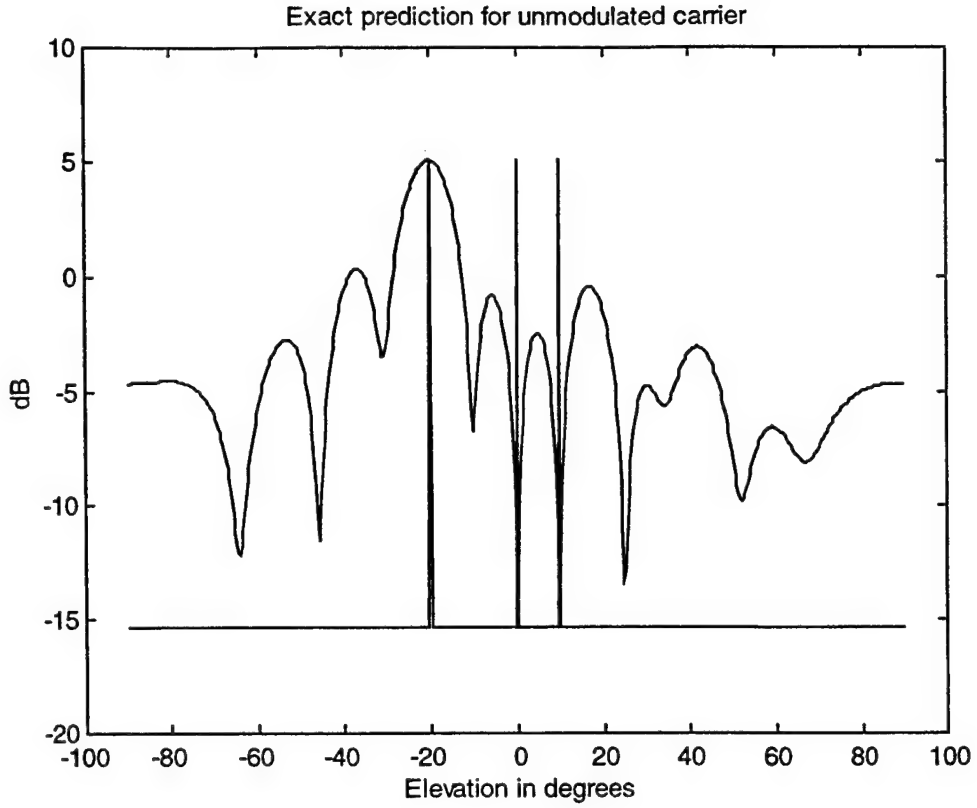
Exact prediction for unmodulated carrier
10
5
0
-5
-10
-15
-20
dB
-100
-80
-60
-40
-20
0
20
40
60
80
100
Elevation in degrees

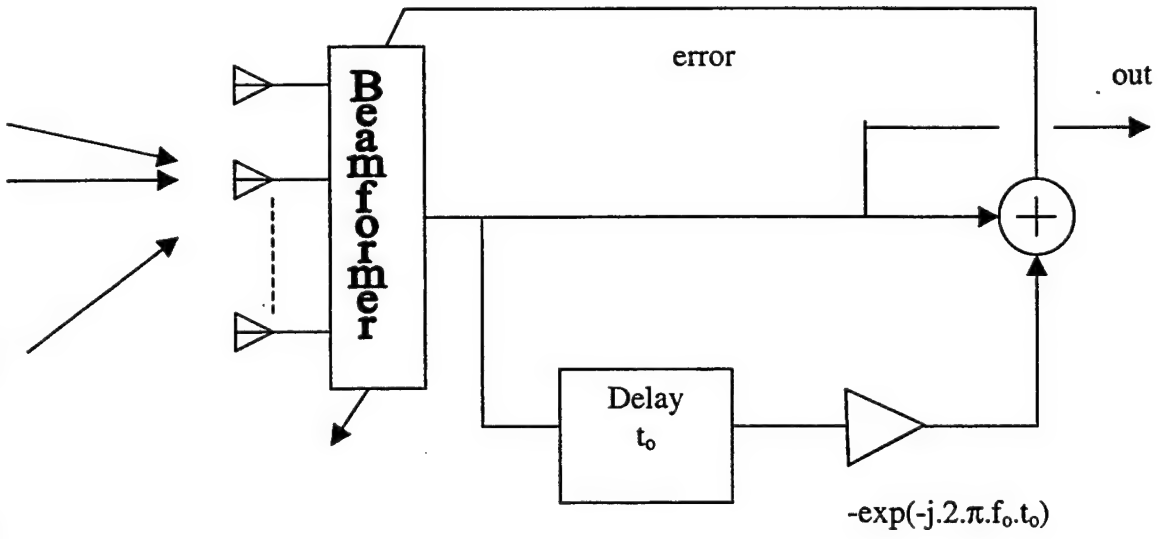
Beamformer
error
out
Delay
t_o
$-\exp(-j.2.\pi.f_o.t_o)$

FIG 4

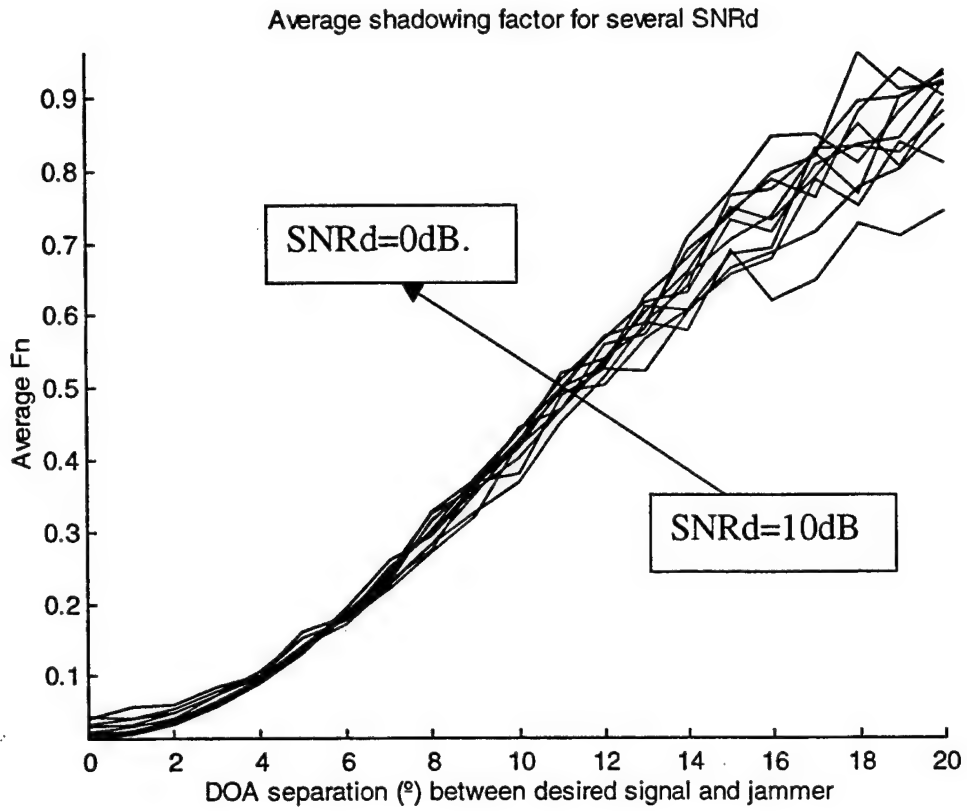
Average shadowing factor for several SNRd
SNRd=0dB.
SNRd=10dB
Average Fn
0.9
0.8
0.7
0.6
0.5
0.4
0.3
0.2
0.1
0
2
4
6
8
10
12
14
16
18
20
DOA separation (º) between desired signal and jammer

FIG 5

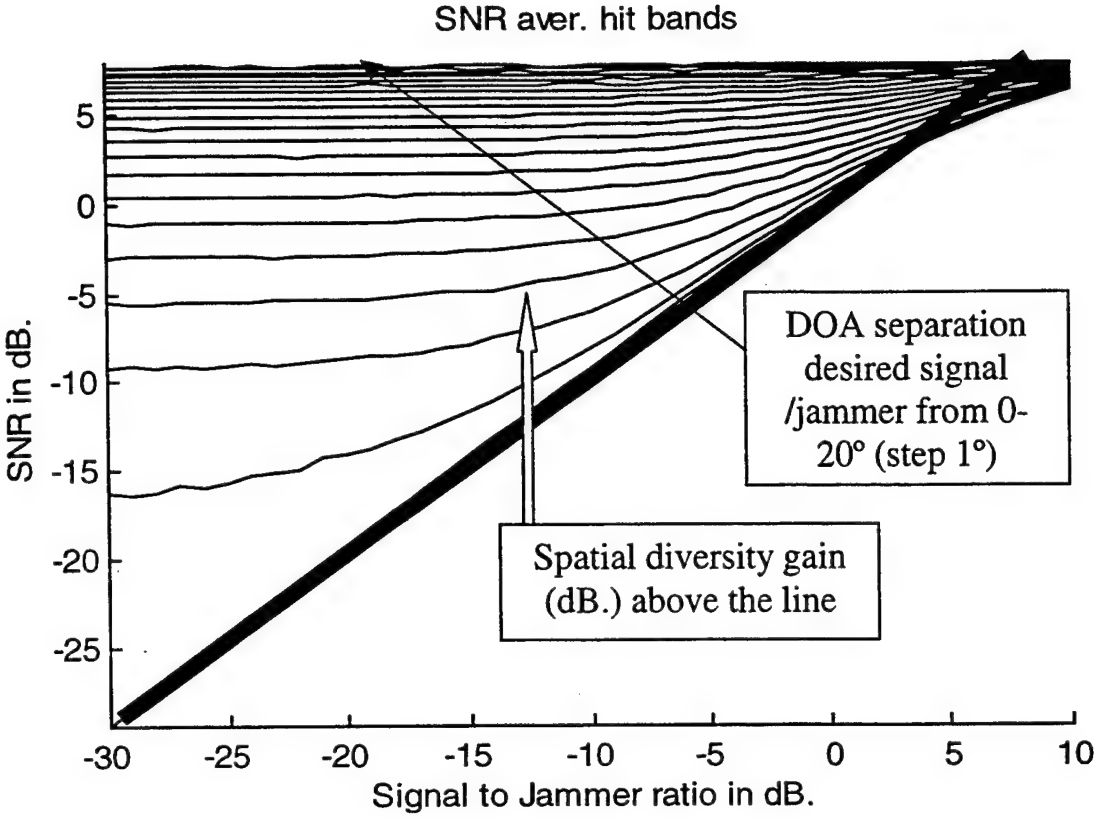
SNR aver. hit bands
SNR in dB.
5
0
-5
-10
-15
-20
-25
-30
-25
-20
-15
-10
-5
0
5
10
Signal to Jammer ratio in dB.
DOA separation desired signal /jammer from 0-20° (step 1°)
Spatial diversity gain (dB.) above the line

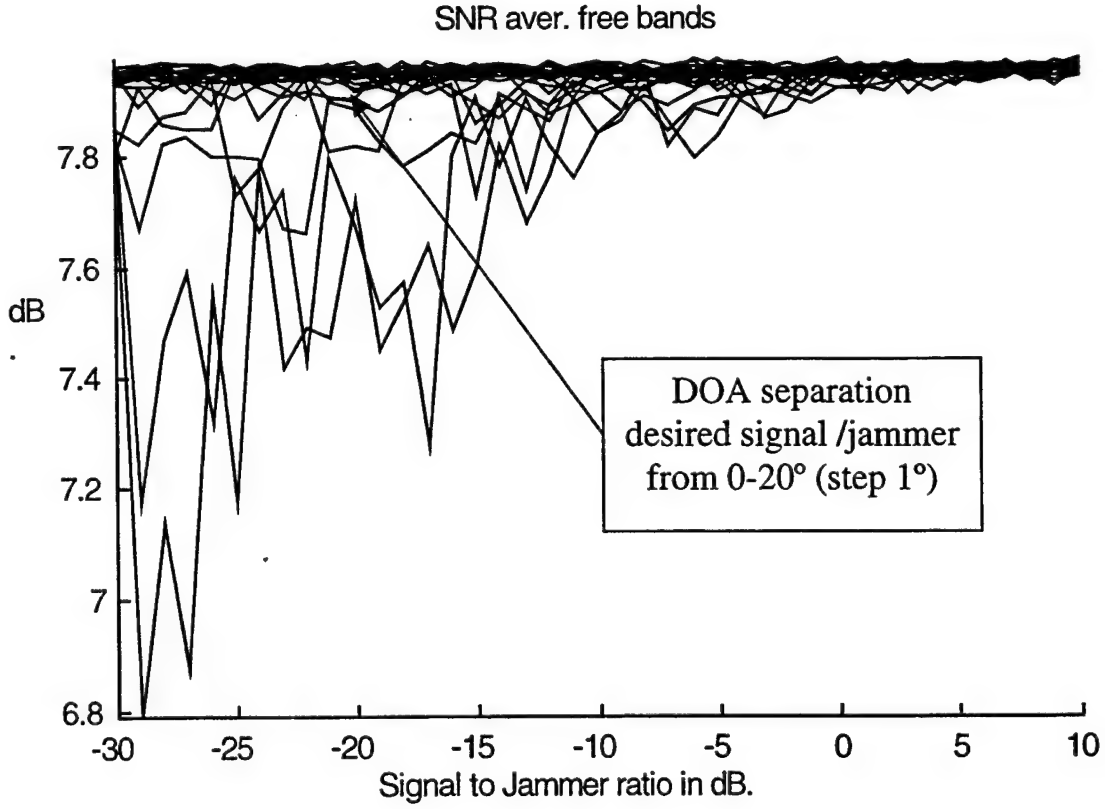
SNR aver. free bands
dB
7.8
7.6
7.4
7.2
7
6.8
-30
-25
-20
-15
-10
-5
0
5
10
Signal to Jammer ratio in dB.
DOA separation desired signal /jammer from 0-20° (step 1°)

FIG 6

Adaptive Array Processing for Multipath Fading Mitigation via Exploitation of Filter Banks*

Yimin Zhang[1], Kehu Yang[2], and Moeness G. Amin[3]

[1] ATR Adaptive Communications Research Laboratories, Kyoto 619-0288, Japan

[2] Institute of Electronics Engineering, Xidian University, Xi'an, Shaanxi 710071, China

[3] Department of ECE, Villanova University, Villanova, PA 19085, USA

E-mail : moeness@ece.vill.edu

Abstract

This paper proposes the subband adaptive array processing method, which is used to mitigate both inter-symbol interference (ISI) and cochannel interference (CCI) in digital mobile communications. The analysis filters enhance the correation of multipath rays in each subband. This enhancement is blind in the sense that no *a priori* knowledge of the arriving signals is required. With the increased coherence, the desired signal can be effectively equalized by subsequent spatial processing. Further, the CCI signals and their multipaths can be suppressed with fewer array degrees-of-freedom. The effect of QMF and DFT filter banks on multipath correlation is delineated.

* Dr. Amin is supported in part by ONR, under Grant #N00014-98-1-0176. Dr. Yang is supported in part by NSFC (Natural Science Foundation of China) under Grant #69602008.

I. Introduction

In land mobile communications, a signal transmitted by a mobile station arrives at a base station reflected and scattered by surroundings, which causes multipath fading. As the demand is increasing for multimedia communications, mobile communication is developing towards high-speed digital wireless networks, where the communication channels is frequency-selective, and the inter-symbol interference (ISI) becomes highly pronounced. Another important problem in mobile communication is cochannel interference (CCI), which is generated due to the frequency reuse in cellular systems.

Adaptive array implementing spatial or spatial-temporal equalizations or diversity techniques prove useful in suppressing both of the ISI and CCI, leading to increased capacity and range [1-8]. The spatial-temporal equalization can be achieved by space-time adaptive processing (STAP) to effectively mitigate ISI and CCI. Such a scheme is composed of an integrated adaptive array and temporal equalizer to perform optimum jointly spatial and temporal signal processing. However, solving both the CCI and ISI problems simultaneously by conventional STAP methods is yet difficult. These methods require either large scale matrix inversion or recursive calculation, or a cascaded form of CCI and ISI cancellers [6-8].

In this paper, we propose an efficient subband adaptive array processing method that utilizes filter banks to mitigate both the CCI and ISI effects in land mobile communications. A subband adaptive array has, in effect, the same function as an STAP system, while the implementation is much easier. The subband adaptive array provides sub-optimal performance in the context of frequency-spatial signal processing, which enhances the signal correlation between multipath rays prior to processing. In subband adaptive arrays, the frequency band of the received signals is divided into smaller bands by the use of filter banks [9]. Proper analysis filters allow a significant increase in the signal correlation between the multipath rays within each subband. Note that such an increase is blind in the sense that it does not require *a priori* knowledge of the arriving signals. As a result of increased correlation, the multipath fading associated with both the desired and the interference signals is reduced, thus yielding faster convergence of the adaptive weight vector as well as fewer degrees-of-freedom (DOF's) required for adequate equalization [10,11].

So far, subband adaptive array methods have been proposed for wideband signal processing.

Subband adaptive arrays have the advantages of reducing the processing rate [14] as well as achieving rapid convergence [12, 15]. Other kind of coherent subspace transformation methods [13, 16] also demonstrate these two advantages.

In this paper, the discussion is mainly focused on the signal correlation enhancement in a frequency-selective fading environment, rather than the conventional consideration on subband signal processing to reduce the signal bandwidth and computational complexity, although such advantages are also shared by our proposed method. The signal correlation enhancement, in essence, converts a frequency-selective fading problem into a flat fading one. In this case, the ISI problem is highly mitigated as the faded signal can be easily equalized by a subsequent spatial combiner. Since the CCI components in each subband are easily removed by the respective narrowband adaptive array, subband adaptive array techniques can simply solve both CCI and ISI problems.

Although many transformation methods can convert a wideband signal into multi-channel narrowband signals, it is shown in this paper that different methods provide different signal correlation enhancement performance. The importance to properly choose the analysis and synthesis filters to obtain good equalization performance by subband signal processing is emphasized.

The paper is organized as follows. In Section II, we first present the framework of adaptive array processing in the presence of multipath rays. It is shown that multipath rays of a signal can be treated as a single ray when their cross-correlation is relatively high. The signal correlation enhancements of multipath signals by using different filter banks are compared in Section III. In Section IV, the analysis of the subband array performance is given. In Section V, simulation examples are provided to confirm the effectiveness of the proposed method.

II. Adaptive Array Framework in the Presence of Multipath Rays

Without a loss of generality, we consider the simple case where a desired signal and a CCI, each with two rays, are incident on an array of N sensors. The received array vector is described as

$$\mathbf{x}(t) = \mathbf{A}(\Theta_D)\mathbf{s}_D(t) + \mathbf{A}(\Theta_I)\mathbf{s}_I(t) + \mathbf{n}(t), \tag{1}$$

where $\mathbf{A}(\Theta_D) = [\mathbf{a}(\theta_{D1}), \mathbf{a}(\theta_{D2})]$ is the collection of the steering vectors for the desired signal, and $\mathbf{s}_D(t) = [s_{D1}(t), s_{D2}(t)]^T$ is the vector which represents the associated complex envelopes at the

presumed phase reference point of the array. Similarly, $\mathbf{A}(\Theta_I) = [\mathbf{a}(\theta_{I1}), \mathbf{a}(\theta_{I2})]$ and $\mathbf{s}_I(t) = [s_{I1}(t), s_{I2}(t)]^T$ are the corresponding vectors for the CCI signal. It is assumed that the desired signal and the CCI signal are independent. We also assume that the elements of the noise vector $\mathbf{n}(t)$ are i.i.d. Gaussian random processes with zero-mean and covariance matrix $\sigma_N^2\mathbf{I}$, where $\mathbf{I}$ is the N x N identity matrix. $s_{D1}(t)$ is used as the direct ray and considered the signal of interest (SOI). The multipath ray $s_{D2}(t)$ can be separated into two components, one is coherent with the SOI and the other is orthogonal to the SOI [17], i.e.,

$$s_{D2}(t) = \rho_D^* \xi_D s_{D1}(t) + s_D^{\perp}(t) \tag{2}$$

where $E[s_D^{\perp}(t) s_{D1}(t)] = 0$, and

$$\rho_D = \frac{E[s_{D1}(t) s_{D2}^*(t)]}{\sigma_{D1}\sigma_{D2}} \tag{3}$$

is the signal correlation between the two rays whose power are $\sigma_D^2 (\triangleq \sigma_{D1}^2)$ and σ_{D2}^2, respectively, $\xi_D = \sigma_{D2}/\sigma_{D1}$. $E[\cdot]$ denotes statistical average and $(\cdot)^*$ denotes complex conjugate. The signal covariance matrix is defined as

$$\begin{aligned}\mathbf{R}'_{DD} &= E[\mathbf{s}_D(t)\mathbf{s}_D^H(t)] \\ &= \sigma_D^2 \begin{bmatrix} 1 & \rho_D\xi_D \\ \rho_D^*\xi_D & |\rho_D\xi_D|^2 \end{bmatrix} + \begin{bmatrix} 0 & 0 \\ 0 & (1-|\rho_D|^2)\sigma_{D2}^2 \end{bmatrix}\end{aligned} \tag{4}$$

where $(\cdot)^H$ denotes complex conjugate transpose. Accordingly, the spatial covariance matrix is given by

$$\begin{aligned}\mathbf{R}_{DD} &= \mathbf{A}(\Theta_D) E[\mathbf{s}_D(t)\mathbf{s}_D^H(t)]\mathbf{A}^H(\Theta_D) \\ &= [\mathbf{a}(\theta_{D1}), \mathbf{a}(\theta_{D2})] \left\{ \sigma_D^2 \begin{bmatrix} 1 & \rho_D\xi_D \\ \rho_D^*\xi_D & |\rho_D\xi_D|^2 \end{bmatrix} + \begin{bmatrix} 0 & 0 \\ 0 & (1-|\rho_D|^2)\sigma_{D2}^2 \end{bmatrix} \right\} \begin{bmatrix} \mathbf{a}^H(\theta_{D1}) \\ \mathbf{a}^H(\theta_{D2}) \end{bmatrix} \\ &= \sigma_D^2 [\mathbf{a}(\theta_{D1}) + \rho_D^*\xi_D \mathbf{a}(\theta_{D2})][\mathbf{a}(\theta_{D1}) + \rho_D^*\xi_D \mathbf{a}(\theta_{D2})]^H + (1-|\rho_D|^2)\sigma_{D2}^2 \mathbf{a}(\theta_{D2})\mathbf{a}^H(\theta_{D2})\end{aligned} \tag{5}$$

The first term of the right side of (5) is constructed from combined signal vector $\tilde{\mathbf{s}}_D(t) = [\mathbf{a}(\theta_{D1}) + \rho_D^*\xi_D \mathbf{a}(\theta_{D2})] s_{D1}(t)$, where the quantity in the brackets

$$\tilde{\mathbf{a}}_D = \mathbf{a}(\theta_{D1}) + \rho_D^* \xi_D \mathbf{a}(\theta_{D2}) \tag{6}$$

represents the generalized steering vector of SOI. The second term in (5) is the contribution to the ISI from the orthogonal components $s_D^{\perp}(t)$. This contribution vanishes asymptotically as $|\rho_D|$ approaches 1.

By assuming that the reference signal $r(t)$ is an ideal replica of the SOI $s_{D1}(t)$, then the correlation vector between the data vector $\mathbf{x}(t)$ and the reference signal $r(t)$ is

$$\mathbf{r}_D = E[\mathbf{x}(t)r^*(t)] = E[\mathbf{x}(t)s_{D1}^*(t)] = \sigma_D^2 \tilde{\mathbf{a}}_D, \tag{7}$$

which coincides with the generalized steering vector of the SOI, given in (6). Thus, the minimum mean square error (MMSE) optimum weight vector is given by [18]

$$\mathbf{w} = \mathbf{R}_{XY}^{-1}\mathbf{r}_D = g\mathbf{R}_N^{-1}\tilde{\mathbf{a}}_D \tag{8}$$

where $g = \sigma_D^2(1 - \sigma_D^2 \tilde{\mathbf{a}}_D^H \mathbf{R}_{XY}^{-1} \tilde{\mathbf{a}}_D)$ is a constant,

$$\mathbf{R}_{XY} = E[\mathbf{x}(t)\mathbf{x}^H(t)] = \mathbf{R}_N + \sigma_D^2 \tilde{\mathbf{a}}_D \tilde{\mathbf{a}}_D^H \tag{9}$$

$$\mathbf{R}_N = (1 - |\rho_D|^2)\sigma_{D2}^2 \mathbf{a}(\theta_{D2})\mathbf{a}^H(\theta_{D2}) + \mathbf{R}_{IN} \tag{10}$$

$\mathbf{R}_N$ is the equivalent covariance matrix of all interfering components, and

$$\mathbf{R}_{IN} = \mathbf{R}_{II} + E[\mathbf{n}(t)\mathbf{n}^H(t)] = \mathbf{R}_{II} + \sigma_N^2 \mathbf{I}. \tag{11}$$

$\mathbf{R}_{II}$ is the covariance matrix of the CCI signal vector, which is defined in (14). By using the matrix inversion formula, we obtain

$$\mathbf{R}_N^{-1} = \mathbf{R}_{IN}^{-1} - \varepsilon \mathbf{R}_{IN}^{-1}\mathbf{a}(\theta_{D2})\mathbf{a}^H(\theta_{D2})\mathbf{R}_{IN}^{-1} \tag{12}$$

where

$$\varepsilon = \frac{(1 - |\rho_D|^2)\sigma_{D2}^2}{1 + (1 - |\rho_D|^2)\sigma_{D2}^2 \mathbf{a}^H(\theta_{D2})\mathbf{R}_{IN}^{-1}\mathbf{a}(\theta_{D2})} \tag{13}$$

which monotonously decreases as $|\rho_D|$ increases.

From the above analysis, the array weight vector will be less influenced by the orthogonal component, $s_D^{\perp}(t)$, as $|\rho_D|$ increases. For the case of $|\rho_D|$ reaching a unit value, the two multipath rays can be considered a single ray, and they can be handled by a single DOF. Consequently, the

frequency-selective fading problem is converted into a flat fading problem. Thus, the channel is equalized by array processing and the ISI problem is solved.

All CCI components are to be suppressed by the spatial signal processing. Therefore, these components can be represented by using eigen-decomposition methods. The covariance matrix of the CCI signal vector, denoted by $\mathbf{R}_{II}$, is expressed as,

$$\mathbf{R}_{II} = \mathbf{A}(\Theta_I)E[\mathbf{s}_I(t)\mathbf{s}_I^H(t)]\mathbf{A}^H(\Theta_I) = \sum_{i=1}^{2} \lambda_{Ii}\mathbf{u}_{Ii}\mathbf{u}_{Ii}^H \tag{14}$$

where λ_{Ii} (i=1,2) are the eigenvalues of $\mathbf{R}_{II}$ and $\mathbf{u}_{Ii}$ are the associated eigenvectors. The two eigenvalues are given by [19]

$$\begin{aligned}\lambda_{I1,2} &= \frac{N}{2}[\sigma_{I1}^2 + \sigma_{I2}^2 + 2\sigma_{I1}\sigma_{I2}\,\mathrm{Re}(\rho_I\beta_I^*)] \\ &\times\left[1 \pm \sqrt{1 - \frac{4\sigma_{I1}^2\sigma_{I2}^2(1-|\beta_I|^2)(1-|\rho_I|^2)}{[\sigma_{I1}^2 + \sigma_{I2}^2 + 2\sigma_{I1}\sigma_{I2}\,\mathrm{Re}(\rho_I\beta_I^*)]^2}}\right]\end{aligned} \tag{15}$$

where σ_{I1}^2 and σ_{I2}^2 are the powers of the two rays of the CCI signal, respectively. ρ_I is the signal temporal correlation coefficient between the two rays, and β_I is the spatial correlation coefficient of the rays, defined as

$$\beta_I = \frac{\mathbf{a}^H(\theta_{I1})\mathbf{a}(\theta_{I2})}{\|\mathbf{a}(\theta_{I1})\|\,\|\mathbf{a}(\theta_{I2})\|} \tag{16}$$

It is clear that λ_{I2} becomes 0 when either or both of $|\rho_I|$ and $|\beta_I|$ become 1. For these cases, the two rays behave as a single ray. Therefore, while the array often needs two DOF's to effectively suppress the two rays with low signal correlation, it suffices only to use a single DOF when the two rays are highly correlated statistically and/or spatially.

III. Signal Correlation Enhancement by Using Filter Banks

In the previous section, we discussed the adaptive array framework in the presence of multipath rays. It is shown that, the increase of the correlation between signal multipath rays converts the frequency-selective problem into a flat fading problem, so that the signal is equalized by array

processing. When this correlation is very high, the multipath rays can be treated as a single equivalent ray. A generalized beam is formed for the multipath rays of the desired signal by a single array DOF so that the rays are combined in the manner of maximum ratio, and the multipath rays of each CCI signal will be suppressed by a single array DOF.

This section discusses the signal correlation enhancement of multipath rays by subband signal processing. We first briefly review the concept of subband signal processing by using filter banks, then give the basic principle of coherency enhancement via subband partition using ideal filters. Next, the implementation based on DFT and QMF filter banks is discussed and the performances of signal correlation enhancement are compared.

A. Subband signal processing by using filter banks

A filter bank is a set of filters linked by sampling operators and sometimes by delays. Fig.1 shows the block diagram of a filter bank. The z-transform of the output $y(n)$ is expressed as

$$Y(z) = T(z)X(z) + \sum_{k=1}^{M-1} A_k(z)X(e^{j2\pi k/M}z) \tag{17}$$

where $X(z)$ is the z-transform of $x(n)$,

$$T(z) = \frac{1}{M}\sum_{k=1}^{M} H^{(k)}(z)F^{(k)}(z) \tag{18}$$

$$A_k(z) = \frac{1}{M}\sum_{k=1}^{M} H^{(k)}(e^{-j2\pi k/M}z)F^{(k)}(z), \tag{19}$$

and M is the number of subbands, and we assume the decimation rate is the same. This filter bank is called maximally decimated filter bank. The first term of the right side of (17) is the non-aliasing component, and the last term is the aliasing component. To realize the perfect reconstruction (PR) of the filter bank, it is required that

$$T(z) = z^{-n_0} \tag{20}$$

and

$$A_k(z) = 0 \quad \text{for } k = 1, 2, \ldots, M\text{-}1 \tag{21}$$

where $n_0 > 0$ is an arbitrary integer.

Under the PR condition, the output of the filter bank is a delayed version of the input of the filter bank without distortion, or

$$y(n) = x(n - n_0). \tag{22}$$

If a filter bank consists of ideal filters is used, that is

$$H^{(k)}(f) = F^{(k)}(f) = \begin{cases} 1, & -\frac{B}{2} + \frac{k-1}{M} B \le f < -\frac{B}{2} + \frac{k}{M} B \\ 0, & elsewhere \end{cases} \tag{23}$$

then clearly the filter bank satisfies the PR condition. Although such a filter bank is not casual, it provides a very simple expression. The expression will be used to analyze the signal correlation enhancement in sub-section B.

A useful type of PR filter bank is DFT filter bank, which is based on DFT and IDFT transforms, as is shown in Fig. 2. The DFT filter bank is discussed in sub-section C.

Quadrature mirror filter (QMF) banks, or more practically, pseudo-QMF banks, are often used to realize efficient subband signal processing with perfect or near-perfect reconstruction (NPR) [9, 20, 21]. A QMF filter has the same construction as Fig. 1, where in a QMF filter bank each of the analysis or synthesis filters can be realized by an FIR filter with finite taps. In a pseudo-QMF bank, the filter bank channels are formed by a series of equidistant frequency shifts of an appropriate prototype filter, and the transfer functions of adjacent channels are approximately power complementary between their center frequencies. We will discuss the pseudo-QMF banks in sub-section D.

B. Basic principle of coherency enhancement via subband partition

Consider a band-limited stochastic signal $s(t)$. For the simplicity of analysis, we assume the power spectrum density function (PSDF), denoted by $p(f)$, is flat within bandwidth B,

$$p(f) = \begin{cases} 1, & -\frac{B}{2} \le f \le \frac{B}{2} \\ 0, & elsewhere. \end{cases} \tag{24}$$

The associated autocorrelation function, denoted by $r(\tau)$, is obtained by the Fourier transformation of $p(f)$, as

$$r(\tau) = E\{s(t)s^*(t-\tau)\} = \frac{\sin(\pi B\tau)}{\pi\tau}. \tag{25}$$

If we equally partition $p(f)$ into M subbands, such as

$$p(f) = \sum_{k=0}^{M-1} p^{(k)}(f), \tag{26}$$

where

$$p^{(k)}(f) = \begin{cases} 1, & -\frac{B}{2} + \frac{k}{M}B \le f < -\frac{B}{2} + \frac{k+1}{M}B \\ 0, & elsewhere \end{cases}, \tag{27}$$

then the autocorrelation function for kth subband signal $s^{(k)}(t)$ will be

$$r^{(k)}(\tau) = E\{s^{(k)}(t)s^{(k)*}(t-\tau)\} = \frac{\sin(\frac{\pi B\tau}{M})}{\pi\tau} e^{j\frac{\pi B\tau}{M}(2k-M-1)}. \tag{28}$$

The signal correlation coefficient of $s(t)$ and its delayed replica $s(t-\tau)$ is then

$$\rho(\tau) = \alpha\frac{r(\tau)}{r(0)} = \alpha\frac{\sin(\pi B\tau)}{\pi B\tau}, \tag{29}$$

where α ($|\alpha|=1$) is a factor used to express the propagation phase difference between $s(t)$ and $s(t-\tau)$. Similarly, for the kth subband signal we have

$$\rho^{(k)}(\tau) = \alpha\frac{r^{(k)}(\tau)}{r^{(k)}(0)} = \alpha\frac{\sin(\pi B\tau/M)}{\pi B\tau/M} e^{j(2k-M-1)\pi B\tau/M}. \tag{30}$$

By comparing (29) and (30), it becomes apparent that the signal correlation of the subband signal is widened M times in the time scale. We note that $|\rho^{(k)}(\tau)|$ does not change with k, which implies that the signal correlation is equally enhanced for the different subbands. For example, when $\tau = 1/B$ we have $\rho(1/B) = 0$, which means two signals are uncorrelated. When the signal is divided into M subbands, then $|\rho^{(k)}(1/B)| = \frac{\sin(\pi/M)}{\pi/M}$ which equals to 0.9936 for M =16. Therefore, the two uncorrelated rays become approximately coherent in the subbands. The correlation $|\rho^{(k)}(\tau)|$ is plotted versus M and is shown by the solid line in Fig. 3 for $B\tau = 1$.

C. Subband partition via DFT filter banks

In the above sub-section, we considered the filter bank based on ideal filters. However, for causal systems, the transfer function of an FIR filter does not have the shape of a rectangular pulse. The most practically used filter banks are based on DFT and QMF filter banks to realize perfect reconstruction or near-perfect reconstruction [9, 21]. In this sub-section we analyze the performance of signal correlation enhancement when DFT filter banks are used.

The discrete Fourier transformation (DFT) of a data sequence $x(n)$ is defined as

$$X(k) = \sum_{n=0}^{M-1} x(n) W^{nk} \quad , \quad k = 0,1,\cdots,N-1 \tag{31}$$

where $W = e^{-j2\pi/M}$. The kth subband output of the DFT is

$$y^{(k)}(t) = \sum_{n=0}^{M-1} x(t - nT_S) e^{-j2\pi(N-1-n)k/N} \quad , \quad 0 \le k \le M-1 \tag{32}$$

where T_S is the sampling duration. Here we assume critical sampling, so that $T_S = 1/B$. The impulse responses of kth subband DFT analysis and synthesis filter can be described as

$$\begin{cases} h_k(n) = e^{-j2\pi(M-1-n)k/M} \\ f_k(n) = e^{j2\pi nk/M} \end{cases} \tag{33}$$
$$0 \le n \le M-1, \quad 0 \le k \le M-1.$$

Then, the z-domain transfer functions of the filters are described

$$\begin{cases} H_k(z) = \sum_{n=0}^{M-1} z^{-n} e^{-j2\pi(M-1-n)k/M} \\ F_k(z) = \sum_{n=0}^{M-1} z^{-n} e^{j2\pi nk/M} \end{cases} \tag{34}$$
$$0 \le k \le M-1$$

respectively, and the frequency response of the kth analysis filter is

$$\begin{aligned} H^{(k)}(f) &= \sum_{n=0}^{M-1} e^{-j2\pi nf} e^{-j2\pi(M-1-n)k/M} \\ &= \frac{\sin(\pi M(f - k/M))}{\sin(\pi(f - k/M))} e^{-j\pi(M-1)(f-k/M)}, \end{aligned} \tag{35}$$

where f denotes the normalized frequency with respect to the signal bandwidth B.

From (35) and

$$p^{(k)}(f) = \left|H^{(k)}(f)\right|^2 p(f), \tag{36}$$

the autocorrelation function and signal correlation coefficient of kth subband filter output signal is obtained as

$$\begin{aligned} r^{(k)}(\tau) &= \int_{-\infty}^{\infty} p^{(k)}(f) e^{j2\pi f\tau} df \\ &= \int_{-\infty}^{\infty} \sum_{n=0}^{M-1} \sum_{m=0}^{M-1} e^{-j2\pi f(n-m)/B} e^{-j2\pi(m-n)k/M} p(f) e^{j2\pi f\tau} df \\ &= \sum_{n=0}^{M-1} \sum_{m=0}^{M-1} e^{-j2\pi(m-n)k/M} r(\tau - \frac{n-m}{B}) \end{aligned} \tag{37}$$

and

$$\rho^{(k)}(\tau) = \alpha r^{(k)}(\tau) / r^{(k)}(0). \tag{38}$$

The signal correlation coefficient is plotted in Fig.4 for the different subbands. It is seen that the curve is flat only when τ/T_S is an integer. At the other cases, the signal correlation coefficient has the largest value at k=0, and the coefficient is very low at $k=\frac{M}{2}$, particularly when the modulo of τ/T_S is 0.5.

The correlation coefficient between the two rays is given as the dotted line in Fig. 3 for $B\tau = 1$ and k =0. $\left|\rho^{(k)}(\tau)\right|$ is approximately 0.935 when M =16. From Fig. 3 it is clear that the DFT filter banks provide meager signal correlation enhancement. From Fig.4 it is seen that $\left|\rho^{(k)}(\tau)\right|$ is even lower when τ / T_S is not an integer and k is close to $M/2$. Thus, filter banks with more powerful correlation enhancement are preferable to reduce the number of subband partitions.

D. Subband partition via QMF filter banks

We now discuss the signal correlation enhancement using pseudo-QMF filter banks. The impulse responses of the pseudo-QMF analysis and synthesis filters $h_k(n)$ and $f_k(n)$ respectively, are cosine-modulated versions of a real and linear-phase impulse response of the prototype filter $h(n)$, i.e.

$$\begin{cases} h_{k'}(n) = 2h(n)\cos\left((2k'+1)\dfrac{\pi}{2M'}(n-\dfrac{N-1}{2})+(-1)^{k'}\dfrac{\pi}{4}\right) \\ f_{k'}(n) = 2h(n)\cos\left((2k'+1)\dfrac{\pi}{2M'}(n-\dfrac{N-1}{2})-(-1)^{k'}\dfrac{\pi}{4}\right) \end{cases}$$
$$0 \le n \le N-1, \quad 0 \le k' \le M'-1, \tag{39}$$

where N is the number of FIR taps. Denote $H(z) = \sum_{n=0}^{N-1} h(n)z^{-n}$ as the z-transform of $h(n)$, the z-transforms of $h_{k'}(n)$ are

$$H^{(k')}(z) = \underbrace{a_{k'}c_{k'}H(zW^{(k+\frac{1}{2})})}_{H^{(k',1)}(z)} + \underbrace{a_{k'}^{*}c_{k'}^{*}H(zW^{-(k'+\frac{1}{2})})}_{H^{(k',2)}(z)} \tag{40}$$

where $W = e^{-j\frac{\pi}{M'}}$, $a_{k'} = e^{j\theta_{k'}}$, $c_{k'} = W^{(k'+\frac{1}{2})(\frac{N-1}{2})}$, and $\theta_{k'} = (-1)^{k'}\dfrac{\pi}{4}$. Due to the mirror effect, the signal correlation is very low for a large k' and non-integer τ/T_S. Therefore, direct utilization of QMF subband filter bank does not bring adequate signal correlation enhancement for different subbands. To solve this problem, we partition each subband analysis filter into two sub-subband filters, $H^{(k',1)}(z)$ and $H^{(k',2)}(z)$. Consequently, in our modified QMF subband processing scheme, the analysis filter bank consists of $2M'$ subband coding (SBC) filter banks while the synthesis filter bank consists of M' QMF banks.

To simplify and unify the notation, we let M=$2M'$, and denote the subband index (k', i) into k so that

$$k = \begin{cases} k' & i = 1 \\ k'+M' & i = 2 \end{cases} \tag{41}$$

Then we have

$$\begin{cases} H^{(k)}(z) = \begin{cases} a_k c_k H(zW^{(k+\frac{1}{2})}) & 0 \le k < \dfrac{M}{2} \\ a^{*}_{k-\frac{M}{2}} c^{*}_{k-\frac{M}{2}} H(zW^{-(k+\frac{1-M}{2})}) & \dfrac{M}{2} \le k < M \end{cases} \\ F^{(k)}(z) = a_k^{*}c_k H(zW^{(k+\frac{1}{2})}) + a_k c_k^{*} H(zW^{-(k+\frac{1}{2})}) \quad 0 \le k < \dfrac{M}{2} \end{cases} \tag{42}$$

and

$$\begin{cases} h_k(n) = \begin{cases} 2h(n)e^{(2k+1)\frac{\pi}{M}(n-\frac{N-1}{2})+(-1)^k\frac{\pi}{4}} & 0 \le k < \frac{M}{2} \\ 2h(n)e^{-(2k-M+1)\frac{\pi}{M}(n-\frac{N-1}{2})-(-1)^{(k-\frac{M}{2})}\frac{\pi}{4}} & \frac{M}{2} \le k < M \end{cases} \\ f_k(n) = 2h(n)\cos\left((2k+1)\frac{\pi}{M}(n-\frac{N-1}{2}) - (-1)^k\frac{\pi}{4}\right) \quad 0 \le k < \frac{M}{2} \end{cases} \tag{43}$$

where for the synthesis filters we only give them for $0 \le k < \frac{M}{2}$, since only $\frac{M}{2}$ filters are required. The kth subband ($k \ge \frac{M}{2}$) uses the same synthesis filter of the ($k - \frac{M}{2}$)-th subband. Fig. 5 shows the configuration of the modified QMF filter bank.

Similar to (37), the autocorrelation functions of the outputs of these two sub-subband filters are obtained as

$$r^{(k)}(\tau) = \begin{cases} \sum_{n=0}^{N-1}\sum_{m=0}^{N-1} h(n)h(m)e^{-j(2k+1)(n-m)}r(\tau - \frac{n-m}{B}) & 0 \le k < \frac{M}{2} \\ \sum_{n=0}^{N-1}\sum_{m=0}^{N-1} h(n)h(m)W^{j(2k+1-M)(n-m)}r(\tau - \frac{n-m}{B}) & \frac{M}{2} \le k < M \end{cases} \tag{44}$$

Since $r^{(k+\frac{M}{2})}$ ($0 \le k < \frac{M}{2}$) is the conjugate of $r^{(k)}$, they have the same amplitude. From (44), it is seen that the signal correlation coefficient between two multipath ray components in kth two QMF sub-subband filter outputs is calculated by

$$\rho^{(k)}(\tau) = \alpha r^{(k)}(\tau)/r^{(k)}(0). \tag{45}$$

Fig. 6 shows the signal correlation coefficient for the different subbands. The FIR coefficients are computed based on [21], and the number of taps is 48, 64, 128, and 256 for M = 4, 8, 16, and 32, respectively. From the figure it is clear that $|\rho^{(k)}(\tau)|$ is flat over the subbands except the minor degradation at the two sub-subbands of k=$\frac{M}{2}$-1 and k=$\frac{M}{2}$ when τ/T_S is not an integer. Therefore, the signal correlation is almost equally enhanced for the different subbands after the subband signal processing based on modified-QMF filter banks.

The signal correlation coefficient is plotted as the dashed line in Fig. 3 for $B\tau = 1$ and k=0. It is evident that the modified QMF-based filter banks have very close signal correlation enhancement

performance to that of the ideal FIR filters.

In the above analysis, M depends on the signal correlation improvement and the requirement of subband processing. In practice, M should be chosen depending on the environment coherence bandwidth [22] and the employed signal bandwidth.

IV. Subband Adaptive Array

A. Concept

In the above sections, we have discussed the signal equalization at a frequency-selective fading environment as the signal correlation between multipath rays is increased, and the signal correlation is enhanced by subband signal processing via exploitation of the filter banks. Therefore, applying the subband signal processing technique to adaptive arrays forms subband adaptive arrays, which is possible to solve both of the CCI and ISI problems in a multipath fading environment. In this section we discuss the concept and the behavior of subband adaptive array.

We now consider the adaptive array implementing the Wiener-Hopf solution, such as the LMS adaptive array, with the modified pseudo-QMF filter banks here. The output of each array sensor and the reference signal are divided into M subbands, respectively. The array is near-perfectly reconstructed after converging to the reference signal. The steady state optimum weight vector at the kth subband is thus given by

$$\mathbf{w}^{(k)} = \mathbf{R}_{XX}^{(k)-1}\mathbf{r}_D^{(k)} \qquad k=1, \ldots, M \tag{46}$$

where

$$\mathbf{R}_{XX}^{(k)} = E[\mathbf{x}^{(k)}(t)\mathbf{x}^{(k)H}(t)] \tag{47}$$

$$\mathbf{r}_D^{(k)} = E[\mathbf{x}^{(k)}(t)r^{(k)*}(t)]\,. \tag{48}$$

From the discussion in Sections 2 and 3, the multipath rays in each subband encounter increases signal correlation, and, asymptotically they behave like a single ray for high values of M.

B. Performance analysis

From (8) and (12), the array output signal-to-interference-plus-noise ratio (SINR) without subband signal processing is obtained as,

$$\begin{aligned}\mathrm{SINR}_0 &= \frac{P_{S0}}{P_{IN0}} = \frac{E\{|\mathbf{w}^H \tilde{s}_D(t)\tilde{\mathbf{a}}_D|^2\}}{E\{\mathbf{w}^H \mathbf{R}_N \mathbf{w}\}} \\ &= \frac{\sigma_D^2 |\tilde{\mathbf{a}}_D^H \mathbf{R}_N^{-1} \tilde{\mathbf{a}}_D|^2}{\tilde{\mathbf{a}}_D^H \mathbf{R}_N^{-1} \mathbf{R}_N \mathbf{R}_N^{-1} \tilde{\mathbf{a}}_D} = \sigma_D^2 \tilde{\mathbf{a}}_D^H \mathbf{R}_N^{-1} \tilde{\mathbf{a}}_D\end{aligned} \tag{49}$$

where P_{S0} is the SOI output power and P_{IN0} the output interfering signal power, respectively. With subband signal processing, the SOI output power, $P_S^{(k)}$, and the output interfering signal power, $P_{IN}^{(k)}$, at the kth subband are given by

$$\begin{aligned}P_S^{(k)} &= \sigma_D^{(k)2} |\mathbf{w}^{(k)H} \tilde{\mathbf{a}}_D^{(k)}|^2 \\ &= \sigma_D^{(k)2} (\tilde{\mathbf{a}}_D^{(k)H} \mathbf{R}_{XX}^{(k)-1} \tilde{\mathbf{a}}_D^{(k)})^2 = g^{(k)2} \sigma_D^{(k)2} (\tilde{\mathbf{a}}_D^{(k)H} \mathbf{R}_N^{(k)-1} \tilde{\mathbf{a}}_D^{(k)})^2\end{aligned} \tag{50}$$

and

$$\begin{aligned}P_{IN}^{(k)} &= \mathbf{w}^{(k)H} \mathbf{R}_N^{(k)} \mathbf{w}^{(k)} \\ &= \sigma_D^{(k)2} \tilde{\mathbf{a}}_D^{(k)H} \mathbf{R}_{XX}^{(k)-1} \mathbf{R}_N^{(k)} \mathbf{R}_{XX}^{(k)-1} \tilde{\mathbf{a}}_D^{(k)} = g^{(k)2} \sigma_D^{(k)2} \tilde{\mathbf{a}}_D^{(k)H} \mathbf{R}_N^{(k)-1} \tilde{\mathbf{a}}_D^{(k)}\end{aligned} \tag{51}$$

respectively, where

$$g^{(k)} = \sigma_D^{(k)2} (1 - \sigma_D^{(k)2} \tilde{\mathbf{a}}_D^{(k)H} \mathbf{R}_{XX}^{(k)-1} \tilde{\mathbf{a}}_D^{(k)}) . \tag{52}$$

The output SINR of a subband adaptive array is expressed as

$$\mathrm{SINR}_{\mathrm{SUB}} = \frac{\sum_{k=0}^{M-1} P_S^{(k)}}{\sum_{k=0}^{M-1} P_{IN}^{(k)}} = \frac{\sum_{k=0}^{M-1} g^{(k)2} \sigma_D^{(k)2} |\tilde{\mathbf{a}}_D^{(k)H} \mathbf{R}_N^{(k)-1} \tilde{\mathbf{a}}_D^{(k)}|^2}{\sum_{k=0}^{M-1} g^{(k)2} \tilde{\mathbf{a}}_D^{(k)H} \mathbf{R}_N^{(k)-1} \tilde{\mathbf{a}}_D^{(k)}} . \tag{53}$$

The SINR improvement by subband array processing is most significant in the following cases. The first case is that, the number of DOF's is less than the total number of rays, but is larger than the total number of the desired and CCI signals, while the signal correlation between the multipath rays is small. Consider a mobile station at high-speed digital communications environment. Although the number of CCI signals is limited, they can arrive with a large number of multipath rays with low

signal correlation. In this case, the conventional adaptive array cannot sufficiently suppress the CCI rays as well as the interfering multipath rays of the desired signal, whereas the subband adaptive array can suppress the CCI rays and combines the multipath rays of the desired signal.

Another case is that, the multipath rays of the desired signal come from a small angular sector so that it is not possible for conventional adaptive array to suppress the interfering multipath while maintaining the proper gain of the desired signal. A subband adaptive array is not sensitive to the problem since it is not necessary for the array to suppress the multipath rays.

V. Performance Simulation

Computational simulations are performed to confirm our analysis. An equi-spaced linear 3-element adaptive array is considered and the interelement spacing is half wavelength. Sample matrix inversion (SMI) method [23] is used to approximate the optimum weights in obtaining the output SINR and bit error rate (BER). Both the desired signal and the interference signals are considered with QPSK modulation, and the roll-off rate is 0.5.

We first consider the case where only the desired signal with two rays is present. It is assumed that $\sigma_{D1}^2 = \sigma_{D2}^2 = 10$ dB, and $\sigma_N^2 = 0$ dB. Fig. 7 shows the output SINR versus the number of subbands, M (In the figures hereafter M=1 denotes the case where the signal is processed without subband decomposition). In Fig. 7, the DOA of the direct ray is 0 degree from the broadside direction. We show two cases where the DOA of the delayed ray is from 40 degrees and 2 degrees, respectively. The time delay between the two rays is T_S so that the two rays are uncorrelated.

For the case of θ_{D2}=40 degrees, the two rays are widely separated in space. With two DOF's, the uncorrelated delayed ray is suppressed, leading to high output SINR is high, even when no subband signal processing is performed. Thus, the improvement by subband signal processing is not significant. However, for the case of θ_{D2}=2 degrees, the output SINR is very low (1.7dB) when no subband signal processing is performed. The degradation of the output SINR is caused by the resolution limitation of the array since the two signals are closed separated. The array output SINR performance is improved rapidly as M increases, which confirms the equalization ability of the subband signal processing.

We add other two multipath rays into the above case. The corresponding array output SINR is shown in Fig. 8. The new multipath rays have the same input signal level, and the DOA's are -20 and -60 degrees, and their delay times relative to the direct ray are $2T_S$ and $3T_S$, respectively. In this case, when no subband signal processing is performed, the four rays are uncorrelated to each other, and the array will try to suppress the three delayed rays. We note that the 3-element array only has two DOF's. Therefore, the array DOF's are not sufficient, and the array cannot provide good performance. It is clear from Fig. 8 that the output SINR is near 0dB. On the other hand, when subband signal processing is performed, the four rays will asymptotically behave as an equivalent ray and the output SINR increases rapidly as M increases. The output SINR exceeds 13dB when $M = 4$ or larger, and the BER is lower than 10^{-5}.

Fig.9 depicts the output SINR when two CCI signals are added to the case considered in Fig.7. The CCI powers are $\sigma_{I1}^2 = \sigma_{I2}^2 = 20$dB, and their DOA's are -20 and -60 degrees, with delay time difference equals to T_S. When no subband signal processing is performed, the array will suppress the delayed ray of the desired signal and the two uncorrelated CCI rays. Similar to the case in Fig.8, the number of DOF's is not sufficient to achieve this task. The result is very poor output SINR as worse as -1.6dB. When subband signal processing is performed, the two rays of the desired signal will be treated as an equivalent single one, and the two rays of the CCI signal as another equivalent ray. Thus, the array DOF's will be sufficient, and the output SINR increases to 7.1dB for $M = 4$, and 12dB for $M = 8$. The corresponding BER performance is shown in Fig.10, which decreases rapidly as M increases.

VI. Conclusion

We have proposed subband adaptive arrays for multipath fading mitigation in wireless communications. It has been shown that subband adaptive arrays, which provide sub-optimal frequency-spatial signal processing, are very effective both in mitigating the inter-symbol interference (ISI) problem caused by frequency-selective fading, and in suppressing the co-channel interference (CCI) signals in mobile communications.

The performance of the adaptive array in the presence of multipath rays has been analyzed. We

have shown that these rays can be considered as a single path when the signal correlation between the rays is high. The analysis of the signal correlation enhancement between the multipath rays by subband signal processing was presented. We have discussed the signal correlation enhancement performance for filter banks using ideal filters, DFT, and modified QMF filters. The excellent performance of modified QMF filter banks, which are practical to use, is also demonstrated. The simulation results confirmed the analyses and the effectiveness of the proposed method to combat the multipath fading for both the desired signal and the CCI signals.

Acknowledgements

The first two authors would like to thank Dr. Bokuji Komiyama, President, Dr. Yoshio Karasawa and Dr. Yoshihiko Mizuguchi, former and current Head of Department 3, all of ATR Adaptive Communications Research Laboratories, for their encouragement and helpful discussions.

References

[1] Y. Ogawa, M. Ohmiya, and K. Itoh, "An LMS adaptive array for multipath fading reduction," *IEEE Trans. Aerosp. Electron. Syst.*, vol.AES-23, no.1, pp.17-23, Jan.1987.

[2] S. Anderson, M. Millnert, M. Viberg, and B. Wahlberg, "An adaptive array for mobile communication systems," *IEEE Trans. Veh. Technol.*, vol.VT-40, pp.230-236, 1991.

[3] Y. Zhang, "Multipath fading equalization by an adaptive array," in *Proc. Int. Symp. Antennas Propagat.*, Sapporo, pp.149-152, Aug. 1992.

[4] N. Ishii and R. Kohno, "Spatial and temporal equalization based on an adaptive tapped-delay-line array antenna," *IEICE Trans. Commun.*, vol.E78-B, no.8, pp.1162-1169, Aug. 1995.

[5] Y. Doi, T. Ohgane, and E. Ogawa, "ISI and CCI canceller combining the adaptive array antennas and the Viterbi equalizer in a digital mobile radio," in *Proc. IEEE VTC*, pp.81-85, April 1996.

[6] T. A. Thomas and M. D. Zoltowski, "Novel receiver signal processing for interference calcellation and equalization in cellular TDMA communications," in *Proc. IEEE ICASSP*, pp.3881-3884, 1997.

[7] J-W. Liang and A. Paulraj, "Two stage CCI/ISI reduction with space-time processing in TDMA cellular networks," in *Proc. 30th Annual Asilomar Conf. on Signals, Systems, and Computers*, Pacific Grove, CA, Nov. 1996.

[8] A. J. Paulraj and C. B. Papadias, "Space-time processing for wireless communications," *IEEE Signal Processing Magazine*, vol.14, no.6, pp.49-83, Nov. 1997.

[9] N. J. Fliege, "*Multirate Digital Signal Processing*," John Wiley, 1994.

[10] Y. Zhang, K. Yang, and M. G. Amin, "Adaptive subband arrays for multipath fading mitigation", in *Proc. IEEE AP-S Int. Symp.*, Atlanta, pp.380-383, June 1998.

[11] --, "Perforemance analysis of subband adaptive arrays in multipath propagation environment," to appear in *Proc. IEEE Signal Processing Workshop on Statistical Signal and Array Signal Processing*, Portland, Sept. 1998.

[12] F. Lorenzelli, A. Wang, D. Korompis, R. Hydson, and K. Yao, "Optimization and performance of broadband microphone arrays," *SPIE*, vol. 2563, pp.158-169, July 1995.

[13] H. Wang and M. Kaveh, "Coherent signal subspace processing for the detection and estimation of angles of arrival of multiple wideband sources," *IEEE Trans. ASSP*, vol.33, no.4, pp.823-831, Aug. 1985.

[14] T. Sekiguchi and Y. Karasawa, "Multidimentional signal processing for antenna arrays," *Tech. Rep. of IEICE*, no.CAS97-89, Jan. 1988.

[15] J. M. Khalab and M. K. Ibrahim, "Novel multirate adaptive beamforming technique," *Electron. Lett.*, vol.30. no.15, pp.1194-1195, 1994.

[16] M. G. Amin, "High resolution direction of arrival estimation of multiple wide-band sources in multichannel adaptive nulling systems," in *Proc. IEEE ICASSP*, Atlanta, May 1996.

[17] J. Yang and A. Swindlehurst, "Maximum SINR beamforming for correlated sources," in *Proc. ICASSP'95*, Detroit, pp.1916-1919, May 1995.

[18] I. J. Gupta, "Effect of jammer power on the performance of adaptive arrays," *IEEE Trans. Antennas Propagat.*, vol.32, no.9, Sept. 1984.

[19] J. E. Hudson, "*Adaptive Array Principles*," Peter Peregrinus, 1989.

[20] R. D. Koipillai and P. P. Vaidyanathan, "New results of cosine-modulated FIR filter banks satisfying perfect reconstruction," in *Proc. IEEE ICASSP*, Toronto, pp.1789-1792, May 1991.

[21] T. Q. Nguyen, "Near-perfect-reconstruction pseudo-QMF banks," *IEEE Trans. Signal Proc.*,

vol.42, pp.65-76, 1994.

[22] W. C. Y. Lee, "*Mobile Communications Design Fundamentals*," second edition, New York: Wiley, 1993.

[23] I. S. Reed, J. D. Mallet, and L. E. Brennan, "Rapid convergence rate in adaptive arrays," *IEEE Trans. Aerosp. Electron. Syst.*, vol.10, pp.853-863, Nov. 1974.

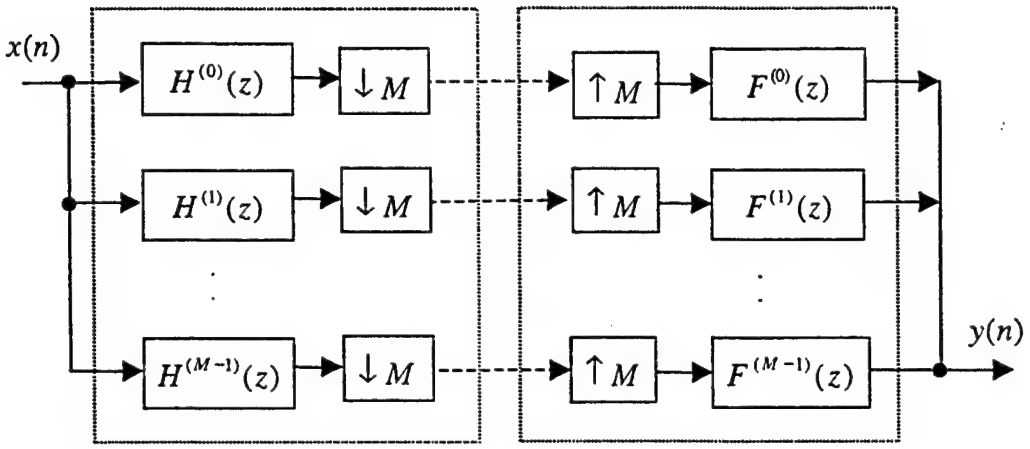

Fig.1 Block diagram of a filter bank

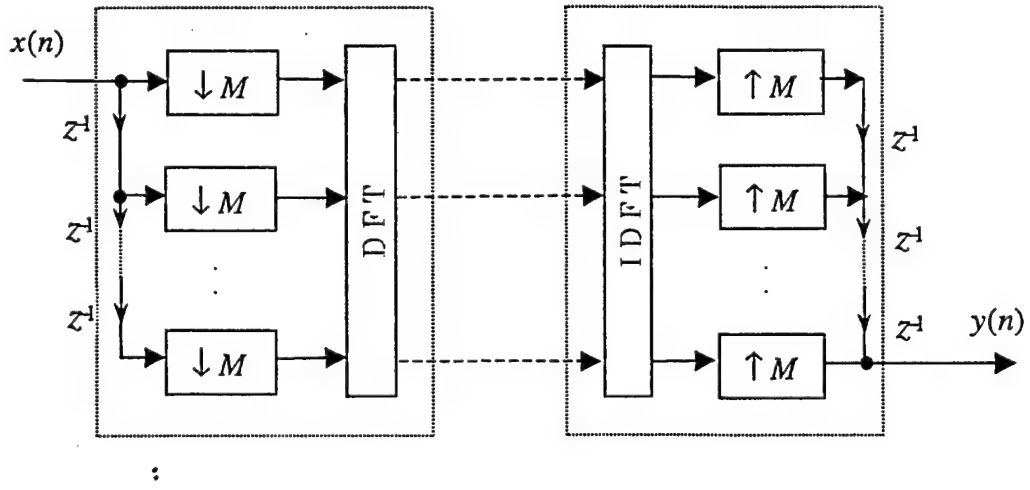

Fig.2 Block diagram of a DFT filter bank

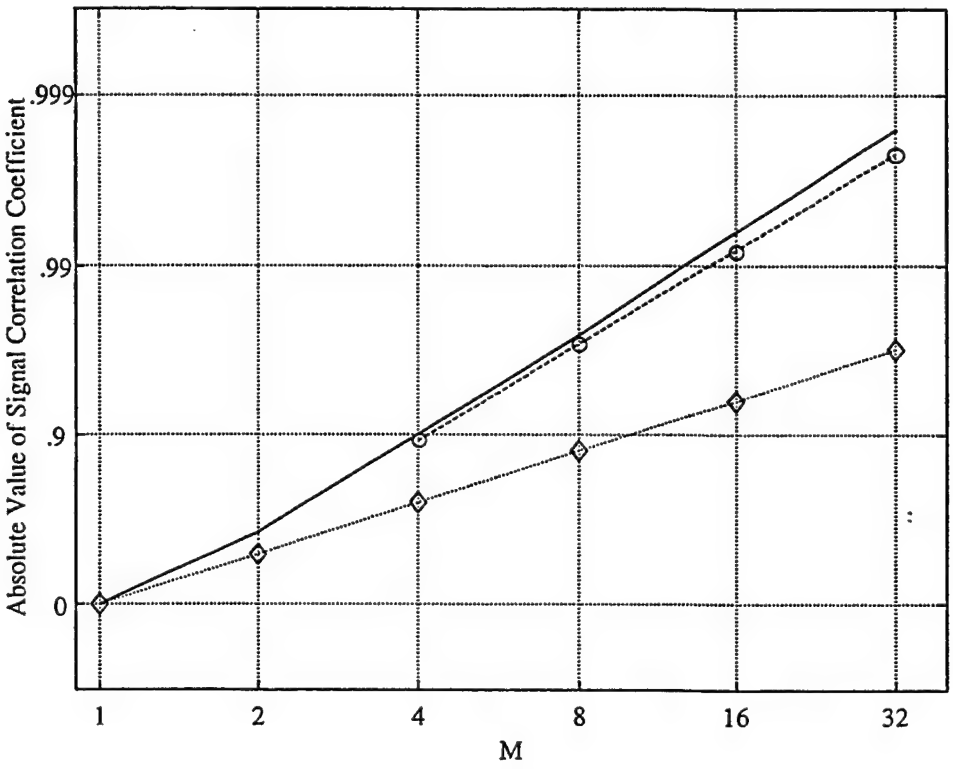

Fig.3 Signal correlation coefficient vs. M for $\tau = T_S$

(—— ideal -<>- DFT —o— QMF)

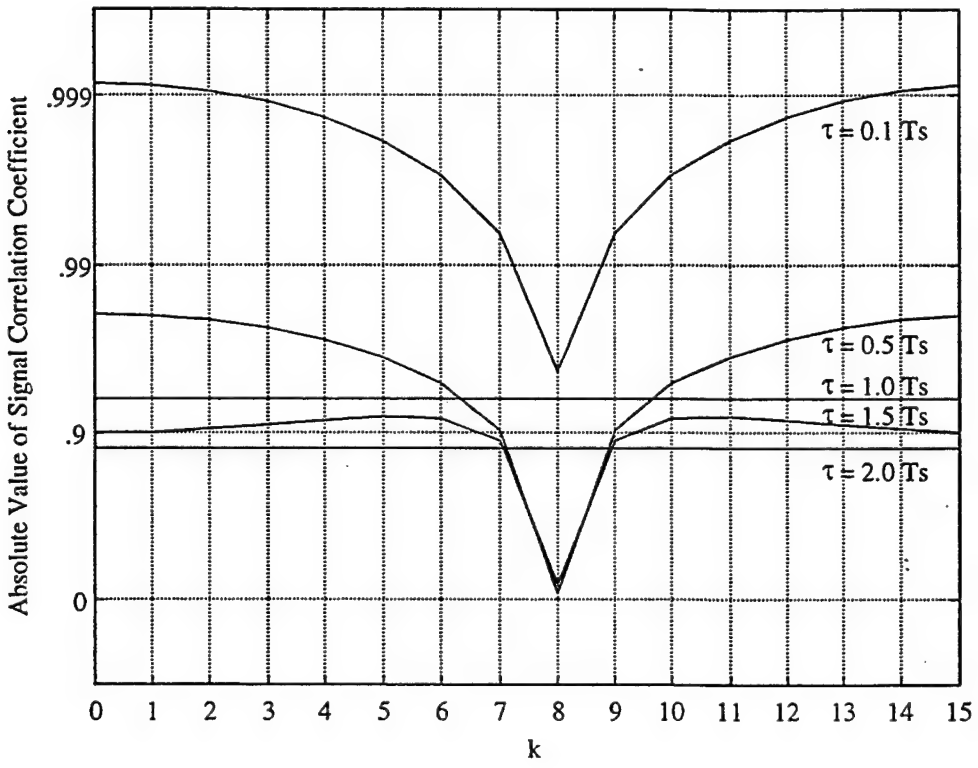

Fig.4 Signal correlation coefficient of DFT filter banks at the different subbands ($M = 16$)

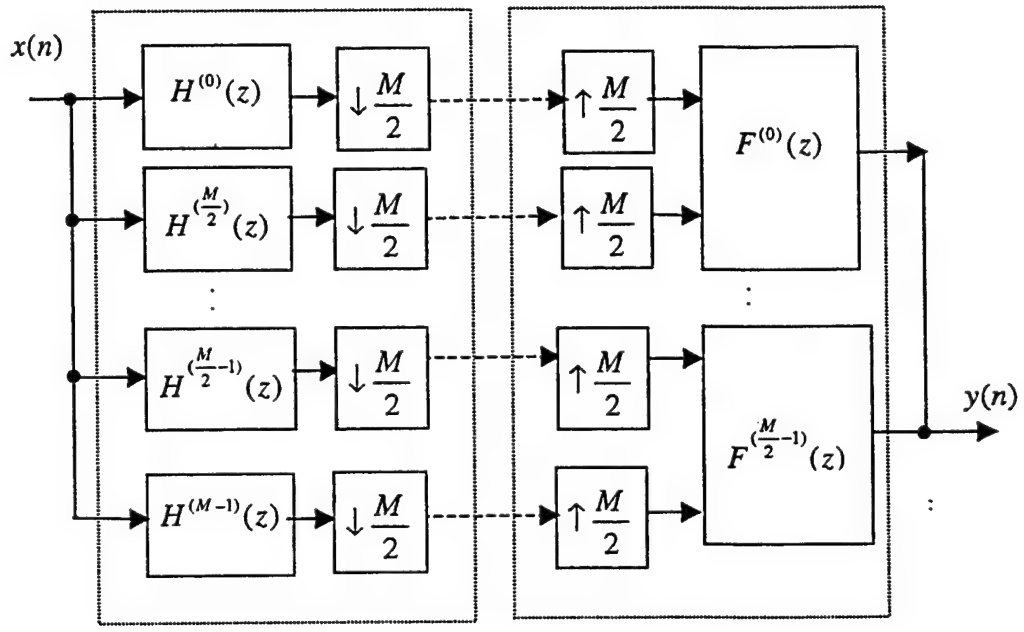

Fig.5 Block diagram of a modified QMF bank

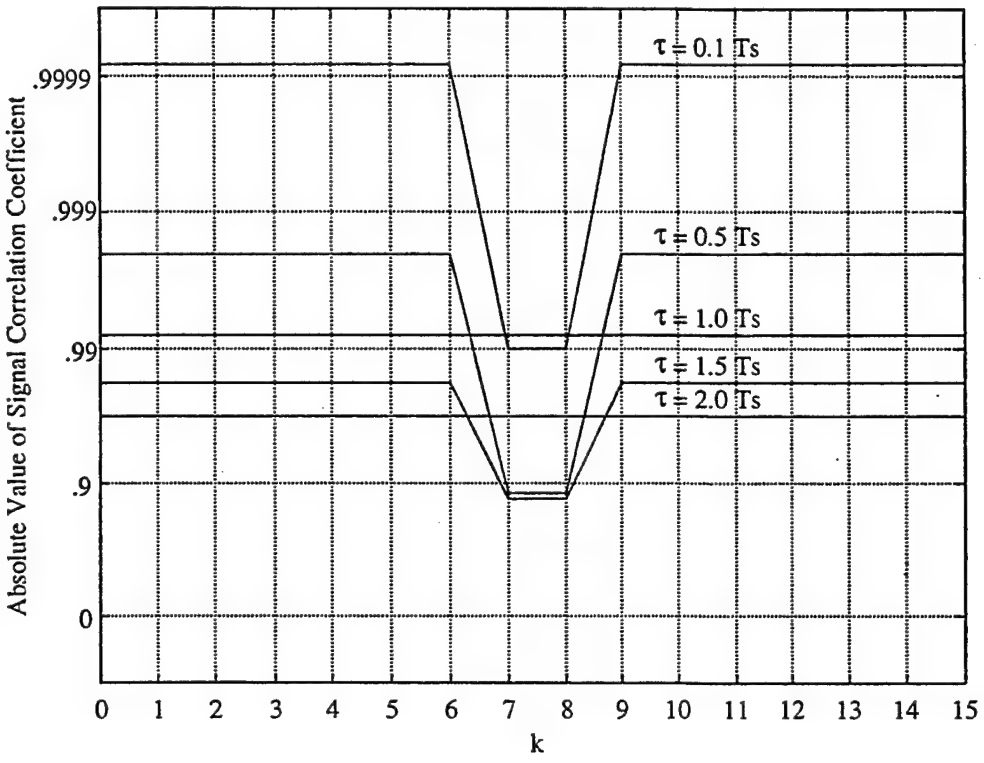

Fig.6 Signal correlation coefficient of modified QMF banks at the different subbands ($M = 16$)

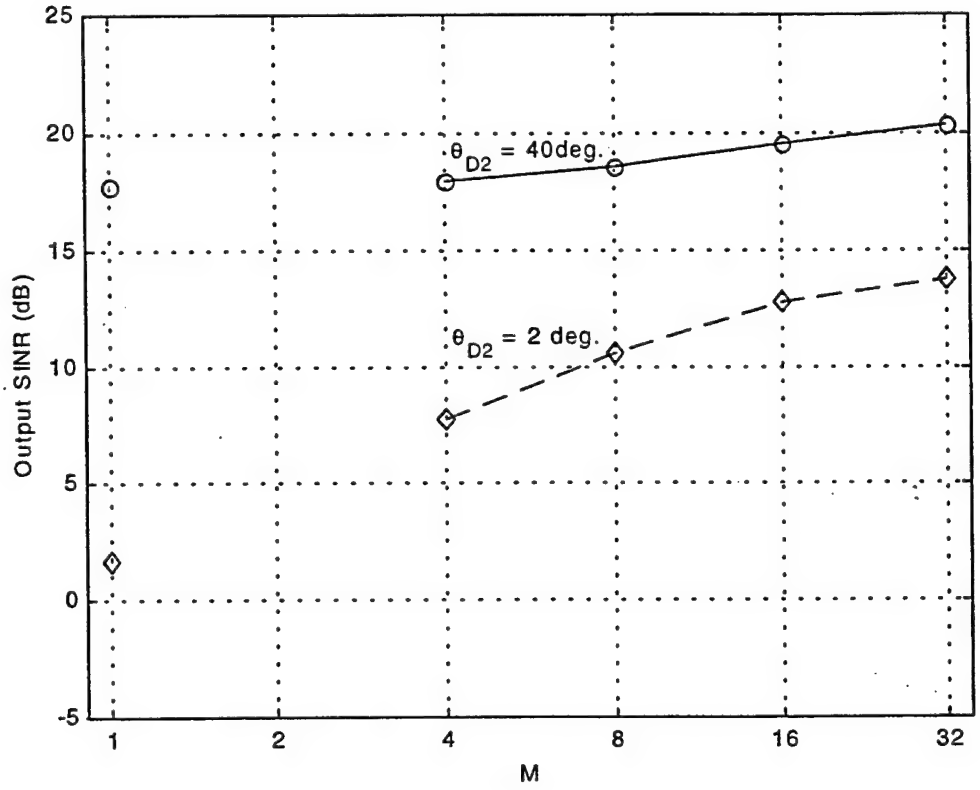

Fig.7 Output SINR vs. M

($\sigma_{D1}^2 = \sigma_{D2}^2 = 10$dB, $\theta_{D1} = 0$ deg., $\tau = T_S$)

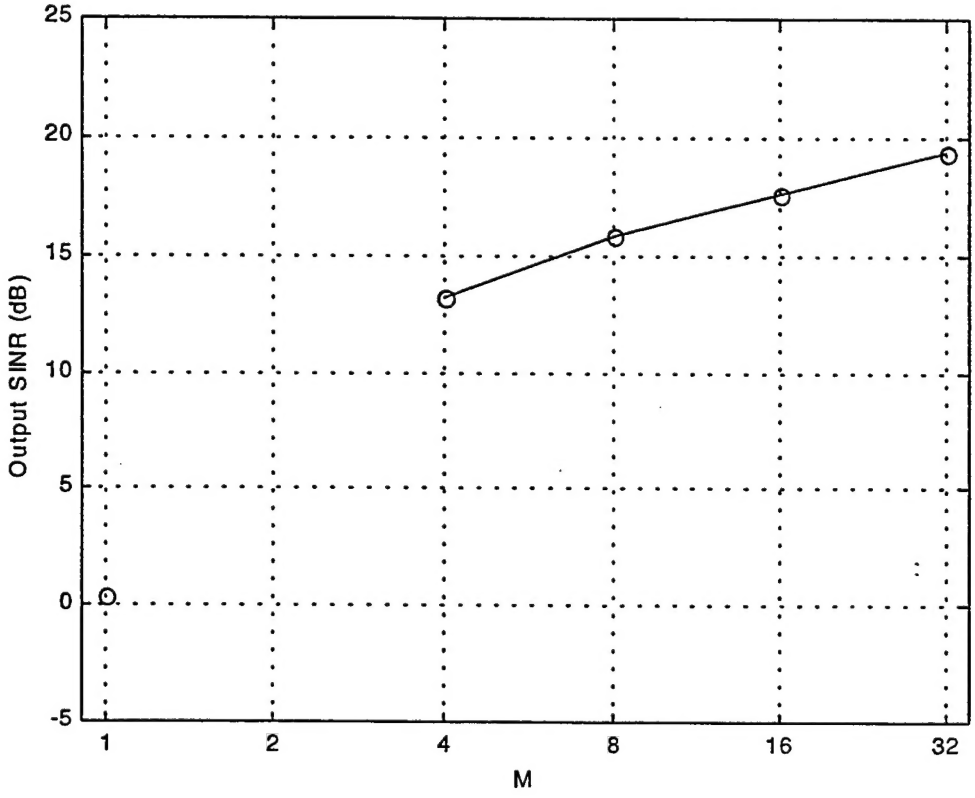

Fig.8 Output SINR vs. M

($\sigma_{D1}^2 = \sigma_{D2}^2 = \sigma_{D3}^2 = \sigma_{D4}^2 = 10$dB, $\theta_{D1} = 0$ deg., $\theta_{D2} = 20$ deg., $\theta_{D3} = -20$ deg., $\theta_{D4} = -60$ deg., $\tau_2 = T_S$, $\tau_3 = 2T_S$, $\tau_4 = 3T_S$)

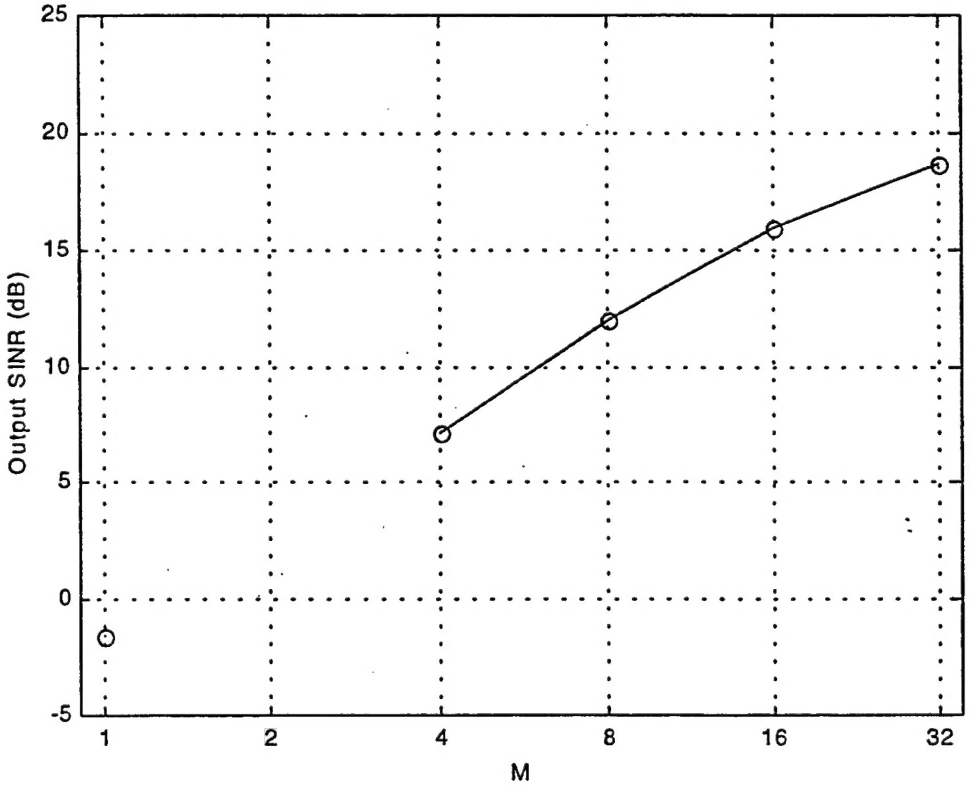

Fig.9 Output SINR vs. M

($\sigma_{D1}^2 = \sigma_{D2}^2 = 10$dB, $\theta_{D1} = 0$ deg., $\theta_{D2} = 20$ deg., $\tau_D = T_S$,

$\sigma_{I1}^2 = \sigma_{I2}^2 = 20$dB, $\theta_{I1} = -20$ deg., $\theta_{I2} = -60$ deg., $\tau_I = T_S$)

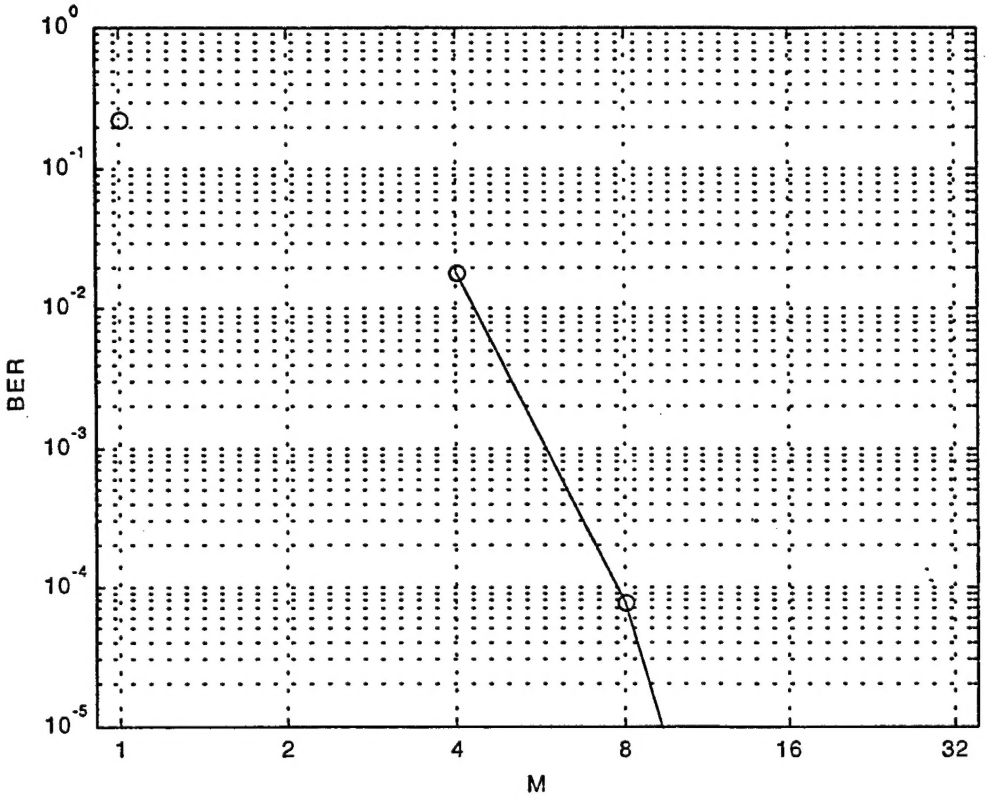

Fig.10 BER vs. M

($\sigma_{D1}^2 = \sigma_{D2}^2 = 10$dB, $\theta_{D1} = 0$ deg., $\theta_{D2} = 20$ deg., $\tau_D = T_S$,
$\sigma_{I1}^2 = \sigma_{I2}^2 = 20$dB, $\theta_{I1} = -20$ deg., $\theta_{I2} = -60$ deg., $\tau_I = T_S$)

REPORT DOCUMENTATION PAGE

Form Approved
OMB No. 0704-0188

1. AGENCY USE ONLY *(Leave blank)*	2. REPORT DATE	3. REPORT TYPE AND DATES COVERED
	October 1st, 1998	Interim: November 15th, 1997- September 30th, 1998

4. TITLE AND SUBTITLE

BLIND TIME-FREQUENCY ANALYSIS FOR SOURCE DISCRIMINATION IN MULTISENSOR ARRAY PROCESSING

5. FUNDING NUMBERS

G- N00014-98-1-0176

6. AUTHOR(S)

Moeness G. Amin

7. PERFORMING ORGANIZATION NAMES(S) AND ADDRESS(ES)

Villanova University
800 Lancaster Ave
Villanova, Pa 19085

8. PERFORMING ORGANIZATION REPORT NUMBER

Acc: 527616

9. SPONSORING / MONITORING AGENCY NAMES(S) AND ADDRESS(ES)

Office of Naval Research (William Miceli)
Ballston Center Tower One
800 North Quincy Street
Arlington VA 22217-5660

10. SPONSORING / MONITORING AGENCY REPORT NUMBER

11. SUPPLEMENTARY NOTES

a. DISTRIBUTION / AVAILABILITY STATEMENT

Approved for Public Release; distribution is Unlimited

12. DISTRIBUTION CODE

13. ABSTRACT *(Maximum 200 words)*

This report includes results on the applications of time frequency distributions in blind source separation and direction finding problems. A novel approach based on time-frequency distributions (TFDs) for separating signals received by a multiple antenna array is developed. The sources have different time-frequency signatures and are instantaneously mixed at the array sensors. The proposed approach provides a significant improvement in performance over the recently introduced spatial time-frequency distributions, specifically for signals with close time-frequency signatures. Spatial averaging of the TFDs of the sensor data is performed to eliminate the interactions of the sources signals in the time-frequency domain, and as such restores important properties of the source TFD matrix. We have also improved nonstationay source signal estimation by performing the blind source separation using ambiguity functions, and as such, avoid the inclusion of cross-terms in the estimation process. Our third contribution to this area is the introduction of the Time-Frequency MUSIC as a new array signal processing method based on time-frequency signal representations. This report also includes contributions to problems of fast computation TFDs, spatial processing for frequency diversity spread spectrum communications as applied to partial jamming mitigation, and subband array processing to combat fading and multipath.

14. SUBJECT TERMS

Blind Source Separation, Direction Finding, Time-Frequency Distributions, Subband Arrays, Spatial Diversity Spread Spectrum Communications

15. NUMBER OF PAGES

85

16. PRICE CODE

17. SECURITY CLASSIFICATION OF REPORT	18. SECURITY CLASSIFICATION OF THIS PAGE	19. SECURITY CLASSIFICATION OF ABSTRACT	20. LIMITATION OF ABSTRACT
UNCLASSIFIED	UNCLASSIFIED	UNCLASSIFIED	